A novel shortcut for computational materials design

Ayoub Aouina

▶ **To cite this version:**

Ayoub Aouina. A novel shortcut for computational materials design. Computational Physics [physics.comp-ph]. Institut Polytechnique de Paris, 2022. English. NNT : 2022IPPAX008 . tel-03662872

HAL Id: tel-03662872
https://theses.hal.science/tel-03662872

Submitted on 9 May 2022

HAL is a multi-disciplinary open access archive for the deposit and dissemination of scientific research documents, whether they are published or not. The documents may come from teaching and research institutions in France or abroad, or from public or private research centers.

L'archive ouverte pluridisciplinaire **HAL**, est destinée au dépôt et à la diffusion de documents scientifiques de niveau recherche, publiés ou non, émanant des établissements d'enseignement et de recherche français ou étrangers, des laboratoires publics ou privés.

INSTITUT POLYTECHNIQUE DE PARIS

NNT : 2022IPPAX008

Thèse de doctorat

A novel shortcut for computational materials design

Thèse de doctorat de l'Institut Polytechnique de Paris
préparée à École Polytechnique

École doctorale n° 626 École Doctorale de l'Institut Polytechnique de Paris
(ED IP Paris)
Spécialité de doctorat : Physique

Thèse présentée et soutenue à Palaiseau, le 01 février 2022 par

AYOUB AOUINA

Composition du Jury :

Emmanuel Fromager Professeur Laboratoire de Chimie Quantique, Université de Strasbourg, France	Président
Silvana Botti Professeur Abbe Center of Photonics, Friedrich Schiller Universität in Jena, Germany	Rapporteure
Neepa Maitra Professeur Department of Physics, Rutgers University at Newark, USA	Rapporteure
Nikitas Gidopoulos Associate Professor Department of Physics, Durham University, UK	Examinateur
Carsten Ullrich Professeur Department of Physics and Astronomy, University of Missouri, USA	Examinateur
Matteo Gatti Chargé de recherche CNRS Laboratoire des solides irradiés, École Polytechnique	Directeur de thèse
Lucia Reining Directrice de recherche CNRS Laboratoire des solides irradiés, École Polytechnique	Directrice de thèse

Contents

List of Figures

List of Tables

List of Abbreviations

QMC	Quantum Monte Carlo
GFFT	Green's Function Functional Theory
DFT	Density Functional Theory
XC	Exchange Correlation
AFQMC	Auxiliary Field Quantum Monte Carlo
KS	Kohn Sham
DM	Density Matrix
HEG	Homogeneous Electron Gas
HK	Hohenberg-Kohn
LDA	Local Density Approximation
GGA	Generalized Gradient Approximation
WDA	Weighted Density Approximation
MAE	Mean Average Error
COT	Connector Theory

To my beloved parents and my generous aunt Nadira.

Chapter 1

Introduction

Computational design of materials reflects the dream of creating new materials with desired properties for various applications, such as photovoltaics, thermoelectrics or nanotechnologies. It is well known in condensed matter physics that the properties of materials originate from a collective behavior of particles, namely, electrons and nuclei which are the fundamental constituents of matter. In most cases, understanding the collective behavior of electrons is necessary to predict and design a large number of materials features. The challenge then is to describe a system with many interacting electrons, which are governed by the laws of quantum mechanics. This problem is known as the quantum many-body problem.

In principle, any system of interacting particles can be fully described via the wavefunctions which are the solutions of the Schrödinger equation. However, the solution of this equation is complicated, and even computationally impossible, for systems of more than a few particles. One possible way to proceed is to approximate the ground state wavefunction and some excited state wavefunctions using stochastic methods such as Quantum Monte Carlo (QMC) [1, 2]. Such methods are based on the minimization of the energy with respect to a trial many-body wavefunctions. They involve very expensive calculations and their cost increases rapidly with the size of the system. This price is due to the excellent quality of the approximation; in particular they yield near-exact estimation for the total energy of the system.

Another possible way to tackle the problem is based on building functionals of more compact quantities. An example is the one-body Green's function [1, 3], which describes the likelihood that an electron added to (or removed from) a material at position $\mathbf{r}$ and time t is found at another position $\mathbf{r}'$ and time t'. The one-body Green's function is the basic building block in Green's function functional theory (GFFT). Much of the success of GFFT is due to the assumption that the interaction between the particles is weak and it can be treated within Many Body Perturbation Theory [4, 1]. However, the perturbation expansion suffers from convergence problems, and making high-order expansions, which implies high computational cost, does not necessarily lead to an improvement.

Another approach to deal with the many body problem is density functional theory (DFT) [5, 6]. It is so efficient that it allows one to run high throughput calculations [7, 8, 9, 10, 11]. According to DFT any observable is

a functional of the ground-state density of electrons, which is the probability to find one of N electrons in a volume of space. The density is a three-dimensional function which makes DFT much cheaper than QMC, however, the DFT functionals are not known and there is no useful systematic prescription how to construct them.

The aim of this thesis is to give a systematic and general approach for approximating observables or other objects. This approach is based on two pillars : first, it suggests to calculate and store the desired quantity in a model system, which is usually a simple system. This allows us to do the calculation with high precision using high-level methods, or to profit from available results. The computational cost does not matter a lot since these calculations are done once and for all. The second pillar consists of making the connection between the model and real systems, i.e, the prescription how to optimize the use of the model data in order to approximate quantities in real systems. This prescription, termed connector, is very general and in principle exact. In practice, it has to be approximated. Once a good connector has been established, one can obtain results for many materials with a modest computational cost. Moreover, it can be seen as a generator for new functionals.

In the next chapter, I will present the theoretical framework of this thesis, mainly the many body problem, density functional theory and density functional matrix theory [12, 13].

Then, in chapter 3, I will introduce the general connector theory and I will show how it can be applied to any quantity, and under which conditions. The discussion will be accompanied with a simple physical example in order to clarify the mathematical scheme. The examples and applications chosen in this thesis are mostly extended systems, although the connector approach is not limited to those in principle.

The aim of chapter 4 is to use the connector theory in order to build a new approximation for the exchange correlation (xc) potential. This quantity plays a central role in DFT, and it is very interesting to study since it describes the most intriguing ingredient of an interacting-particle system, namely the exchange and correlation effects.

As a first attempt toward testing the connector approximation of the xc potential, I evaluated and studied the performance of the approximation of a non-local functional in chapter 5. The encouraging results obtained from this study was the primary motivation for chapter 6, in which I considered the *true* xc potential functional. The purpose of this chapter is to conduct a comparative study of the electronic densities obtained using the connector functional and several popular DFT functionals with respect to a benchmark density of a given material. This topic initiates a collaboration with S. Chen and S. Zhang who calculated the benchmark densities in three prototypical solids using Auxiliary Field QMC [14], which is known to be very accurate. Given the availability of the QMC density, I inverted it in order to obtain a near-exact xc potential. This allowed me to directly compare it to the approximate functionals, including the connector approximation. The details of the inversion and the results are discussed in chapter 7. After accomplishing this, I used the inverted xc potential to extract the xc contribution from the

total energy, which was computed using QMC [14]. This xc energy served as a benchmark to test a connector functional which I designed specifically for the xc energy in chapter 8.

In chapters 9 and 10, I present two different applications of the connector theory beyond DFT and the xc potential. In the first application, I discuss a way to estimate for a given Hamiltonian, the density directly from a *connector* potential. In the second application, I use the Kohn-Sham density matrix to illustrate how the connector can approximate a non-local object. Finally, in chapter 11 I will draw conclusions and give my vision of promising directions for the future.

Chapter 2

Theoretical Background

The underlying physical laws necessary for the mathematical theory of a large part of physics and the whole of chemistry are thus completely known, and the difficulty is only that the exact application of these laws leads to equations much too complicated to be soluble.

Paul Dirac

In this chapter, I will review the theoretical concepts and the methods used to accomplish my thesis. I will start by the original problem which is the description of a system of interacting electrons. Then, I will discuss some independent-electron approximations as a way to tackle the many body problem. These approximations paved the way to density functional theory (DFT), which is considered as the state-of-art method to study the electronic structure. I will introduce the DFT formalism and I will present the approximations that make it practical. Following that, I will present the density matrix functional theory which requires more information than DFT but provides direct access to more observables. In all the rest of my thesis, equations are written in atomic units: $e^2 = \hbar = m_e = 1$ where e is the electron charge and m_e its mass. The unit of length is then a Bohr$\approx$ 0.529Å and the unit of energy is a Hartree$\approx$ 27.211eV.

2.1 The Many Body Problem

One of the most important and challenging problems in physics and chemistry is the many-body problem. The issue is to describe a system of many interacting electrons and nuclei. The size of these systems ranges from few particles, as in the case of atoms, to the order of the Avogadro number $N \sim 10^{23}$ particles, which is the case of solids. The good news is that, at least as far as today's insight allows us to judge, we know all the laws that govern these particles from quantum and statistical mechanics. We can then write

their Hamiltonian, which contains the main information about the system. It reads[1]

$$\hat{H} = -\sum_i \frac{\nabla_i^2}{2} - \sum_I \frac{\nabla_I^2}{2M_I} + \frac{1}{2}\sum_{i\neq j} \frac{1}{|\mathbf{r}_i - \mathbf{r}_j|} + \frac{1}{2}\sum_{I\neq J} \frac{Z_I Z_J}{|\mathbf{R}_I - \mathbf{R}_j|} - \sum_{i,I} \frac{Z_I}{|\mathbf{r}_i - \mathbf{R}_I|}, \tag{2.1}$$

where electrons and their positions are denoted by i and r_i, nuclei by I and R_I. M_I is the I-th nucleus mass and Z_I its atomic number. The first two terms represent the kinetic energy of electrons and nuclei. The next two terms represents electron-electron interaction and nucleus-nucleus interaction. The last term is the Coulomb interaction between electrons and nuclei.

2.1.1 Schrödinger equation

According to the first postulate of quantum mechanics, the state of the system at time t is completely specified by a mathematical object, called the wavefunction[2] $\psi(\{\mathbf{R}_I\}, \{\mathbf{r}_i\}, t) \equiv \psi(\mathbf{R}_1, \mathbf{R}_2, ..., \mathbf{R}_N, \mathbf{r}_1, \mathbf{r}_2, ..., \mathbf{r}_N, t)$. This wavefunction is the solution of the time-dependent Schrödinger equation, which reads

$$i\frac{\partial\psi(\{\mathbf{R}_I\}, \{\mathbf{r}_i\}, t)}{\partial t} = \hat{H}\psi(\{\mathbf{R}_I\}, \{\mathbf{r}_i\}, t). \tag{2.2}$$

The eigenstate of $\hat{H}$ at time $t = 0$ satisfies the time-independent Schrödinger equation

$$\hat{H}\psi(\{\mathbf{R}_I\}, \{\mathbf{r}_i\}) = E\psi(\{\mathbf{R}_I\}, \{\mathbf{r}_i\}). \tag{2.3}$$

The solution of this equation allows us to extract all the information contained in the Hamiltonian (2.1) at $t = 0$. This is more than enough for a system in equilibrium to determine many of its properties. However, equation (2.3) can be solved analytically at most for two particles and numerically for very few particles. The challenge arises from the Coulomb interaction, which couples the motions of all particles in the system, and hence requires simultaneous solution of (2.3) for the entire system. Furthermore, the wavefunction ψ depends on the positions and spins of the system's $N \sim 10^{23}$ particles. Thus, even if we were able to compute the wavefunction, storing it would need an astronomical number of memory units, which is simply beyond the capabilities of modern computers and is expected to stay so in the foreseeable future. To address this difficulty, clearly we need to make approximations [15].

2.1.2 The Born–Oppenheimer approximation

The difficulty of the many-body problem lies in the fact that the Hamiltonian (2.1) cannot be written as a sum of independent particles, since the Coulomb

[1] Relativistic effects and external perturbation are not considered.
[2] The spin coordinates will not be shown for the rest of the thesis.

interaction completely couples the motions of electrons and nuclei. However, the kinetic energy operator of the nuclei in (2.1) is proportional to the inverse nuclear mass $1/M$, which is very small compared to the electronic mass, $\frac{m_e}{M} \approx 10^{-4}$. Therefore, one can assume the nuclei to be fixed in their instantaneous positions and treat their kinetic energy as a perturbation. The electrons then move under the effect of the nuclear potential $V_{\text{ext},\mathbf{R}}(\mathbf{r} \equiv \{\mathbf{r_i}\})$ with fixed $\mathbf{R} \equiv \{\mathbf{R_I}\}$, and the electron-electron Coulomb repulsion. The pertinent Hamiltonian for the electrons is then

$$\hat{\mathcal{H}} = -\sum_i \frac{\nabla_i^2}{2} + \frac{1}{2}\sum_{i\neq j} \frac{1}{|\mathbf{r}_i - \mathbf{r}_j|} + V_{\text{ext},\mathbf{R}}(\mathbf{r}). \tag{2.4}$$

For a given state l and configuration $\mathbf{R}$, the Schrödinger equation for the electronic system reads

$$\left[-\sum_i \frac{\nabla_i^2}{2} + \frac{1}{2}\sum_{i\neq j} \frac{1}{|\mathbf{r}_i - \mathbf{r}_j|} + V_{\text{ext},\mathbf{R}}(\mathbf{r})\right] \varphi_{\mathbf{R}}^{(l)}(\mathbf{r}) = E^{(l)}(\mathbf{R})\varphi_{\mathbf{R}}^{(l)}(\mathbf{r}), \tag{2.5}$$

where $\varphi_{\mathbf{R}}^{(l)}(\mathbf{r})$ is an electronic wavefunction, which is a function of the position of all electrons $\mathbf{r}$. It also depends on the nuclear positions: this dependence is included as a subscript $\mathbf{R}$. The superscript l labels the element of the complete set of eigenstates for the electrons at each $\mathbf{R}$. The eigenvalues $E^{(l)}(\mathbf{R})$ are the associated electronic energies, which also depend on the nuclear position.

Let us now decompose the full wavefunction for a given state starting from the following ansatz

$$\psi(\mathbf{r}, \mathbf{R}) = \sum_l \eta^{(l)}(\mathbf{R})\varphi_{\mathbf{R}}^{(l)}(\mathbf{r}), \tag{2.6}$$

where $\eta^{(l)}(\{\mathbf{R}\})$ are functions of the nuclear positions. They are the coefficients that weight the electronic states $\varphi^{(l)}$. Now we apply the Hamiltonian (2.1) to (2.6) and, using (2.5), we obtain

$$\begin{aligned}\hat{H}\sum_l \eta^{(l)}(\mathbf{R})\varphi_{\mathbf{R}}^{(l)}(\mathbf{r}) = \quad & \textstyle\sum_l \eta^{(l)}(\mathbf{R}) \left(E^{(l)}(\mathbf{R}) + \hat{V}_{nn} + \sum_J \frac{-\nabla_J^2}{2M_J}\right) \varphi_{\mathbf{R}}^{(l)}(\mathbf{r}) \\ & + \textstyle\sum_{J,l} \varphi_{\mathbf{R}}^{(l)}(\mathbf{r}) \frac{-\nabla_J^2 \eta^{(l)}(\mathbf{R})}{2M_J} + \sum_{J,l} \frac{-\nabla_J \eta^{(l)}(\mathbf{R}) \nabla_J \varphi_{\mathbf{R}}^{(l)}(\mathbf{r})}{M_J},\end{aligned} \tag{2.7}$$

where $\hat{V}_{nn} = \frac{1}{2}\sum_{I\neq J} \frac{Z_I Z_J}{|\mathbf{R}_I - \mathbf{R}_j|}$ is the nuclear Coulomb interaction. We multiply this equation on the left by $\varphi_{\mathbf{R}}^{*(m)}(\mathbf{r})$ and we integrate over $\mathbf{r}$. Using (2.3), this yields

$$E\,\eta^{(m)}(\mathbf{R}) = \left(E^{(m)}(\mathbf{R}) + \hat{V}_{nn} + \sum_i A_{l,m}(\mathbf{R}) + \sum_J \frac{-\nabla_J^2}{2M_J} + \sum_i B_{l,m}(\mathbf{R})\right) \eta^{(m)}(\mathbf{R}), \tag{2.8}$$

with

$$A_{l,m}(\mathbf{R}) = -\sum_J \frac{1}{2M_J} \int d\mathbf{r} \varphi_{\mathbf{R}}^{*(m)}(\mathbf{r}) \nabla_J^2 \varphi_{\mathbf{R}}^{(l)}(\mathbf{r}), \tag{2.9}$$

$$B_{l,m}(\mathbf{R}) = -\sum_J \frac{1}{M_J} \int d\mathbf{r} \varphi_{\mathbf{R}}^{*(m)}(\mathbf{r}) \nabla_J \varphi_{\mathbf{R}}^{(l)}(\mathbf{r}) \, \nabla_J. \tag{2.10}$$

In the Born-Oppenheimer approximation [16], the electrons are assumed to follow adiabatically the motion of the nuclei, i.e., they remain in the given state m as the nuclei move, and there is no change of state from m to l. This means all the off-diagonal terms of $A_{l,m}$ and $B_{l,m}$ are neglected. The diagonal terms $B_{m,m}$ vanish if the $\varphi_{\mathbf{R}}^{m}(\mathbf{r})$ can be chosen to be real and the number of electrons, N, is fixed. This can be shown as follows

$$\begin{aligned} B_{m,m} &= -\sum_J \frac{1}{M_J} \int d\mathbf{R} \int d\mathbf{r} \varphi_{\mathbf{R}}^{*(m)}(\mathbf{r}) \nabla_J \varphi_{\mathbf{R}}^{(m)}(\mathbf{r}) \, \nabla_J \\ &= -\sum_J \frac{1}{M_J} \int d\mathbf{R} \nabla_J \int d\mathbf{r} \frac{1}{2} \left| \varphi_{\mathbf{R}}^{(m)}(\mathbf{r}) \right|^2 \nabla_J \\ &= -\sum_J \frac{1}{M_J} \int d\mathbf{R} \nabla_J \frac{N}{2} \nabla_J \\ &= 0. \end{aligned} \tag{2.11}$$

Thus, for each electronic state m, the nuclear motion is given by a purely nuclear equation, which reads

$$\left[-\sum_J \frac{1}{2M_J} \nabla_J^2 + U^{(m)}(\mathbf{R}) \right] = E\eta^{(m)}(\mathbf{R}), \tag{2.12}$$

with $U^{(m)}(\mathbf{R}) = V_{nn}(\mathbf{R}) + E^{(m)}(\mathbf{R}) + A_{m,m}(\mathbf{R})$, which represents a modified potential for the nuclei. The term $A_{m,m}(\mathbf{R})$ is very small since it is proportional to the inverse nuclear mass. It can also be neglected if the electron are more localized around the nuclei. Here, the term $E^{(m)}(\mathbf{R})$ can be interpreted as an *electronic glue* for the lattice [17].

In conclusion, the Born-Oppenheimer approximation allows us to decouple the dynamics of the electrons from the one of the nuclei. It is considered as excellent approximation [18], except when the adiabatic surfaces, defined by $E^{(m)}(\mathbf{R})$, are degenerate or nearly degenerate. In this case, the transition probability between different electronic states is significant, and so we cannot neglect the off-diagonal terms of $A_{l,m}$ and $B_{l,m}$. For all systems studied in this thesis, we will use the Born-Oppenheimer approximation. Moreover, we will use the *frozen-core* approximation. This means the inner electrons, known as core electrons, will be attached to their nuclei in a fixed state which makes a positively charged ion structure. This approximation is justified since only the valence electrons play an important role in the interatomic interaction.

Even with these approximations, the many-body problem remains very difficult due to the long range Coulomb interaction between electrons, and it is still impossible to store their wavefunction.

2.2 Observables

Our aim when studying the many-body problem is to understand and predict materials properties. These properties can be measured experimentally and we call them observables. For electrons whose state is described by the wavefunction φ, any time-independent observable at zero temperature can be calculated as an expectation value of a linear operator $\hat{O}$

$$\langle \hat{O} \rangle = \langle \varphi | \hat{O} | \varphi \rangle , \tag{2.13}$$

where φ is assumed to be normalized.

One interesting observable, that we will use often in this thesis, is the charge density of electrons. It is given by the expectation value of the density operator $\hat{n}(\mathbf{r}) = \sum_i \delta(\mathbf{r} - \mathbf{r}_i)$,

$$n(\mathbf{r}) = N \int d\mathbf{r}_2 ... d\mathbf{r}_N |\varphi(\mathbf{r}, \mathbf{r}_2, \mathbf{r}_3, ..., \mathbf{r}_N)|^2, \tag{2.14}$$

where N is the total number of electrons.

The other natural observables of the electronic system is the total energy, which is the expectation value of the Hamiltonian (2.4). Since we use the adiabatic approximation, the energy that results from the nuclear Coulomb interaction, E_{nn}, is a constant. This constant can be added to the zero of energy which yields

$$E = \langle \hat{\mathcal{H}} \rangle + E_{nn} = \langle \hat{T}_e \rangle + \langle \hat{V}_{ee} \rangle + \int d\mathbf{r} V_{\text{ext}}(\mathbf{r}) n(\mathbf{r}) + E_{nn}, \tag{2.15}$$

where $\hat{T}_e$ denotes the kinetic energy of electrons, and $\hat{V}_{ee}$ denotes the electronic Coulomb interaction operator.

One can see from above that observables are integrated objects and by calculating the wavefunction we have obtained too many details that we do not necessarily need to calculate physical quantities.

2.3 The variational principle

Here, we present the variational principle, which is a very powerful concept in mathematics and is widely used in theoretical physics. Suppose that we have a system with a Hamiltonian $\hat{\mathcal{H}}$, and we do not know the ground state energy, E_0, and the ground state wavefunction, φ_0, that verifies

$$\hat{\mathcal{H}} \varphi_0 = E_0 \varphi_0. \tag{2.16}$$

Now, if we choose any trial wavefunction φ, and we calculate its energy E, then the variational theorem guarantees

$$E[\varphi] = \langle \varphi | \hat{\mathcal{H}} | \varphi \rangle \geq E_0. \tag{2.17}$$

Thus, the wavefunction which most accurately describes the ground state of the system is the one which minimizes the total energy, i.e.,

$$E_0 = \min_{\{\varphi\}} \langle \varphi | \hat{\mathcal{H}} | \varphi \rangle . \tag{2.18}$$

This makes physical sense because the ground-state energy is, by definition, the lowest energy; hence, the energy E cannot be less than the energy of the ground-state wavefunction. The latter can be found using the method of Lagrange multipliers, by varying the wavefunction φ in (2.17), subject to the constraint $\langle \varphi | \varphi \rangle = 1$.

The variational principle is very useful for guiding approximations for the ground-state many-body wavefunction. It is the essence of stochastic methods like variational Monte Carlo [1].

2.4 Independent-particle methods

The solution of the many-body Schrödinger equation is challenging due to the Coulomb interaction between electrons. This interaction takes the form of a two-body operator in the Hamiltonian. Because of the Coulomb interaction, it is not possible to write the Hamiltonian as a sum of one body operators, and so we cannot factorize the many-body wavefunction. However, the independent-particle methods give us a way to approximate the interacting system by a non-interacting one, where the Schrödinger equation can be solved easily. The idea is to replace the two-body interaction term by an effective term representing the average action of all electrons on one of them. In other words, we admit that there is an approximation where finally the two-body term is replaced by a term depending only on the variables of one electron. Hence, we formally find a picture of the system where the effective Hamiltonian is a sum of independent pieces, and thus the many-body wavefunction is expressed as product or Slater determinant of a set of single-electron orbitals. Indeed, in this picture we assume that electrons are uncorrelated, although it is possible to make them obey the Pauli exclusion principle.

2.4.1 Hartree approximation

One of the earliest attempts to approximate the many-body problem using an independent-particle picture was made by Hartree [19]. The approximation is based on two steps: first we assume the wavefunction to be a product of a

set of single-electron orbitals[3]

$$\varphi^{\mathrm{H}}(\mathbf{r}_1, \mathbf{r}_2, ..., \mathbf{r}_N) = \phi_1(\mathbf{r}_1)\phi_2(\mathbf{r}_2)... \phi_N(\mathbf{r}_N), \tag{2.19}$$

where the orbitals are orthonormal. The second step is to use the variational principle (2.18) to obtain the effective Hamiltonian whose eigenstates are the orbitals that construct the full wavefunction φ^{H}. To do this, we use the Lagrange multipliers method to perform the minimization (2.18), under the normalization condition of the orbitals. This implies that we vary the expectation value of the Hamiltonian (2.4) with respect to the orbitals $\phi_i(\mathbf{r_i})$, and introduce the normalization condition via the Lagrange multipliers ε_i

$$\delta\left[\left\langle \varphi^{\mathrm{H}}\right| \mathcal{H} \left|\varphi^{\mathrm{H}}\right\rangle - \sum_i \varepsilon_i(\langle\phi_i|\phi_i\rangle - 1)\right] = 0. \tag{2.20}$$

The Hamiltonian $\mathcal{H}$, defined in (2.4), can be written as

$$\hat{\mathcal{H}} = \sum_i \hat{H}_1(i) + \frac{1}{2}\sum_{i\neq j} \hat{V}_{ee}(i,j), \tag{2.21}$$

where $\hat{H}_1(i)$ is the single-electron Hamiltonian and $\hat{V}_{ee}(i,j) = \frac{1}{|\mathbf{r}_i - \mathbf{r}_j|}$. Using (2.21) in (2.20) and considering only the variation of the bra $\left\langle \varphi^{\mathrm{H}}\right|$, we get for the first term

$$\left\langle \delta\varphi^{\mathrm{H}}\right| \sum_i \hat{H}_1(i) \left|\varphi^{\mathrm{H}}\right\rangle = \sum_i \langle\delta\phi_i| \hat{H}_1(i) |\phi_i\rangle . \tag{2.22}$$

For the operator $\hat{V}_{ee}(i,j)$, we get

$$\begin{aligned}\frac{1}{2}\sum_{i\neq j}\left\langle \delta\varphi^{\mathrm{H}}\right| \hat{V}_{ee}(i,j) \left|\varphi^{\mathrm{H}}\right\rangle &= \frac{1}{2}\left(\sum_{i\neq j}\langle\delta\phi_i\phi_j| \hat{V}_{ee}(i,j) |\phi_i\phi_j\rangle + \sum_{i\neq j}\langle\phi_i\delta\phi_j| \hat{V}_{ee}(i,j) |\phi_i\phi_j\rangle\right) \\ &= \sum_{i\neq j}\langle\delta\phi_i| \left(\langle\phi_j| \hat{V}_{ee}(i,j) |\phi_j\rangle\right) |\phi_i\rangle . \end{aligned} \tag{2.23}$$

Now we sum all the resulting terms from (2.20), which yields

$$\sum_i \left[\langle\delta\phi_i| \left(\hat{H}_1(i) + \sum\nolimits'_{j\neq i}\langle\phi_j| \hat{V}_{ee}(i,j) |\phi_j\rangle - \varepsilon_i\right) |\phi_i\rangle\right] = 0 \tag{2.24}$$

Since this must hold for all possible $\left\langle \delta\varphi_i^{\mathrm{H}}\right|$ and $\left|\delta\varphi_i^{\mathrm{H}}\right\rangle$, this can be satisfied only if

$$\left[\hat{H}_1(i) + \sum\nolimits'_{j\neq i}\langle\phi_j| \hat{V}_{ee}(i,j) |\phi_j\rangle\right] |\phi_i\rangle = \varepsilon_i |\phi_i\rangle , \tag{2.25}$$

where the primed sum is a single sum over all j different from i. We rewrite equation (2.25), replacing the notation $\mathbf{r}_i$ by $\mathbf{r}$, we obtain

[3] To be more precise, we should include the spin by expressing the wavefunction in terms of spinors.

$$\left[-\frac{\nabla^2}{2} + V_{\text{ext}}(\mathbf{r}) + V_{\text{Hartree}}(\mathbf{r}) + V^i_{\text{SIC}}(\mathbf{r})\right]\phi_i(\mathbf{r}) = \varepsilon_i\phi_i(\mathbf{r}), \tag{2.26}$$

where

$$V_{\text{Hartree}}(\mathbf{r}) = \int d\mathbf{r}' \frac{n(\mathbf{r}')}{|\mathbf{r}-\mathbf{r}'|} \quad \text{and} \quad V^i_{\text{SIC}}(\mathbf{r}) = -\frac{1}{2}\int d\mathbf{r}' \frac{|\phi_i(\mathbf{r}')|^2}{|\mathbf{r}-\mathbf{r}'|}. \tag{2.27}$$

The term $V_{\text{Hartree}}(\mathbf{r})$ is known as Hartree potential, and the potential $V^i_{\text{SIC}}(\mathbf{r})$ is the self-interaction correction of the Hartree potential. It guarantees that an electron in orbital $\phi_i(\mathbf{r})$ does not interact with itself, but only with the $(N-1)$ remaining electrons of the system. The term $V^i_{\text{SIC}}(\mathbf{r})$ is often neglected, that is why we often say that the Hartree equations contain a self-interaction term. This was not the case in the original derivation of Hartree equations, as shown in (2.26).

In conclusion, the Hartree approximation allows us to treat each electron as an independent particle living in an effective potential, generated by the other electrons. This picture yields an approximation for the many-body wavefunction, and hence we can calculate properties of real systems. Unfortunately, the Hartree approximation does not yield particularly satisfactory results. For instance, it predicts that there will be no binding energy keeping the electrons in a uniform system [20]. This, of course, contradicts experimental evidence that electrons require a finite amount of energy to be released from solids. The shortcomings of Hartree approximation can be understood from two points of view: first, the electrons are treated independently and so the correlation of their motion, due to the Coulomb interaction, is neglected. Second, we supposed that the wavefunction can be written as product of orbitals, and so the variational principle can only search through a restricted domain of wavefunctions, which does not necessarily contain the exact ground-state wavefunction. In addition to that, a wavefunction that takes the form (2.19) does not obey the Pauli exclusion principle. This last issue was resolved by an improved approximation, which we will present in the following section.

2.4.2 Hartree-Fock approximation

In order to satisfy the Pauli principle, Fock proposed to replace the wavefunction used in Hartree theory with an appropriate linear combination, known as a Slater determinant [21]

$$\varphi^{\text{HF}}(\mathbf{r}_1, \mathbf{r}_2, \ldots, \mathbf{r}_N) = \frac{1}{\sqrt{N!}}\begin{vmatrix} \phi_1(\mathbf{r}_1) & \phi_1(\mathbf{r}_2) & \ldots & \phi_1(\mathbf{r}_N) \\ \phi_2(\mathbf{r}_1) & \phi_2(\mathbf{r}_2) & \ldots & \phi_2(\mathbf{r}_N) \\ \vdots & \ddots & \ddots & \vdots \\ \vdots & \ddots & \ddots & \vdots \\ \phi_N(\mathbf{r}_1) & \phi_N(\mathbf{r}_2) & \ldots & \phi_N(\mathbf{r}_N) \end{vmatrix}, \tag{2.28}$$

where $1/\sqrt{N!}$ is the normalization factor. By writing the wavefunction as in (2.28), the Pauli principle is taken into account mathematically. Indeed, the determinant ensures that the wavefunction of the system is antisymmetric under exchange of any pair of electrons. This means if we swap an electron for another, the wavefunction remains unchanged except for a change of sign. The wavefunction will then vanish, indicating zero probability, as two electrons with the same orbital and spin approach each other.

Similarly to the previous section, we apply the variational principle using the ansatz (2.28), and we obtain the Hartree-Fock equations

$$\left[\frac{-\nabla^2}{2} + V_{\text{ext}}(\mathbf{r}) + V_{\text{Hartree}}(\mathbf{r}) + V_{\text{x}}^i(\mathbf{r})\right]\phi_i(\mathbf{r}) = \varepsilon_i\phi_i(\mathbf{r}), \tag{2.29}$$

with

$$V_{\text{x}}^i(\mathbf{r}) = -\frac{1}{2}\left[\sum_j \int d\mathbf{r}' \frac{\phi_j^*(\mathbf{r}')\phi_i(\mathbf{r}')}{|\mathbf{r}-\mathbf{r}'|}\right]\frac{\phi_j(\mathbf{r})}{\phi_i(\mathbf{r})}. \tag{2.30}$$

This term is the so-called exchange potential. It is the direct result of incorporating the Pauli principle via an antisymmetrised wavefunction. Note that the sum in (2.30) can be separated as

$$V_{\text{x}}^i(\mathbf{r}) = -\frac{1}{2}\left[\sum_{j\neq i} \int d\mathbf{r}' \frac{\phi_j^*(\mathbf{r}')\phi_i(\mathbf{r}')}{|\mathbf{r}-\mathbf{r}'|}\right]\frac{\phi_j(\mathbf{r})}{\phi_i(\mathbf{r})} - \frac{1}{2}\int d\mathbf{r}' \frac{|\phi_i(\mathbf{r}')|^2}{|\mathbf{r}-\mathbf{r}'|}. \tag{2.31}$$

The second term is exactly the self-interaction correction of the Hartree potential, $V_{\text{SIC}}^i(\mathbf{r})$. This is to say that the Hartree-Fock Hamiltonian is free of the self-interaction. Note also that the term $V_{\text{x}}^i(\mathbf{r})$ is always negative, which leads to a lower total energy energy than in the Hartree approximation. Thus, the Hartree-Fock approximation is better than the Hartree one. It improves the electron density, and it binds atoms into molecules and solids. However, this binding is usually too weak [20]. The deficiency stems from the fact that electrons are still treated independently, by neglecting their correlation, which is of course incorrect.

2.4.2.1 Koopmans' theorem

In order to make use of the variational principle, taking into account the normalization condition, we introduced the Lagrange multipliers ε_i. These quantities have a dimension of energy as one can see from the Hartree-Fock equations (2.29), but do they have a physical meaning? To answer this question let us calculate the required energy to remove an electron from a given orbital k

$$E^N - E_k^{N-1} = \langle\varphi|\,\hat{\mathcal{H}}\,|\varphi\rangle - \left\langle\varphi_k^{N-1}\right|\hat{\mathcal{H}}_k^{N-1}\left|\varphi_k^{N-1}\right\rangle, \tag{2.32}$$

where E_k^{N-1}, and φ_k^{N-1} is the energy and the wavefunction of the system respectively, after removing an electron from an orbital k, and

$$\hat{\mathcal{H}}_k^{N-1} = \sum_{i \neq k} \hat{H}_1(i) + \frac{1}{2} \sum_{\substack{i \neq j \\ i,j \neq k}} \hat{V}_{ee}(i,j). \tag{2.33}$$

To evaluate this difference , we first make the following assumptions:

- the wavefunction of the system, φ, is a single Slater determinant.
- removing the k-th electron has no effect on the orbitals of other electrons.

Clearly, these are approximations. In principle, the many-body wavefunction is not a single Slater determinant, and the removal of one electron will affect the entire system, and so the orbitals would not be the same. By considering these approximations, the wavefunction φ_k^{N-1} is then obtained by omitting the k-th row and the k-th column of the Slater determinant. This yields

$$\begin{aligned} E_k^N - E_k^{N-1} &= \langle \phi_k | \left[\frac{-\nabla^2}{2} + V_{\text{ext}}(\mathbf{r}) + V_{\text{Hartree}}(\mathbf{r}) + V_{\text{x}}^k(\mathbf{r}) \right] | \phi_k \rangle \\ &= \varepsilon_k. \end{aligned} \tag{2.34}$$

So the meaning of the eigenvalue ε_k is the energy required to remove an electron from orbital k. This result is known as Koopmans' theorem [22].

2.5 Exchange and correlation

Electrons are interacting particles and it is difficult to describe them within an independent-particle picture. Indeed, the Hartree-Fock approximation succeeded to capture a very important effect, known as the exchange, but it ignores another effect resulting from the electrostatic correlation of electrons. This correlation effect is essential in the description of electrons; together with the exchange, they make a sort of *glue* that binds atoms together to form molecules and solids [20].

In the case of the Hartree-Fock approximation, the exchange effect leads to a term that lowers the total energy. The physical picture of this term lies in the Pauli principle. It implies that the region surrounding each electron is depleted from any electron with the same quantum number, which creates a positive *exchange hole*. The same thing happens in the case of correlation because of the electrostatic repulsion, which gives rise to a *correlation hole.* In order to give a more quantitative aspect to the exchange and correlation holes, it is convenient to work with the joint probability, $n(\mathbf{r}, \mathbf{r}')$, of finding two electrons at the point $\mathbf{r}$ and $\mathbf{r}'$

$$n(\mathbf{r}, \mathbf{r}') = \int d\mathbf{r}_3 ... \, d\mathbf{r}_N |\varphi(\mathbf{r}, \mathbf{r}', ..., \mathbf{r}_N)|^2, \tag{2.35}$$

which can be seen as a sum of the joint probability of uncorrelated electrons and an extra term $\Delta n(\mathbf{r}, \mathbf{r}')$

$$n(\mathbf{r}, \mathbf{r}') = n(\mathbf{r})n(\mathbf{r}') + \Delta n(\mathbf{r}, \mathbf{r}'), \tag{2.36}$$

where $\Delta n(\mathbf{r}, \mathbf{r}')$ is a measure of the interdependence of the electrons, which vanishes in case of independent electrons. This term can be written as

$$\Delta n(\mathbf{r}, \mathbf{r}') = n(\mathbf{r})n_{\mathrm{xc}}(\mathbf{r}, \mathbf{r}'), \tag{2.37}$$

where $n_{\mathrm{xc}}(\mathbf{r}, \mathbf{r}')$ is the exchange correlation hole, which can be expressed as a sum of an exchange and a correlation hole

$$n_{\mathrm{xc}}(\mathbf{r}, \mathbf{r}') = n_{\mathrm{x}}(\mathbf{r}, \mathbf{r}') + n_{\mathrm{c}}(\mathbf{r}, \mathbf{r}'). \tag{2.38}$$

There are at least two exact constraints on the exchange hole, $n_{\mathrm{x}}(\mathbf{r}, \mathbf{r}')$: (i) it is always negative, and (ii) the integral of $n_{\mathrm{x}}(\mathbf{r}, \mathbf{r}')$ over $\mathbf{r}'$ yields[4] -1. The correlation hole, instead, must integrate to zero, which means that it just redistributes the hole's density.

Similarly to the exchange, the correlation energy is always negative for the ground state [23].

In conclusion, exchange and correlation are essential physical contributions to the interacting electrons system. Their importance was highlighted thanks to Hartree and Hartree-Fock theory. To improve these approximations further, it is critical to accurately describe the exchange and correlation effects. The theory that made a further improvement and revolutionized the field of electronic structure came in 1964 [5]. It can also be formulated using an independent-particle picture, but it includes the exchange correlation effects in a smart way, making an in principle exact theory.

2.6 Density Functional Theory

The wavefunction is a powerful fundamental quantity, and once it is known all the properties of the system follow. However, it is too complicated to deal with, since it depends on the position and the spin of each electron of the system, which leads to a huge number of degrees of freedom. In addition to that, the wavefunction does not have a clear physical interpretation and it is not interesting for itself. What makes it interesting is the fact that all observables are expectation values of the wavefunction. This implies an integration over all its variables. Therefore the wavefunction is a kind of an *intermediate* object that reveals to us what we want to know about the system with too much cost. Thus, one can ask whether there is another optimized way to calculate the observables, without passing by the wavefunction. In fact, if we

[4] This is a consequence of the Pauli exclusion principle.

compute the Hartree energy we get

$$\left\langle \hat{V}_{\text{Hartree}} \right\rangle = \frac{1}{2} \int d\mathbf{r} d\mathbf{r}' \frac{n(\mathbf{r}) n(\mathbf{r}')}{|\mathbf{r} - \mathbf{r}'|}, \tag{2.39}$$

which means that the only needed quantity here is the electronic density. However, this is no longer obvious when it comes to the kinetic energy

$$\left\langle \hat{T}_e \right\rangle = -\frac{1}{2} \sum_i \int d\mathbf{r}_1 ... d\mathbf{r}_N \varphi^*(\mathbf{r}_1, \mathbf{r}_2, .., \mathbf{r}_N) \nabla_i^2 \varphi(\mathbf{r}_1, \mathbf{r}_2, .., \mathbf{r}_N). \tag{2.40}$$

Thomas-Fermi theory [24, 25] was the first attempt to change the paradigm by giving an approximation to the kinetic energy in terms of the density. The approximation consists in replacing the homogeneous density in the kinetic energy function of the homogeneous electron gas (HEG) by the local density of the system. This yields the following functional for the total energy:

$$E^{\text{TF}}[n] = C \int d\mathbf{r} n(\mathbf{r})^{5/3} + \frac{1}{2} \int d\mathbf{r} d\mathbf{r}' \frac{n(\mathbf{r}) n(\mathbf{r}')}{|\mathbf{r} - \mathbf{r}'|} + \int n(\mathbf{r}) V_{\text{ext}}(\mathbf{r}), \tag{2.41}$$

with $C = \frac{3}{10}(3\pi^2)^{2/3}$. In order to find the ground state density, the Thomas-Fermi functional (2.41) must be minimized with respect to $n(\mathbf{r})$, and subject to the constraint that the number of electrons is conserved $\int d\mathbf{r} n(\mathbf{r}) = N$. This approach yields good approximations for the density and the total energy of an atom, but it turns out to be very rough for molecules and solids [26, 27, 28]. This shortcoming is due to two main factors:

- Using a very simple approximation for the kinetic energy, which represents a significant portion of the total energy, and so even a small error has an important impact on the result.
- Treating the electrons interaction classically in the functional (2.41), and so a very important term is missed, which is the exchange and correlation energy, as discussed in Sec. 2.4.2.

In 1964, Hohenberg and Kohn [5] confirmed the usefulness of using the ground-state density instead of the many-body wavefunction. Most importantly, they proved that it is the the sufficient information to know all the ground-state observables. This breakthrough led to an in principle exact theory known as Density functional theory (DFT), with approximations in practice, which makes electronic structure calculations much faster without sacrificing too much the accuracy.

2.6.1 The Hohenberg-Kohn theorem

Hohenberg and Kohn (HK) [5] formulated and proved the following two theorems, which provide a strong mathematical foundation for the development of modern DFT methods:

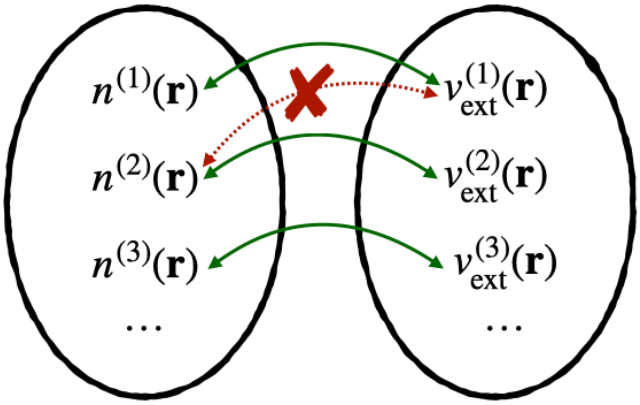

FIGURE 2.1: One-to-one mapping between the density and the external potential.

HK theorem I: Proof of existence the external potential $V_{\text{ext}}(\mathbf{r})$ is, up to a constant, a unique functional of the density $n(\mathbf{r})$; since, in turn $V_{\text{ext}}(\mathbf{r})$ defines the many-body Hamiltonian $\hat{\mathcal{H}}$, then the full many-body state is a unique functional of $n(\mathbf{r})$.

HK theorem II: Variational principle The ground-state energy functional has a minimum at the exact ground state density $n(\mathbf{r})$.

In other words, the first theorem states that there is one-to-one mapping between the density and the wavefunction. In fact, if we know the wavefunction then it is evident, from the definition of the density (2.14), that it is well defined. Now, our goal is to prove the opposite. For the sake of simplicity, let us first assume that the ground state is non-degenerate. Then we suppose that we have two different external potentials $V_{\text{ext}}(\mathbf{r})$ and $V'_{\text{ext}}(\mathbf{r}')$ where

$$V_{\text{ext}}(\mathbf{r}) - V'_{\text{ext}}(\mathbf{r}) \neq constant. \tag{2.42}$$

The two potentials define two different Hamiltonians, $\hat{\mathcal{H}}$ and $\hat{\mathcal{H}}'$, which have two different ground-state wavefunctions, φ and φ'. Let us now assume that φ and φ' have the same ground-state density $n(\mathbf{r})$, this yields

$$E_0 = \langle\varphi|\,\hat{\mathcal{H}}\,|\varphi\rangle < \langle\varphi'|\,\hat{\mathcal{H}}\,|\varphi'\rangle = \langle\varphi'|\,\hat{\mathcal{H}}' - \sum_i V'_{\text{ext}}(\mathbf{r}_i) + \sum_i V_{\text{ext}}(\mathbf{r}_i)\,|\varphi'\rangle\,, \tag{2.43}$$

from which it follows

$$E_0 < E'_0 + \langle\varphi'|\sum_i \left[V_{\text{ext}}(\mathbf{r}_i) - V'_{\text{ext}}(\mathbf{r}_i)\right]|\varphi'\rangle\,, \tag{2.44}$$

or

$$E_0 < E'_0 + \int d\mathbf{r}\left[V_{\text{ext}}(\mathbf{r}) - V'_{\text{ext}}(\mathbf{r})\right] n(\mathbf{r}). \tag{2.45}$$

Similarly for $E_0' = \langle \varphi' | \hat{\mathcal{H}}' | \varphi' \rangle$ we obtain

$$E_0' < E_0 - \int d\mathbf{r} \left[V_{\text{ext}}(\mathbf{r}) - V_{\text{ext}}'(\mathbf{r}) \right] n(\mathbf{r}) \tag{2.46}$$

Now we sum the right and left hand side of (2.44) and (2.46), and we get

$$E_0 + E_0' < E_0 + E_0', \tag{2.47}$$

which is a contradiction. Hence, we have proved by *reductio ad absurdum* that two different ground-state wavefunctions cannot yield the same ground-state density. In conclusion we have demonstrated that there is a one-to-one correspondence between the ground-state wavefunction and the density.

The first Hohenberg-Kohn theorem implies that the expectation value of any physical observable of the system is a unique functional of the ground-state density $n(\mathbf{r})$. Therefore, the total ground-state energy is a functional of the density, and it can be written as

$$E_v[n] = F[n] + \int d\mathbf{r} n(\mathbf{r}) V_{\text{ext}}(\mathbf{r}), \tag{2.48}$$

where $F[n]$ is a universal functional for any many-electrons system. The subscript v denotes that the functional of the energy is well defined, once the external potential is fixed. Since there is a bijection between the wavefunction and the density, one can reformulate the variational principle to be a search for the density that minimizes $E_v[n]$, keeping the number of electrons fixed. This is the second HK theorem.

The Hohenberg-Kohn theorems establish the uniqueness of the density-potential, they do not give access neither to the density $n(\mathbf{r})$, nor to the energy functional $E_v[n]$. This may seem useless from a practical point of view. In any case, these theorems gave birth to an in principle exact theory, which is a very useful as a guideline to build and improve approximations. Putting this together with the fact that an important portion of $F[n]$ is accessible from Hartree theory, namely the Hartree energy, these facts are probably the major motivation that fueled the search to make DFT practical. This goal was achieved thanks to the Kohn-Sham method.

2.6.2 Kohn-Sham approach

DFT is the most widely used method to study interacting electrons. The credit for its success goes largely to the Kohn-Sham (KS) approach [29]. The idea of this approach is similar to Hartree and Hartree-Fock theory. It consists of using the independent-particle picture to calculate properties of the interacting system. While in the Hartree-Fock approximation one uses the wavefunction as fundamental variable to calculate observables, the Hohenberg-Kohn theorem has proved that a three dimensional function, namely the density $n(\mathbf{r})$, is sufficient to know *everything* about the system. In the Kohn-Sham approach, the density is used as the fundamental variable, and instead of using an independent-particle system to construct the wavefunction, it is used

to calculate the exact density of the interacting system

$$n(\mathbf{r}) = \sum_i |\phi_i(\mathbf{r})|^2, \tag{2.49}$$

where $\phi_i(\mathbf{r})$ are the orbitals of the independent-particle system, which is called the *auxiliary system*.

In addition, Kohn and Sham suggested to re-write the total energy functional (2.48) as follows

$$E_{\mathrm{KS}}[n] = T_s[n] + \int d\mathbf{r} n(\mathbf{r}) V_{\mathrm{ext}}(\mathbf{r}) + E_{\mathrm{Hartree}}[n] + E_{\mathrm{xc}}[n], \tag{2.50}$$

with $T_s[n]$ is the kinetic energy functional of the non-interacting system, which can be calculated as :

$$T_s[n] = \sum_i \langle \phi_i | -\frac{\nabla_i^2}{2} | \phi_i \rangle , \tag{2.51}$$

and $E_{\mathrm{Hartree}}[n]$ is the Hartree energy functional given in (2.39). The last term, $E_{xc}[n]$, encompasses the exchange correlation effects. Equation (2.50) reflects the genius of the Kohn-Sham approach for two reasons:

- First, it explicitly separates out the non-interacting kinetic energy, which is very useful since we have learned from Thomas-Fermi theory that it is particularly important to approximate the kinetic energy as accurately as possible.
- Second, it encodes all the unkown interacting information in the exchange correlation functional, $E_{\mathrm{xc}}[n]$, which represents a small part of the energy. This term does not have the same quantitative definition as in the case of Hartree-Fock theory, but it describes the same qualitative effect.

Note that it is not obvious in (2.51) that $T_s[n]$ is a functional of the density; but this becomes clear, if we apply the HK theorem to the non-interacting system.

Now, we need to determine the non-interacting system. In order to do so, we make use of the variational principle and we minimize the KS functional (2.50) subject to a normalization constraint. Since T_s is expressed as a functional of the orbitals, it is more convenient to vary $E_{\mathrm{KS}}[n]$ with respect to $\phi_i^*(\mathbf{r})$. This yields

$$\begin{aligned} \frac{\delta E_{\mathrm{KS}}}{\delta \phi_i^*(\mathbf{r})} &= \frac{\delta T_s}{\delta \phi_i^*(\mathbf{r})} + \int d\mathbf{r}' \frac{\delta \left\{ \int d\mathbf{r}'' n(\mathbf{r}'') V_{\mathrm{ext}}(\mathbf{r}'') + E_{\mathrm{Hartree}}[n] + E_{\mathrm{xc}}[n] \right\}}{\delta n(\mathbf{r}')} \frac{\delta n(\mathbf{r}')}{\delta \phi_i^*(\mathbf{r})} \\ &= \frac{\delta T_s}{\delta \phi_i^*(\mathbf{r})} + \int d\mathbf{r}' V_{\mathrm{KS}}(\mathbf{r}') \frac{\delta n(\mathbf{r}')}{\delta \phi_i^*(\mathbf{r})}, \end{aligned} \tag{2.52}$$

where $V_{\mathrm{KS}}(\mathbf{r}')$ is called the Kohn-Sham potential. Using the expressions of $n(\mathbf{r})$ and T_s given in (2.49) and (2.51) respectively, we get

$$\frac{\delta T_s}{\delta \phi_i^*(\mathbf{r})} = -\frac{1}{2}\nabla^2 \phi_i(\mathbf{r}) \quad \text{and} \quad \frac{\delta n(\mathbf{r}')}{\delta \phi_i^*(\mathbf{r})} = \phi_i(\mathbf{r}')\delta(\mathbf{r}-\mathbf{r}'). \tag{2.53}$$

Now we introduce the Lagrange multipliers, ε_i, to take into account the orthonormalization constraints

$$\int d\mathbf{r}\phi_i^*(\mathbf{r})\phi_j(\mathbf{r}) = \delta_{i,j}, \tag{2.54}$$

and it follows

$$\left\{-\frac{1}{2}\nabla^2 + V_{\mathrm{KS}}(\mathbf{r})\right\}\phi_i(\mathbf{r}) = \varepsilon_i \phi_i(\mathbf{r}). \tag{2.55}$$

Hence, we obtained single-electron equations, which are known as Kohn-Sham equations. They are self-consistent equations, since the term $V_{\mathrm{KS}}(\mathbf{r})$ requires the density as an input. The KS potential represents an effective local potential acting on an electron at point $\mathbf{r}$. Being local is a very useful feature of this potential, since it extremely simplifies the calculations.

From (2.52) we can see that $V_{\mathrm{KS}}(\mathbf{r}, [n])$ is a functional derivative of density functionals, and so it is a functional of the density, it reads

$$V_{\mathrm{KS}}(\mathbf{r}, [n]) = V_{\mathrm{ext}}(\mathbf{r}) + V_{\mathrm{Hartree}}(\mathbf{r}, [n]) + v_{xc}(\mathbf{r}, [n]), \tag{2.56}$$

where $V_{\mathrm{ext}}(\mathbf{r})$ is the external potential that defines the system and fixes the non-universal part of the energy functional. The term $V_{\mathrm{Hartree}}(\mathbf{r}, [n])$ refers to the Hartree potential defined previously in (2.27), and $v_{\mathrm{xc}}(\mathbf{r}, [n])$ is the exchange correlation (xc) potential. It is the unknown part in the KS potential, that is not accessible in any practical way and must be approximated. The approximation of the xc potential is critical in DFT since it determines the quality of the estimated density and total energy.

2.6.2.1 Local density approximation

The first approximation that has been considered for the exchange correlation potential was proposed by Kohn and Sham in their original paper [29]. They suggested to consider a system with slowly varying density[5] locally as a homogeneous electron gas (HEG), and so one can write

$$E_{\mathrm{xc}}^{\mathrm{LDA}}[n] = \int d\mathbf{r} n(\mathbf{r})\epsilon_{\mathrm{xc}}(n(\mathbf{r})), \tag{2.57}$$

where $\epsilon_{\mathrm{xc}}(n = n(\mathbf{r}))$ in a point $\mathbf{r}$ is the exchange-correlation energy per particle of a HEG with constant density $n = n(\mathbf{r})$. It can be viewed as the sum of an exchange and correlation contribution

$$\epsilon_{\mathrm{xc}}(n) = \epsilon_{\mathrm{x}}(n) + \epsilon_{\mathrm{c}}(n). \tag{2.58}$$

[5] Kohn and Shame defined the regime of slowly varying density by the conditions $r_s/r \ll 1$, where r_s is the Wigner Seitz radius, and r_0 is a typical length over which there is a noticeable change in the density

The exchange term, $\epsilon_x(n)$, commonly called *Dirac exchange* [30], is known exactly: it reads

$$\epsilon_x(n) = \frac{-3}{4}\left(\frac{3n}{\pi}\right)^{1/3}. \tag{2.59}$$

For the correlation part, $\epsilon_c(n)$, there is no exact analytical expression. Nevertheless, this term has been calculated in the HEG to a near-exact accuracy with Quantum Monte Carlo (QMC) methods by Ceperley and Alder [31]. These calculations proved to be extremely useful in developing approximations for the xc potential, which were critical in making DFT practical. One of the widely used parametrization of the QMC results was established by Perdew and Zunger [32]. It reads

$$\epsilon_c(r_s) = \begin{cases} -0.0480 + 0.0311\ln(r_s) - 0.0116 r_s + 0.0020 r_s \ln(r_s), & \text{for } r_s < 1 \\ -0.1423/(1 + 1.0529\sqrt{r_s} + 0.3334 r_s), & \text{for } r_s > 1, \end{cases} \tag{2.60}$$

with $r_s = (4\pi n/3)^{-1/3}$. The local density approximation (LDA) for the xc potential is the functional derivative of (2.57), which can be written as

$$v_{xc}^h(\mathbf{r}) = \epsilon_{xc}(n(\mathbf{r})) + n(\mathbf{r})\left.\frac{d\epsilon_{xc}(n)}{dn}\right|_{n=n(\mathbf{r})}. \tag{2.61}$$

The basic idea of the LDA is then to estimate the xc potential of an inhomogeneous system by using at each point $\mathbf{r}$ the results of a HEG with homogeneous density equal to the local density $n(\mathbf{r})$ of the inhomogeneous system, as illustrated in Fig. 2.2. This approximation is reasonable for a system where the density varies slowly, but this condition is not always satisfied in practice. However, the LDA is surprisingly efficient: it yields fairly good description of bulk solids and their surfaces [33]. Its application covers even very inhomogeneous systems like atoms and molecules. This success was justified later by the fact that LDA satisfies several exact constraints, and especially the sum rule on the xc hole [34]. In general, the LDA works well when the physics of the system is nearsighted [35], i.e., an effect at $\mathbf{r}'$ beyond a certain distance does not significantly influence the physics at point $\mathbf{r}$. It is worth noting that LDA is the basis of most modern exchange-correlation functionals.

2.6.2.2 Generalized Gradient approximation

The largest source of error in the LDA comes from the exchange energy, which is often underestimated, while the correlation energy is often overestimated even though, in absolute value, its contribution to the total energy is smaller [23]. These two errors tend to cancel each other. To improve the accuracy of DFT calculations, we need better approximations for the exchange-correlation functional. Some attempts [36] were based on the idea of defining a functional of the local density $n(\mathbf{r})$ and the magnitude of its gradient

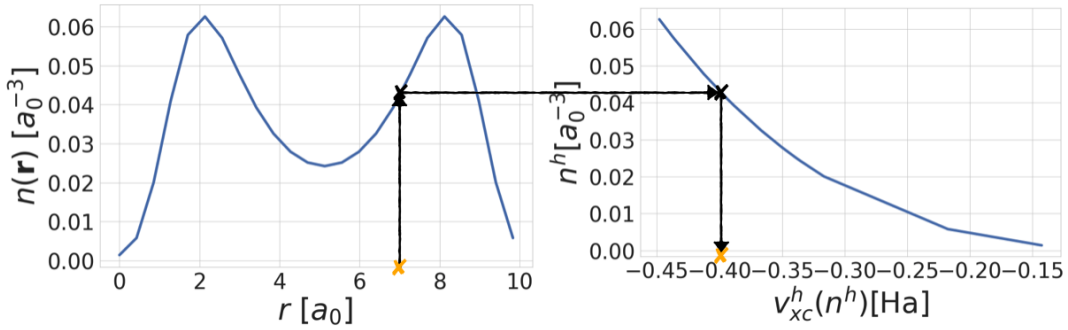

FIGURE 2.2: LDA scheme. On the left we have the density of silicon along direction (100). On the right we have the xc potential of the HEG, v_{xc}^h, as a function of the homogeneous density n^h. To estimate the xc potential at point $\mathbf{r}$ we read the density $n(\mathbf{r})$, then we approximate the value of $v_{\text{xc}}(\mathbf{r})$ for silicon by $v_{\text{xc}}^h(n(\mathbf{r}))$.

$|\nabla n(\mathbf{r})|$ in order to take into account the inhomogeneity of the system. In order to obtain this kind of functionals, the LDA is treated as the first term of a Taylor series development, then the exchange-correlation energy is expanded in terms of the gradients of the density [37, 38]. This form of functionals is known as the Gradient Expansion Approximation (GEA). Unfortunately, this gives worse results than the LDA. Indeed, the xc hole no longer satisfies the conditions [39] which ensured that LDA has some physical sense. In order to correct these problems, the GEA functionals have been modified to make them respect some desired properties in the limit of large gradient. This led to the Generalized Gradient Approximation (GGA), which contributed significantly to the success of DFT [23]. The form of this functional can be written as

$$E_{\text{xc}}^{\text{GGA}}[n] = \int d\mathbf{r} n(\mathbf{r}) \epsilon_{\text{x}}(n(\mathbf{r})) F_{\text{xc}}(n(\mathbf{r}), |\nabla n(\mathbf{r})|), \tag{2.62}$$

with F_{xc} is the xc enhancement factor. Often the contributions for exchange and correlation are developed separately:

$$F_{\text{xc}}\left(n(\mathbf{r}), |\nabla n(\mathbf{r})|\right) = F_{\text{x}}\left(n(\mathbf{r}), |\nabla n(\mathbf{r})|\right) + F_{\text{c}}\left(n(\mathbf{r}), |\nabla n(\mathbf{r})|\right). \tag{2.63}$$

There are numerous forms for the enhancement factors proposed by Becke [40], and Perdew and coworkers [41, 42, 43]. They constructed these factors in a non-empirical way by imposing as many exact constraints as possible on the xc functional. Among the non-empirical GGA functionals, here we present the Perdew, Burke and Ernzerhof (PBE) functional [44] which is one of the most remarkable and successful ones.

The exchange enhancement factor for PBE is given by

$$F_x = 1 + \kappa - \frac{\kappa}{1 + \beta\pi^2 s(\mathbf{r})^2/3\kappa}, \tag{2.64}$$

with $\kappa = 0.804$, $\beta = 0.066725$, and $s(\mathbf{r})$ is the dimensionless reduced density gradient defined as

$$s(\mathbf{r}) = \frac{|\nabla n(\mathbf{r})|}{2n(\mathbf{r})k_F(\mathbf{r})}, \tag{2.65}$$

where $k_F(\mathbf{r})$ is the Fermi wavevector associated to the local density $n(\mathbf{r})$, which is related to the density as $k_F(\mathbf{r}) = \left(3\pi^2 n(\mathbf{r})\right)^{1/3}$.

For the correlation part, we have

$$F_c = \frac{1}{\epsilon_x(n(\mathbf{r}))}\left[\epsilon_c(n(\mathbf{r})) + \gamma \ln\left\{1 + \frac{\left(1 + At^2\right)\beta t^2/\gamma}{1 + At^2 + A^2t^4}\right\}\right], \tag{2.66}$$

where $t = |\nabla n(\mathbf{r})|/2k_s(\mathbf{r})n(\mathbf{r})$, with the Thomas-Fermi screening wave number $k_s(\mathbf{r}) = \sqrt{4k_F(\mathbf{r})/\pi}$, $\gamma = 0.031091$, and

$$A = \frac{\beta/\gamma}{\exp\left[-\epsilon_c(n(\mathbf{r}))/\gamma\right] - 1}. \tag{2.67}$$

Compared to the LDA, the computational cost of PBE is modestly higher, but it yields more accurate results for the exchange and correlation energies of atoms and for the atomization energies of molecules and solids.

Finally, in order to obtain the xc potential of the GGA functional, one has to calculate the functional derivative of (2.62). This derivative is not straightforward as in case of LDA, but there are different approaches [23] to handle it.

2.6.2.3 Hybrid functionals

Another class of approximations for the xc potential consists of using the Hartree-Fock method to add the exact exchange energy part, or the exact exchange hole, while the correlation part is calculated using DFT approximated functional, e.g., LDA, non-empirical or empirical GGA functionals. This class of approximations is called "hybrid functionals". They were first introduced by Becke [45] and have since undergone many improvements [46, 47]. They are often used by going beyond the Kohn-Sham scheme with its local potential to a generalized Kohn-Sham (GKS) scheme [48, 49], where the potential is non-local, similar to Hartree-Fock. This changes the nature of the auxiliary system and is the reason for the fact that one finds in general band gaps closer to the measured ones. This improvement comes with high increase in computing cost.

2.7 One-body reduced density matrix

So far we have discussed two extreme approaches to calculate observables of a real system. The first one is based approximating the wavefunction, which is sufficient to obtain a comprehensive description of the system, but it is highly challenging to approximate. The second one is DFT, which tells

us that all the physical properties of the system are functionals of the density, however there is no systematic way to determine these functionals. So the fewer details we calculate, the more it becomes difficult to express observables. This suggests to look for a compromise: one could try to build functionals of an intermediate object between the wavefunction and the density, in order to directly access more observables and at the same time avoid the challenge of storing functions that depend on a larger number of electron coordinates.

In particular, instead of using the wavefunction, on can consider the density matrix, $\Gamma^{(N)}$, which conceptually plays the same role as the wavefunction since it encodes all of the system's information. It is defined as follows:

$$\Gamma^{(N)}\left(\mathbf{r}_1,\ldots,\mathbf{r}_N;\mathbf{r}'_1,\ldots,\mathbf{r}'_N\right) \equiv N!\varphi^*\left(\mathbf{r}'_1,\ldots,\mathbf{r}'_N\right)\varphi\left(\mathbf{r}_1,\ldots,\mathbf{r}_N\right). \tag{2.68}$$

The n-body reduced density matrix (n-RDM) is then obtained as

$$\begin{aligned}\Gamma^{(n)}\left(\mathbf{r}_1,\ldots,\mathbf{r}_n;\mathbf{r}'_1,\ldots,\mathbf{x}'_n\right) =& \frac{N!}{(N-n)!}\int d\mathbf{r}_{n+1}\ldots d\mathbf{r}_N\varphi^*\left(\mathbf{r}'_1,\ldots,\mathbf{r}'_n,\mathbf{r}_{n+1},\ldots,\mathbf{r}_N\right)\\ &\times\varphi\left(\mathbf{r}_1,\ldots,\mathbf{r}_n,\mathbf{r}_{n+1},\ldots,\mathbf{r}_N\right).\end{aligned} \tag{2.69}$$

For the one-body reduced density matrix (1-RDM) $\gamma \equiv \Gamma^{(1)}$, the expression reduces to

$$\gamma\left(\mathbf{r},\mathbf{r}'\right) = N\int d\mathbf{r}_2\ldots d\mathbf{r}_N\varphi^*\left(\mathbf{r}',\mathbf{r}_2,\ldots,\mathbf{r}_N\right)\varphi\left(\mathbf{r},\mathbf{r}_2,\ldots,\mathbf{r}_N\right). \tag{2.70}$$

By definition, the diagonal elements of the 1-RDM yield the density

$$n(\mathbf{r}) = \gamma(\mathbf{r},\mathbf{r}) = N\int d\mathbf{r}_2\ldots d\mathbf{r}_N\varphi^*\left(\mathbf{r},\mathbf{r}_2,\ldots,\mathbf{r}_N\right)\varphi\left(\mathbf{r},\mathbf{r}_2,\ldots,\mathbf{r}_N\right), \tag{2.71}$$

and their sum is normalized to the number of electrons

$$\mathrm{Tr}\,\gamma\left(\mathbf{r},\mathbf{r}'\right) \equiv \int d\mathbf{r}\gamma(\mathbf{r},\mathbf{r}) = N. \tag{2.72}$$

As one can see from (2.70), the 1-RDM provides us with additional non-local information about the system while maintaining a manageable storage size.

2.7.1 Observables as functional of the 1-RDM

The Gilbert extension [12] of the Hohenberg-Kohn theorem states that there is one-to-one mapping between the 1-RDM and the ground-state wavefunction, which means that any observable can in principle be expressed as functional of the 1-RDM. If the observable has a bi-local operator, it can be cast explicitly as

$$O[\gamma] = \int d\mathbf{r}d\mathbf{r}'\hat{O}(\mathbf{r},\mathbf{r}')\gamma(\mathbf{r},\mathbf{r}'). \tag{2.73}$$

This allows us to write the entire kinetic energy functional as

$$T[\gamma] = -\frac{1}{2}\int d\mathbf{r}'\nabla^2\,\gamma(\mathbf{r},\mathbf{r}')\Big|_{\mathbf{r}=\mathbf{r}'}. \tag{2.74}$$

The exchange energy is also accessible using the 1-RDM: it reads

$$E_{\mathrm{x}}[\gamma] = -\frac{1}{2}\int d\mathbf{r}'d\mathbf{r}\frac{\gamma(\mathbf{r}',\mathbf{r})\gamma(\mathbf{r},\mathbf{r}')}{|\mathbf{r}-\mathbf{r}'|}. \tag{2.75}$$

Trivially, the Hartree energy can be expressed using the 1-RDM since we know its explicit functional in terms of the density. The only unknown term of the total energy is the correlation energy, which still needs to be approximated in this case. The correlation energy is typically very small compared to other terms. However, it is important, and is difficult to find in RDMFT. One remarkable approximation to E_{xc} is given by Müller [50]. Thus, the 1-RDM provides access to the biggest part of the total energy. In practice, the 1-RDM, for the ground state, is determined via minimization of the total energy functional, subject to the constraint that it is ensemble N-representable [12, 51].

As in DFT we have to find the functionals and the density, in RDMFT we also have to find the RDM functionals and the 1-RDM. In a later chapter, I will try to find an approximation for the functional $\gamma[n]$.

Chapter 3

Connector theory

In physics, modeling plays a central role to explain real phenomenons. It consists of generating physical representations that approximate a real system in order to understand and predict its behavior. Clearly, the simpler this representation, the more accurate we can calculate the quantities that we are interested in. In this thesis we call a model a simple system that can be described with high precision. Very often, this kind of systems are far from reality and connection to real materials is needed. To illustrate this point, let us take an example. Suppose that we want to calculate the frequency, ω_p, of a plasmon in a simple semiconductor like silicon. This quantity can be expressed by a simple formula for the homogeneous electron gas (HEG). In atomic units, it reads

$$\omega_p^h = \sqrt{4\pi n_h},$$

where n_h is the homogeneous density of the gas. To make use of this formula, one can use the HEG as model for the material by substituting n_h by the average density of the material $\bar{n}$. The resulting plasmon frequency is

$$\omega_p = \sqrt{4\pi \bar{n}}.$$

In silicon $\bar{n} = 0.0296\ a_0^{-3}$ and the resulting ω_p is 16.6 eV, which is a fairly good estimate of the experimental value 16.8 eV [52]. This approximate description can be turned into a new question: how to choose the density n_h in order to optimize the approximation of the real plasmon frequency ω_p, or even to get the exact value? This question can be generalized for any quantity that we want to import from a model. In this chapter we will answer the general question by a prescription termed connector theory. I will keep the discussion very general to be valid for any quantity of interest. I describe the general ideas of the theory and I set the conditions that must be fulfilled in order to use it. Then, in the next chapters I will discuss the application of the connector theory to approximate the charge density and related quantities like the exchange correlation potential and the density matrix.

3.1 The idea of connector

Here we first start by introducing the idea of the connector in a simple example where we know all quantities. The aim of using that example is to give a

concrete description of the idea. Then, we present the general formalism of the connector theory.

3.1.1 Introductory example

Suppose that we want to calculate, for example, the Hartree potential $v_H(\mathbf{r},[n])$ of some real finite system. This quantity is known in the model system that we choose as a sphere of HEG of given radius R, characterized by the homogeneous density n_h inside the sphere, and with Hartree potential $v_R^{H,\text{sphere}}(n_h)$. A similar model has been used in [53] to construct exchange functionals. The Hartree potentials in the real and the model system read, respectively

$$v_H(\mathbf{r},[n]) = \int d\mathbf{r}' \, \frac{n(\mathbf{r}')}{|\mathbf{r}-\mathbf{r}'|} \quad \text{and} \quad v_R^{H,\text{sphere}}(n_h) = n_h \int_R d\mathbf{r}' \, \frac{\mathbf{1}}{|\mathbf{r}-\mathbf{r}'|}. \tag{3.1}$$

In a nutshell, the connector approach suggests to calculate and store the result for a series of homogeneous spheres of different densities n_h. Then, we ask the question: what is the density $n_h^c \equiv n_h$ that enables us to import the Hartree potential from the table of the model to simulate the result of a real molecule? In this example, the exact answer is the solution of the following equation

$$\int d\mathbf{r}' \, \frac{n(\mathbf{r}')}{|\mathbf{r}-\mathbf{r}'|} \;=\; n_h^c \int_R d\mathbf{r}' \, \frac{\mathbf{1}}{|\mathbf{r}-\mathbf{r}'|}. \tag{3.2}$$

This yields

$$n_h^c(\mathbf{r},[n],R) = \int d\mathbf{r}' \, \frac{n(\mathbf{r}')}{|\mathbf{r}-\mathbf{r}'|} \Big/ \int_R d\mathbf{r}' \, \frac{1}{|\mathbf{r}-\mathbf{r}'|} \tag{3.3}$$

The result, n_h^c, is a positive and real number, so it is a well defined density for the model. Knowing this exact *connector*, one could determine the exact Hartree potential from the table of model results as follows

$$v_H(\mathbf{r},[n]) = v_R^{H,\text{sphere}}(n^c(\mathbf{r},[n],R)). \tag{3.4}$$

However, the lhs of (3.2) is in principle unknown. It is the full Hartree potential of the real system that we want to approximate. As a solution to this issue, the connector scheme suggests to use equivalent approximations for $v_H(\mathbf{r},[n])$ and $v_R^{H,\text{sphere}}(n_h)$ on the left and right hand sides of (3.2). A very rough approximation is to set $\frac{1}{|\mathbf{r}-\mathbf{r}'|} \approx c'\,\delta(|\mathbf{r}-\mathbf{r}'|)$ in (3.2), and by making use of (3.4), we obtain

$$n_h^c(\mathbf{r},[n],R) = n(\mathbf{r}) \quad \text{and} \quad v_H(\mathbf{r}) \approx n(\mathbf{r}) \int_R d\mathbf{r}' \, \frac{\mathbf{1}}{|\mathbf{r}-\mathbf{r}'|}, \tag{3.5}$$

for $\mathbf{r}$ inside the sphere of radius R. This is simply the LDA, with a final result that depends on the radius R that was chosen for the model. The result does not depend on the constant factor, c', which cancels out. Instead, if we think that the interaction is so long range that it is essentially constant over some

range of interest, $\frac{1}{|\mathbf{r}-\mathbf{r}'|} \approx c''$, then we get

$$n_h^c(\mathbf{r}, [n], R) = \bar{n} \quad \text{and} \quad v_H(\mathbf{r}) \approx \bar{n} \int_R d\mathbf{r}' \, \frac{1}{|\mathbf{r} - \mathbf{r}'|}, \tag{3.6}$$

where $\bar{n}$ is the average density in the sphere. In order to see whether we have gained anything, we have to compare these two connector results with the results that we would have obtained with a similar effort, by making the same approximations *directly* on the quantities of interest. This yields for the first and second case, respectively

$$v_H(\mathbf{r}) \approx c' \, n(\mathbf{r}) \quad \text{and} \quad v_H(\mathbf{r}) \approx c'' N, \tag{3.7}$$

where N is the number of electrons in the sphere.

The comparison of these and the corresponding connector results illustrates two points. First, the connector results are stable with respect to details of the approximation (in this example, they are independent of c' or c''). Second, whereas the direct approximation screws up the results brutally, the connector results are still correct in certain regimes. For example, the first approximation is correct for $\mathbf{r}$ inside a molecule with a slowly varying charge distribution if its size is smaller than R, while in the second approximation the connector result recovers the correct long range limit far from the molecule.

To summarize, in this example we have used a new approach, termed the connector theory, to approximate the Hartree potential in a finite real system. This approach requires the knowledge of two ingredients, (i) the quantity of interest in the model, which was the Hartree potential of the HEG sphere in this example; (ii) an approximation for the quantity in the real system. In our case we obtained an approximate $v_H(\mathbf{r}, [n])$ by making $\frac{1}{|\mathbf{r}-\mathbf{r}'|} \approx c' \, \delta(|\mathbf{r} - \mathbf{r}'|)$ or $\frac{1}{|\mathbf{r}-\mathbf{r}'|} \approx c''$. The next step is to use an equivalent approximation in the model and establish a connection between the model and the real system via a connector, n_h^c in our example. Finally, we use this connector to take the real quantity from the model table, as done in (3.5) and (3.6).

3.1.2 General formalism

The connector theory is a general approach, it is not limited to a specific example. The idea can be generalized as follows: suppose that we want to calculate an observable or quantity O for real system. Generally, this quantity is a function or functional of a set of parameters or function Q, and it can depend on additional variable x, so $O = O(x; Q)$. In the example above, O is the Hartree potential $v_H(\mathbf{r}, [n])$, Q is a function: the density $n(\mathbf{r}')$ and x is the position vector $\mathbf{r}$. In most cases $O(x; Q)$ is difficult or impossible to calculate in a real material without approximations, or even unknown. However, it may be possible to calculate $O(x; Q)$ for some Q in a restricted domain: this restricted domain defines a model. For the Hartree potential example, Q is the electron density and we restrict it to homogeneous densities, the model is

a sphere of HEG. Connector theory aims at using the model results in order to simulate systems where Q lies outside the model domain. The underlying hypothesis is that not all details of the parameters that describe the real system are equally important. The aim is therefore to find, for a given real system where $Q \equiv Q^R$, another $Q \equiv Q^c$ that lies in the model domain, such that

$$O(x; Q^R) = O(x; Q^c_x). \tag{3.8}$$

Note the subscript x of Q^c_x, which indicates that Q^c is allowed to be different for every value of the argument x. Of course, it could still be impossible to fulfill equality (3.8) if one restricts the model domain too severely. However, if the model is flexible enough such that the equation can be satisfied in principle, one can try to find the one or more Q^c_x for which the equality holds. We call Q^c_x the connector.

In the following we suppose that the model is described by only one effective parameter $\mathcal{Q}$ or, when there are more parameters, we can choose one that will be used to fulfill (3.8). This restriction can be dropped, but it is often useful and we keep it here for clarity. In this case, in the model the functional or multi-dimensional function can be represented by a scalar function, $O(x; Q^c_x) \to \mathcal{O}_x(\mathcal{Q}^c_x)$. For example, in the HEG sphere the one parameter $\mathcal{Q}$ is its number density n_h, so $v_H(\mathbf{r}; [n]) \to v_R^{H,\text{sphere}}(n_h)$, where $v_R^{H,\text{sphere}}$ corresponds to $\mathcal{O}$ and n_h to $\mathcal{Q}$. Equation (3.8) is then formally solved,

$$\mathcal{Q}^c_x = \mathcal{O}_x^{-1}(O(x; Q^R)). \tag{3.9}$$

and the resulting connector Q^c_x is used to get the final result for the real system using the model,

$$O(x; Q^R) = \mathcal{O}_x(\mathcal{Q}^c_x). \tag{3.10}$$

In practice, one will tabulate $\mathcal{O}_x$, and once a connector $\mathcal{Q}^c_x$ is given, for any real system we will simply use these data instead of calculating $O(x; Q^R)$, which will make calculations extremely efficient.

In order for the method to be useful, three conditions should be fulfilled. The first is the validity of the underlying connector hypothesis:

- **[A]** On its domain of definition, $\mathcal{O}_x(\mathcal{Q}^c_x)$ must yield all values that $O(x; Q^R)$ can take on its domain, i.e., the Q^R of interest.

The Q^R which define the domain of interest depend on the range of physical systems one wants to explore; this range does not necessarily include *all possible* physical systems. The domain of O, on the other hand, defines the model system. If for certain Q^R and/or x (3.8) cannot be fulfilled, we have to change model by changing its domain, i.e. the range of allowed Q^c_x.

[**A**] is the only necessary condition, but there is also a question of uniqueness in (3.9): $\mathcal{O}^{-1}$ may require boundary conditions in order to be well defined. This is not a problem of principle, but may create difficulties for the design of approximations. We therefore require:

- **[B]** When the inverse $\mathcal{O}^{-1}$ of $\mathcal{O}$ is not unique, it should at least be possible to specify a unique choice among the possible $\mathcal{O}_i^{-1}$.

Conditions **[A]** and **[B]** settle the framework, but nothing has been gained in practice: the unknown $O(x;Q^R)$ still enters the calculation of the connector in (3.9). Therefore, for connector theory to be of practical interest we have to add:

- **[C]** The connector ansatz must suggest a strategy for approximations.

In the introductory example, we have approximated the Coulomb interaction by making $\frac{1}{|\mathbf{r}-\mathbf{r}'|} \approx c'\,\delta(|\mathbf{r}-\mathbf{r}'|)$. This has enabled us to calculate an approximation for the connector in (3.9) without knowing the full $O(x;Q^R) \equiv v_H(\mathbf{r},[n])$. This step is fundamental for the connector scheme. It suggests to make *in the calculation of the connector* (3.9) an *equivalent* approximation to O and $\mathcal{O}$,

$$\mathcal{Q}_x^{c,\mathrm{approx}} = (\mathcal{O}_x^{\mathrm{approx}})^{-1}(O^{\mathrm{approx}}(x;Q^R)). \tag{3.11}$$

The final approximate connector result is obtained as

$$O(x;Q^R) \approx O_x^c \equiv \mathcal{O}_x(\mathcal{Q}_x^{c,\mathrm{approx}}). \tag{3.12}$$

While the model observable $\mathcal{O}$ is supposed to be well known, it is important to approximate it in (3.11) in the same way as O of the real system, whereas the exact model function $\mathcal{O}$ is used in (3.12): in this way, the result becomes exact in two limits: when the approximation becomes increasingly good, even for a very restricted model, and when the domain of the model system tends towards that of the real system, even using a very rough approximation. In practice, one will not be able to perform the exact calculation, but away from these limits, using the equivalent approximation for $O^{\mathrm{approx}}(x;Q^R)$ and $\mathcal{O}_x^{\mathrm{approx}}(\mathcal{Q})$ still leads to error canceling, and the limiting behavior indicates that results can be improved in a controllable way. How far the model system can be chosen from the real system depends on the quality of the approximation, and vice versa, how rough the approximation is that one can tolerate depends on the closeness of the model and the real system. This dual dependence is a source of the power of the connector approach. It implies that the approximate connector result (3.12) is expected to be superior to the direct approximation $O^{\mathrm{approx}}(x;Q^R)$, without additional computational cost. This benefit is magnified when the model incorporates significant characteristics of the real system, such as the same Coulomb interaction as in the example above. Therefore, the primary effort and intuition in connector theory will be directed at selecting an appropriate model. In Fig. 3.1 we present a summary of the connector scheme discussed in this section.

3.2 First order connector

The approximation of the real and the model quantity shown in (3.11) is a crucial step to design a connector. One interesting and intuitive approximation is the first order expansion around a fixed function or parameter, $\mathcal{Q}_0$,

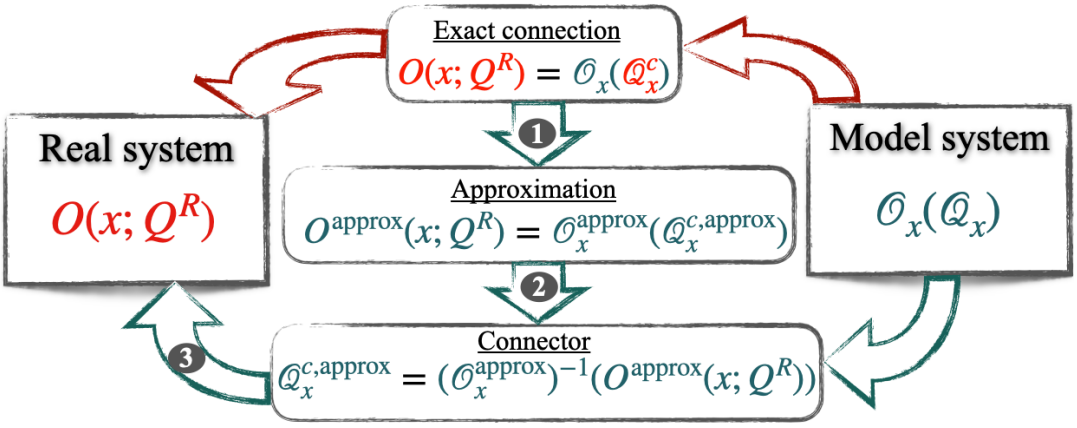

FIGURE 3.1: Summary of the connector scheme. The quantities in green are supposed to be available, while those in red are unknown. Importing the model table via the exact connection, $\mathcal{Q}_x^c$, is not possible since it requires the knowledge of $O(x;Q)$. Instead, the connector scheme suggests to approximate, equivalently, the right and left hand sides of the exact connection equation. Then, we invert the resulting equation to get $\mathcal{Q}_x^{c,\text{approx}}$. Finally, we use this connector to import the model table and approximate the real quantity as $O(x;Q^R) \approx \mathcal{O}_x(\mathcal{O}_x^{c,\text{approx}})$.

from the domain that defines the model. This approximation yields the so-called, first order connector. It reads

$$\mathcal{Q}_x^{c,\text{approx}} = \frac{\int dx' w(x,x') Q^R(x')}{\int dx' w(x',x)}, \tag{3.13}$$

where

$$w(x,x') \equiv \left.\frac{\delta \mathcal{O}(x;Q)}{\delta Q(x'))}\right|_{Q=\mathcal{Q}_0}. \tag{3.14}$$

We can interpret this first order connector as follows: in order to use the model table effectively, we need an amount of information about the physics of the real system. This information is contained in Q, and it is selected by the weight w linearly. In the next chapters we will mainly use this connector to test the theory.

3.2.1 Features of this connector

In order to design the first order connector for a quantity O we need two ingredients

- Table of $\mathcal{O}$ in the model system.
- Linear response, w, of O evaluated in the model system.

By construction, this connector guarantees :

- The zero-order term of the quantity O expansion, $O(x;Q)\big|_{Q=\mathcal{Q}_0}$, provided that the model is a limit case of the real system.

- The exact first-order term that results from expanding the real Q around a particular point, which we call the reference point.

Then, the connector extrapolates the higher-order terms of O. The quality of this extrapolation depends, mainly, on the error cancellation, which is the reason why the connector approximation can go beyond the linear approximation. Physically, it depends on how well the model reflects properties of the real system.

3.2.2 Optimizing the reference point

In general, the quality of the connector approximation depends also on the reference point of the expansion. An optimized choice can improve the quality of the connector in this situation. The choice of the reference point can be based on physical intuition or on a more systematic method like using the known exact constraints or minimizing a cost function that makes a compromise between the desired constraints.

3.3 High order connector or other approximations

While the first order expansion is one possibility for approximating the connector, it is not the only one. To improve the connector approximation, we may use higher order expansions. This is particularly useful for inhomogeneous systems such as molecules. Another feasible approximation is to approximate the Coulomb interaction's long range behavior or to make use of the single electron case, which we will do in the chapter about the density matrix. A more promising way to improve the connector approximations, however, is to tabulate new inhomogeneous models that go beyond the HEG.

Chapter 4

The exchange correlation potential

In Kohn-Sham (KS) density functional theory (DFT) [29], the exchange correlation (xc) potential, $v_{\text{xc}}(\mathbf{r}, [n])$, is a central quantity that needs to be approximated. A lot of of work has been invested in order to give an accurate approximation to the xc potential. One famous approximation to v_{xc} is the local density approximation (LDA) which was proposed from the very beginning by Kohn and Sham. It suggests to see the real system locally as a homogeneous electron gas (HEG) with a density, n^h, equal to the local density of the real system. The xc potential is then approximated as

$$v_{\text{xc}}(\mathbf{r}, [n]) = v^h_{\text{xc}}\left(n^h = n(\mathbf{r})\right),$$

where $v^h_{\text{xc}}(n^h)$ is the xc potential of the HEG at density n^h. This function can be derived from the xc energy per particle of the HEG, which is available thanks to an analytical parameterization based on quantum Monte Carlo (QMC) calculations [31, 32]. Using the LDA for the v_{xc}, the KS-DFT becomes a practical method that gives a remarkably realistic description of bulk solids and their surfaces. However, the LDA showed many shortcomings. For example, it fails in predicting the image potential [54], it does not accurately describe the dissociation of molecules [55] and it is less reliable in the case of localized electron charge [56]. These shortcomings and other motivated the search for reliable xc potential functionals beyond the LDA, which is still a subject of intense research (see e.g. [57, 58, 59, 60, 61, 62, 39, 63, 44, 64, 65, 66, 67]). The aim of this chapter is to use the connector theory to design a new density functional for the xc potential, and to explain in which way it leads to an improvement with respect to the LDA.

Let us first analyze the LDA from a connector point of view. The LDA uses the HEG as a model system in which the correlation energy has been calculated once for all using QMC. The HEG's results are then reused indefinitely. This is a tremendous benefit and it is one of the most important reason for the early success of DFT. In order to use these results in the real system, the LDA proposes the local density as a connector. This suggestion is based on Kohn's intuition of nearsightedness [29, 68, 35], where the xc potential at point $\mathbf{r}$ is not influenced by any change of the density at point $\mathbf{r}'$ different from $\mathbf{r}$. This hypothesis leads to a simple connector that allows us to use the HEG results for any system. However, it provides no guidance on how to optimize the model's use in a systematic way. Instead, this guidance is

provided by the connector scheme discussed in the previous chapter. Here, as in LDA, I will use the HEG to simulate the xc potential in a real system. However, the connector will not be the local density but it will be based on a first order expansion of the exact connection between the model and the real system. I will design a non local approximation and I will explain how to improve it systematically. The Ch. 6 will be dedicated to examine the quality of the connector approximation of the xc potential by looking at the resulting density.

4.1 Exact connector

In order to design improvable approximations, it is very useful to start from an in principle exact solution that represents the objective that we are heading for. This is the first step of the connector scheme, Fig. 3.1. In the case of the xc potential with the HEG as a model system, we are looking for a homogeneous density $n^c_{\mathbf{r}}$ that makes $v^h_{xc}(n^c_{\mathbf{r}})$ equal to the xc potential of the real material in each point $\mathbf{r}$. This is equivalent to looking for the exact connector from condition (3.10), which reads in this case

$$v_{\rm xc}(\mathbf{r},[n]) = v^h_{\rm xc}(n^c_{\mathbf{r}}). \tag{4.1}$$

Note that $n^c_{\mathbf{r}}$ is a homogeneous density, the subscript $\mathbf{r}$ indicates that at each point $\mathbf{r}$, where we want to calculate the xc potential, we may choose a different homogeneous density $n^h \equiv n^c_{\mathbf{r}}$ for the HEG. This flexibility is crucial, because otherwise the exact condition (4.1) could not be fulfilled. In this way, instead, all $v_{\rm xc}$ of real systems can be reached as long as they are negative, as the HEG spans all negative values, so condition [A] is fulfilled. It should be noted that the condition will often be fulfilled straight away, but there could be exceptions. In particular, if one is interested, for example, in the dissociation of linear molecules, one must be aware of the fact that the correlation contribution of these one-dimensional systems leads to a positive bump in $v_{\rm xc}(\mathbf{r})$, see, e.g., [69, 70, 71, 72, 73] whereas the exchange-correlation potential in the HEG is always negative. Therefore, if one wants to use the HEG to simulate these systems, additional action, such as an extension of the domain, would be required to fulfill condition [A]. In what follows, we assume the $v_{\rm xc}$ of real systems is always negative, which is the most common case. The exact connector is the solution of (4.1), which reads

$$n^c_{\mathbf{r}} = (v^h_{\rm xc})^{-1}(v_{\rm xc}(\mathbf{r},[n])). \tag{4.2}$$

Indeed, we gain nothing from this equation in practice. We have just moved the problem from looking for the $v_{\rm xc}(\mathbf{r},[n])$ to the search of the connector $n^c_{\mathbf{r}}$. However, this connector serves as the objective that we seek to achieve in order to optimize the use of the model results. Once the model is chosen, the next step that turns the connector theory into a useful tool is to apply an equivalent approximation to both sides of (4.1). This allows us to invert the equation and obtain an approximate connector. It should be noted that

a very rough approximation can yield a very good connector, which is close to the exact one. This is due to the error cancellation that may occur when we generalize, i.e., we plug in the exact function of the HEG, the connector obtained at the approximation level.

4.2 Using the first order connector

Our goal now is to find an approximate connector, for which (3.11) reads

$$n_{\mathbf{r}}^{c,\text{approx}} = (v_{\text{xc}}^{h,\text{approx}})^{-1}(v_{\text{xc}}^{\text{approx}}(\mathbf{r},[n])) \,. \tag{4.3}$$

One interesting $n_{\mathbf{r}}^{c,\text{approx}}$ is the first order connector presented in the last chapter. This means we use a first order expansion of the v_{xc} around a given homogeneous density n_0 [29, 74] and use this approximation in the connector scheme, as shown in Fig. 4.1, to derive a new functional.

Using a first-order expansion as approximation in (4.1) yields:

$$\int d\mathbf{r}'(n(\mathbf{r}') - n_0) f_{\text{xc}}(|\mathbf{r}-\mathbf{r}'|, n_0) = (n_{\mathbf{r}}^{c,\text{approx}} - n_0) f_{\text{xc}}^h(n_0), \tag{4.4}$$

where $f_{\text{xc}}(|\mathbf{r}-\mathbf{r}'|, n_0) = \delta v_{\text{xc}}(\mathbf{r},[n])/\delta n(\mathbf{r}')|_{n=n_0}$ is the static nonlocal xc kernel of the HEG with density n_0, and $f_{\text{xc}}^h(n_0) = dv_{\text{xc}}^h(n_h)/dn_h\big|_{n_h=n_0}$ is its limit of zero wavevector, which corresponds to the case where variations are restricted such that the density remains homogeneous, i.e., we remain within the parameter space given by the model. The zeroth order term $v_{\text{xc}}^h(n_0)$ cancels on both sides. Finally, inverting the equation we get the approximate connector

$$n_{\mathbf{r}}^{c,\text{approx}}([n]) = \frac{1}{f_{\text{xc}}^h(n_0)} \int d\mathbf{r}' \; n(\mathbf{r}') f_{\text{xc}}(|\mathbf{r}-\mathbf{r}'|, n_0). \tag{4.5}$$

For a density of the real system that varies slowly with respect to variations of the f_{xc} we can take out the density from the integral and the connector yields the LDA, which is exact in this limit [29]. For a very quickly varying density in a periodic system the connector yields the mean density, as one would expect, and which is instead completely missed by the LDA. The approximate connector interpolates between these two limits: it displays the degree of nearsightedness of the xc potential, which is given by

$$v_{\text{xc}}^c(\mathbf{r},[n]) = v_{\text{xc}}^h\left(n^h = n_{\mathbf{r}}^{c,\text{approx}}([n])\right). \tag{4.6}$$

This equation is equivalent to (3.12). The functional $v_{xc}^c(\mathbf{r},[n])$ is non-local, i.e., a variation of the density at point $\mathbf{r}'$ different from $\mathbf{r}$ influences the connector xc potential at point $\mathbf{r}$. However, the impact of this variation depends on the distance between the two points, $|\mathbf{r}-\mathbf{r}'|$, and it is averaged by the xc kernel of the HEG, $f_{\text{xc}}(|\mathbf{r}-\mathbf{r}'|, n_0)$. The latter has been computed using QMC calculations [75], and a parametrization of the results is available [76]. This

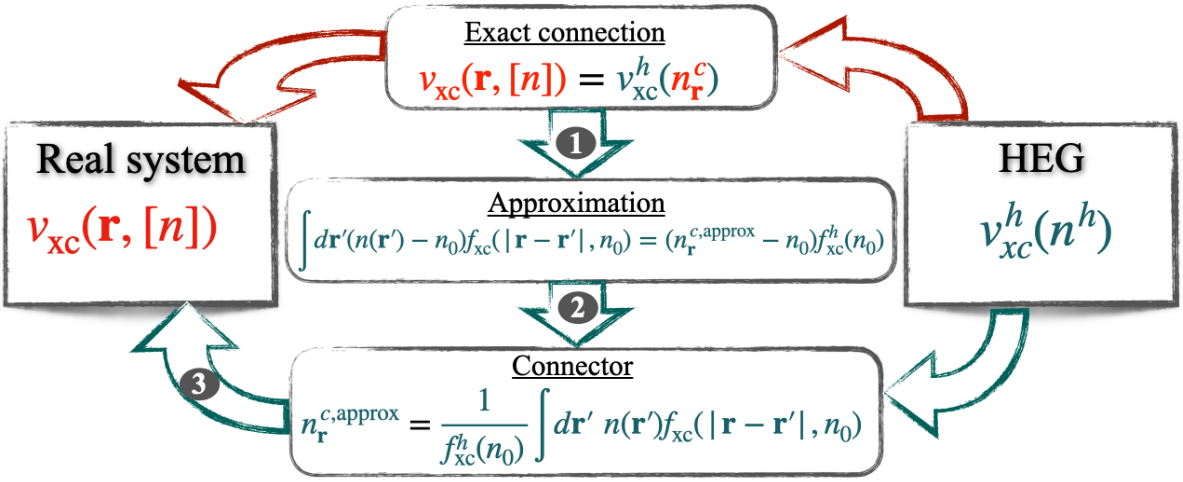

FIGURE 4.1: Connector scheme for the xc potential. The quantities in green are available, while those in red are unknown. The exact connector $n^c_{\mathbf{r}}$ is unknown. In order to get an approximate connector, we the linear expansion in the right and left hand sides of the exact connection equation. Then, we invert the resulting equation to get $n^{c,\text{approx}}_{\mathbf{r}}$. Finally, we use this connector in the function v^h_{xc} to import the xc potential of the HEG that approximates the real quantity at each point $\mathbf{r}$.

means that, similarly to the LDA, one can in principle benefit from high-level calculations performed once and for all in the model.

The connector approximation is not yet well defined, because the linear approximation in (4.4) depends on the homogeneous density n_0 around which we expand. This reference density may be chosen to be a different one for every point $\mathbf{r}$ where we calculate the potential. The following sections will examine several possible choices for n_0.

4.3 The reference density of the expansion

Here, we discuss two ways to select the density at which we evaluate the first order expansion. The first way relies on physical intuitions to determine which density best represents the real system at each point $\mathbf{r}$. The second way is to define the optimal reference density as the one that fulfills the maximum number of exact constraints on the xc potential.

4.3.1 Intuitive choices

Here we presents four intuitive and remarkable choices for n_0, which will be tested in Ch. 6.

4.3.1.1 Mean density

One of the simplest choice to the reference density n_0 is the mean density. With this n_0 the linear approximation can work well for a system with a density that oscillate about its mean. In practice, this means at each iteration of the KS-loop we take $n_0 = \frac{1}{V}\int d\mathbf{r} n(\mathbf{r})$, where V is the volume of the finite system or the unit cell in a periodic system, and $n(\mathbf{r})$ is the output density in that iteration.

4.3.1.2 Local density

One may think that the most important physics of the system is nearsighted and so use the local density to evaluate the xc kernel in (4.5). This yields $n_0 = n(\mathbf{r})$, note here that n_0 is different for each point $\mathbf{r}$. In the next chapter we will use this choice in the connector to approximate a target functional and compare the results to those obtained via direct linear approximation and LDA.

4.3.1.3 Symmetric choice with an equivalent one in the model

As we can see in (4.5), the xc kernel, $f_{xc}(|\mathbf{r}-\mathbf{r}'|, n_0)$, depends on the distance between two points, $\mathbf{r}$ and $\mathbf{r}'$. In order to specify the density, n_0, we can make an analogy with LDA and consider the xc kernel to be bi-nearsighted. Then we take the average of the density at the two points to get $n_0 = \frac{n(\mathbf{r})+n(\mathbf{r}')}{2}$ [77]. This choice of n_0 is not suitable for the macroscopic xc kernel, $f^h_{xc}(n_0)$, which stems from approximating the model. In fact if $n(\mathbf{r})$ represents the density of the real inhomogeneous system, then $n(\mathbf{r}')$ will not find a meaning in $f^h_{xc}(n_0)$. As a solution to that and for the sake of approximating the model and the real system in an equivalent way, we use the following reference density for the model: $n_0^{\text{model}} = \frac{n(\mathbf{r})+n_{\mathbf{r}}^{c,\text{approx}}}{2}$. At the end we get for the connector

$$n_{\mathbf{r}}^{c,\text{approx}} = \frac{1}{f_{xc}\left(\frac{n(\mathbf{r})+n_{\mathbf{r}}^{c,\text{approx}}}{2}\right)} \int d\mathbf{r}' f_{xc}\left(|\mathbf{r}-\mathbf{r}'|, \frac{n(\mathbf{r})+n(\mathbf{r}')}{2}\right) n(\mathbf{r}'). \quad (4.7)$$

This is a self-consistent equation, so to solve it numerically, we pick a first guess for the connector $n_{\mathbf{r}}^{c,\text{approx}}$ and we keep iterating until convergence.

4.3.1.4 Self consistent connector

If we have a functional of the density, its linear approximation should be exact at the density where we perform the expansion. And it should approximate the functional around this reference density relatively well. In our case, we want to design a connector, $n_{\mathbf{r}}^{c,\text{approx}}$, that makes the $v^h_{xc}(n_{\mathbf{r}}^{c,\text{approx}})$ very close to the real functional. At the same time, we have $v^h_{xc}(n_0)$ which appears as the zero-order term of the linear expansion. If we want this term to be close to the real functional, $v_{xc}([n], \mathbf{r})$, for any density $[n]$, we should set

n_0 to be equal to the connector density, $n_0 = n_{\mathbf{r}}^{c,\text{approx}}$, because it is designed for this purpose. This leads to a self-consistent connector.

Another way to obtain the self-consistent connector is to look for the density n_0 that makes the first order term of the expansion vanish. This means

$$\int d\mathbf{r}' f_{\text{xc}}(|\mathbf{r}-\mathbf{r}'|, n_0)(n(\mathbf{r}') - n_0) = 0. \tag{4.8}$$

Solving this equation for n_0 we re-find $n_0 = n_{\mathbf{r}}^{c,\text{approx}}$. To use this connector in practice we start from an initial guess for n_0 then we update n_0 as follows

$$n_0^{k+1} = \frac{1}{f_{\text{xc}}(n_0^k)} \int d\mathbf{r}' f_{xc}(|\mathbf{r}-\mathbf{r}'|, n_0^k) n(\mathbf{r}'), \tag{4.9}$$

where k labels the iterations. After sufficient iterations, n_0^k converge to a specific homogeneous density and so the value of n_0 is no longer arbitrary.

4.3.2 Using exact constraints

Another way to fix the reference density, n_0, can be to use exact constraints on the xc potential, which is a strategy that can successfully lead to the development of new functionals [66]. Suppose that n_0 is a functional of the density, so it can be written as

$$n_0 = \int d\mathbf{r}' n(\mathbf{r}') g([n], \mathbf{r}, \mathbf{r}'), \tag{4.10}$$

where $g([n], \mathbf{r}, \mathbf{r}')$ is a functional that can depend on the density or not. In the limit where the density $n(\mathbf{r})$ tends to a homogeneous density $\bar{n}$, i.e., the real system becomes equal to the HEG model, the connector (4.5) should tend to the same density $\bar{n}$. This implies $n_0 \to \bar{n}$, and so:

$$\int d\mathbf{r}' g(\bar{n}, \mathbf{r}, \mathbf{r}') = 1. \tag{4.11}$$

This condition is satisfied by all the reference density choices discussed in the previous section. In order to make a further step one can choose an ansatz for $g([n], \mathbf{r}, \mathbf{r}')$, a normalized Gaussian weight for example, and tune its parameters to satisfy the zero force theorem [78, 79]. This theorem reflects the fact that interaction among particles cannot generate a net force, it can be written as:

$$\int d\mathbf{r} n(\mathbf{r}) \nabla v_{xc}(\mathbf{r}, [n]) = 0, \tag{4.12}$$

and so in our case

$$\int d\mathbf{r} n(\mathbf{r}) \nabla v_{xc}^h(n_{\mathbf{r}}^{c,\text{approx}}[n]) = 0. \tag{4.13}$$

In practice, the parameters that define $g([n], \mathbf{r}, \mathbf{r}')$ can be different for each material, they are determined numerically, which makes it easier to satisfy (4.13). For additional constraints, one can define a cost function and minimize it to satisfy as many constraints as possible.

The use of exact constraints can be an interesting strategy to fix the reference density. I have not yet used it in the practical applications, but more analysis is planned for future work. In the present thesis I have explored the performance of the intuitive choices described in 4.3.1.

4.4 Separation of the exchange and correlation contributions

In DFT, the majority of the approximate xc functionals are constructed by summing separately the exchange and correlation components. Separating the exchange component from the full functional can be useful, since exact relations exist for exchange under uniform density and spin scaling. Using connector theory, we can also separate $v_{\rm xc}(\mathbf{r})$ into two contributions, e.g., $v_{\rm x}(\mathbf{r}) + v_{\rm c}(\mathbf{r})$, and design distinct connectors for each contribution. This means that, for the systems of interest, we suppose that condition **[A]** of Ch. 2 can be met, and thus an exact connector exists in principle, for both pieces. This would mean that

$$\begin{aligned} v_{\rm x}(\mathbf{r}) &= v_{\rm x}^h(n^c_{\mathbf{r},{\rm x}}) \\ v_{\rm c}(\mathbf{r}) &= v_{\rm c}^h(n^c_{\mathbf{r},{\rm c}})\,, \end{aligned} \tag{4.14}$$

where $n^c_{\mathbf{r},{\rm x}}$and $n^c_{\mathbf{r},{\rm c}}$ are the exact connector for the exchange and correlation potentials, respectively. In this case, the first order connector for the exchange (correlation) is obtained by substituting the xc kernel, f_{xc}, in (4.5) exclusively by the exchange (correlation) kernel. One way to extract this exchange (correlation) kernel from the Corradini's one [76] is to exclude terms generated from the correlation (exchange) contributions. The same separation technique was used for another xc kernel in [80].

The exchange and correlation contributions can then be easily separated in the connector approach. However, it is useful to clarify some points. According to (4.14), each contribution is calculated with its own connector in principle, and there is no reason to suppose the connector that reproduces exactly the exchange contribution, $n^c_{\mathbf{r},{\rm x}} = (v_{\rm x}^h)^{-1}(v_{\rm x}(\mathbf{r};[n]))$, to be the same as the exact connector for the correlation contribution $n^c_{\mathbf{r},{\rm c}} = (v_{\rm c}^h)^{-1}(v_{\rm c}(\mathbf{r};[n]))$, nor to equal the xc connector, $n^c_{\mathbf{r}}$. As a consequence, even when a consistent approximation, such as the linear expansion, is chosen for all pieces, most often also the approximate connectors will be different. This is a general remark about dividing an object of interest into two or more contributions; it is not specific to the separation presented here or to $v_{\rm xc}$. This kind of separation can be used to improve results: suppose that the individual contributions are of quite different nature, for example, that they exhibit a different degree of nearsightedness or naturally suggest a perturbation expansion in a different parameter, or around a different zero order. This would allow one to find a more accurate approximation for each contribution on its own and hence also to improve the final result in many cases. Even when it is not advantageous, however, the fact that connectors are in principle different for every piece of

interest has to be kept in mind whenever one is interested, for some reason, in the individual pieces: when the connector n^c is designed to approximate the sum, it is possible that some single pieces are not well described. This is not a failure of the connector approximation, but of the way it is applied.

4.5 Gradient correction

The first order connector can work well for periodic systems but is probably less accurately for an atom, because this real system is far from the model, which is the HEG. For this reasons I followed the reasoning done in [38] to derive an explicit gradient correction to the connector xc potential defined in (4.6). I obtained the expression

$$v_{\mathrm{xc}}([n],\mathbf{r}) = v^c_{\mathrm{xc}}([n],\mathbf{r}) - \alpha_1 \delta n(\mathbf{r}) \nabla^2_{\mathbf{r}} n(\mathbf{r}) + (\alpha_1 - \frac{\alpha_2}{2}) |\nabla_{\mathbf{r}} n(\mathbf{r})|^2 \qquad (4.15)$$

where α_1 and α_2 are coefficients related to the functional derivatives of the xc potential, and they are numerically available. The detailed derivation of (4.15) and the expressions of α_1 and α_2 are given in the appendix A. For weakly varying density, the expression above goes back to the original first order connector result.

To summarize, in this chapter I have developed a non-local functional for the xc potential based on connector theory. The free parameter of this functional can be chosen and optimized using nearsightedness arguments and/or exact constraints. In practice, this functional can be used to calculate the charge density of materials using the self-consistent Kohn-Sham equation. Additionally, a gradient correction to the connector functional has been proposed. I have implemented and tested the gradient corrected expression for model cases, with results that are promising in some respects but not conclusive. In the present work, I concentrate on the straightforward linear expansion and the question of the starting point of the expansion.

Chapter 5

Approximating a non-local functional

In the previous chapter, I proposed an approximate functional for the xc potential using connector theory. The next natural step is to evaluate the quality of the resulting functional. Since the exact functional is unknown, it is not possible to make a direct comparison. The alternative is to investigate the charge density that is created by the connector potential for given materials. This requires the implementation of the connector approximation in a DFT-code and use it in a self consistent cycle to obtain the density. Of course, this is an interesting topic and I will discuss it in the next chapter. However, this study is technically demanding, so I thought it would be better to start first with an analytical study for a toy system before jumping to real materials.

We know that the xc potential is a non-local density functional. If the connector approximation works for an arbitrary density functional, it is likely to work for the *true* xc potential as well. That is why I decided to take an established non-local functional as target and investigate the performance of the connector approximation on it. In principle, any functional can be the target, but to increase the likelihood of the result's transferability, I picked a non-local xc potential functional based on a weighted density approximation.

In the following, I will start by presenting the target functional and explain how it is constructed. Then, I will study two distinct connector descriptions for the target functional. The first one is obtained by using an approximation of the Coulomb interaction in the connector scheme. The second description is obtained thanks to the first order connector. The connector results will be compared to direct approximations[1] in order to estimate error cancellation and emphasize the improvement made by connector theory. Finally, I will consider the question of treating the exchange and correlation contributions separately by constructing a connector for each part. A summary of the results of this chapter can be found in [81].

[1] A *direct approximation* means the one that yields an approximation for the quantity of interest without using the model. The result of this approximation is denoted by $O^{\text{approx}}(x; Q^R)$ in the connector scheme illustrated in Fig. 3.1. It can be a linear expansion or any other approximation.

5.1 Target functional

We choose as target functional an expression based on a weighted density approximation (WDA) of the xc hole n_{xc} [57, 58, 59, 60], with the weight function proposed in [61]. The xc energy reads:

$$E_{xc}^{WDA}[n] = \int d\mathbf{r}d\mathbf{r}' \frac{n(\mathbf{r})n(\mathbf{r}')}{2|\mathbf{r}'-\mathbf{r}|} C(\tilde{n}(\mathbf{r},\mathbf{r}'))\left(1 - e^{\frac{-\lambda(\tilde{n}(\mathbf{r},\mathbf{r}'))}{|\mathbf{r}-\mathbf{r}'|^5}}\right), \tag{5.1}$$

with $\tilde{n}(\mathbf{r},\mathbf{r}') = [n(\mathbf{r}) + n(\mathbf{r}')]/2$ [82]. The functions C and λ, which depend on $\tilde{n}$, are determined by making E_{xc} exact in the HEG limit, i.e.,

$$\lim_{[n]\to\bar{n}} \int \frac{n(\mathbf{r}')}{2|\mathbf{r}'-\mathbf{r}|} C(\tilde{n}(\mathbf{r},\mathbf{r}'))\left(1 - e^{\frac{-\lambda(\tilde{n}(\mathbf{r},\mathbf{r}'))}{|\mathbf{r}-\mathbf{r}'|^5}}\right) = \epsilon_{xc}(\bar{n}), \tag{5.2}$$

and by ensuring the validity of the xc hole sum rule, which reads

$$\int d\mathbf{r}' n_{xc}(\mathbf{r}, \mathbf{r}'-\mathbf{r}) = -1. \tag{5.3}$$

By taking the functional derivative of E_{xc}^{WDA} with respect to the density, we obtain the exchange-correlation potential v_{xc}^{WDA} given in the appendix (B.2), as well as the functions C and λ (B.1). This potential is the target functional that we want to reproduce. We should emphasize here that our purpose is to compare the connector functional to the target one, not to analyze the quality of the density produced by each potential.

As a "real" system, we choose a toy example for solids with periodic inhomogeneous density, $n(\mathbf{r}) = A\cos(\mathbf{a}\cdot\mathbf{r}) + B$, that depends on the parameters A and B, and the reciprocal lattice vector $\mathbf{a}$ which determines the speed of variation of the density. In the following, the density parameters are chosen so that the maximum density and $\mathbf{a}$ correspond to the case of solid argon. For the connector scheme, we will use the HEG as a model.

5.2 Connector from approximating the Coulomb interaction

The target functional v_{xc}^{WDA} depends explicitly on the Coulomb interaction, as we can see in (B.2). This enables us to design connectors based on approximations of the Coulomb interaction itself. A first rough approximation could be to cut the Coulomb interaction $1/r$ beyond a short distance $r = r_c$, without renormalizing the remaining short-range part of the interaction. Because v_{xc}^{WDA} entirely arises from the Coulomb interaction, removing a significant part of the interaction reduces the potential, and even makes it vanish with the cutoff radius $r_c \to 0$. This means that the cutoff-Coulomb approximation applied directly to the system of interest completely suppresses the xc potential and is therefore a very bad approximation. For the case of the connector, the same approximation is applied to the xc potential of the HEG,

$v_{\rm xc}^h(n^h) \equiv v_{\rm xc}^{\rm WDA}(\mathbf{r}, n^h)$. The approximate connector is then obtained by solving

$$v_{\rm xc}^{h,\rm approx}(n_{\mathbf{r}}^{c,\rm approx}) = v_{\rm xc}^{\rm WDA,approx}(\mathbf{r}, [n]) \tag{5.4}$$

By decreasing the radius r_c, the density in (B.2) becomes slowly varying between the integration limits, for a given point $\mathbf{r}$. The right hand side of (5.4) therefore tends to $v_{\rm xc}^{h,\rm approx}(n(\mathbf{r}))$ and $n_{\mathbf{r}}^{c,\rm approx} \to n(\mathbf{r})$. Thus, the connector result, $v_{\rm xc}^h\left(n^h = n_{\mathbf{r}}^{c,\rm approx}\right)$, tends to LDA. This means that the connector does not apply the previous approximation globally to the potential, but only to how the potential in a given point "sees" the environment, limiting it, for $r_c \to 0$, to the environment close to the point $\mathbf{r}$ where the potential is calculated. We can therefore expect a much more meaningful result than what one would obtain by using the approximation directly in the system of interest, namely here, $v_{\rm xc} \approx 0$.

In Fig. 5.1 we show the target potential $v_{\rm xc}^{\rm WDA}$ for our toy system. We also show the resulting potential obtained when the Coulomb interaction $1/r$ is truncated beyond a very short distance $r_c = 0.1a_0$ where a_0 is the Bohr radius, less than 2% of the unit cell length. Applying this approximation directly to $v_{\rm xc}^{\rm WDA}$ yields a nearly vanishing xc potential, as shown in the figure and as expected. The result of the connector using the same approximation shows a huge improvement over the direct approximation. It does not tend towards zero but to the LDA which gives a much better description of the target. As explained above, this is thanks to the use of the model to simulate the real system and the error cancellation due to the connector construction. Therefore, the LDA can be seen as a prototype illustration of the power of the connector theory in this example.

Nevertheless, the LDA description is not perfect: it has large errors, especially in low-density regions. From the point of view of the connector, this is due to the crude approximation to the Coulomb interaction. In principle, we can fix this inaccuracy by increasing the range of the Coulomb interaction and thus systematically approaching the exact result. However, this approximation would be of limited practical interest.

5.3 Results of first order connector

The first order connector is a general and practical approximated connector. It can be used for any quantity as shown in (3.13). In the last chapter, we have derived this connector, (4.5), in order to build an approximate functional for the unknown xc potential. Here, we want to test this connector by reproducing $v_{\rm xc}^{\rm WDA}$. Before using (4.5), we must adapt it to the target functional, the xc kernel $f_{\rm xc}$ has to be consistent with the $v_{\rm xc}$ that one is heading for. Therefore, for this test we should not use expressions for $f_{\rm xc}$ given in the literature, but we have to calculate the functional derivative of our target xc potential, and evaluate it at the constant density n_0. The resulting $f_{\rm xc}^{\rm WDA}$ can be found in the Appendix, B.3.

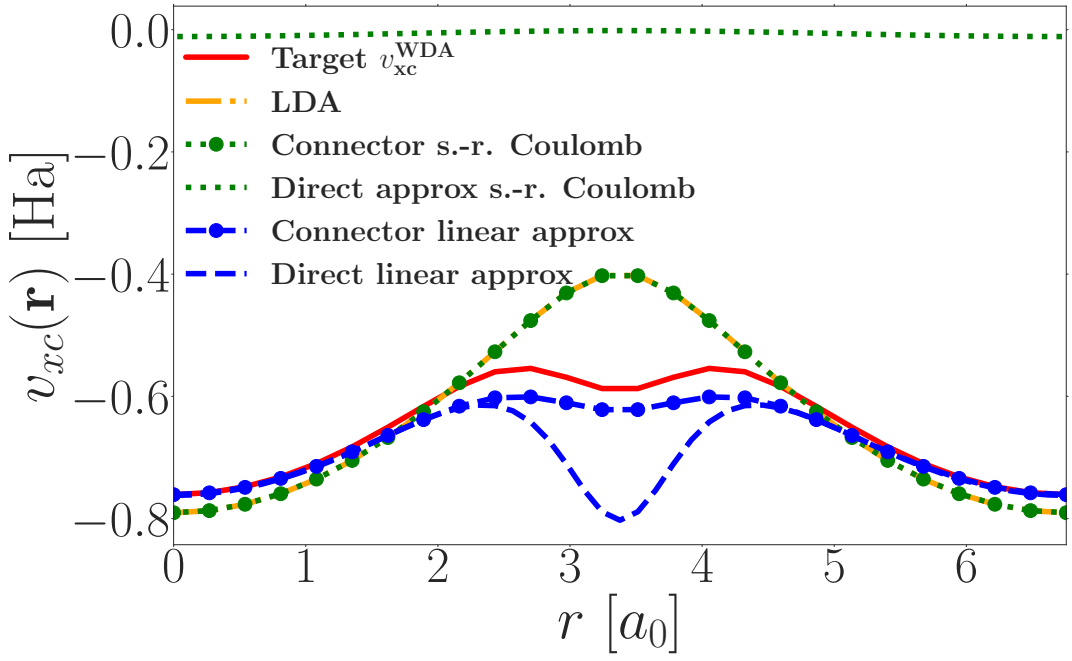

FIGURE 5.1: Target $v_{\mathrm{xc}}^{\mathrm{WDA}}(\mathbf{r})$ (red line), and approximations, for a system with periodic density. Coulomb cutoff at short-range (s.-r.): direct approximation (dotted green) and used in COT (dotted green with filled circles); linear expansion: direct approximation (blue dashed) and used in COT (blue dashed with filled circles); LDA (yellow line). Minimum and maximum densities are 0.0402 a_0^{-3} and 0.3776 a_0^{-3}, reciprocal lattice vector $a = 0.93\ a_0^{-1}$. Note that regions of high and low density can be deduced by looking at $v_{\mathrm{xc}}^{\mathrm{LDA}}$, which is a monotoneous function of $n(\mathbf{r})$.

As discussed in the previous chapter, there are several possibilities for the homogeneous density n_0 around which we expand. This density can be chosen differently for every point $\mathbf{r}$ at which we calculate the potential. To focus on the improvement over the LDA, we choose the local density $n(\mathbf{r})$ for n_0. This means that the direct approximation is a first-order expansion around the LDA.

Let us begin by analyzing the performance of the linear approximation itself, applied directly to the potential without using the connector scheme. The comparison in Fig. 5.1 demonstrates that the WDA potential is well described by the direct linear approximation in regions of high density (large $|v_{\mathrm{xc}}^{\mathrm{WDA}}|$), but not in the low density regions.

We now move on to connector results, and first investigate the connector density $n_{\mathbf{r}}^c$ given by (4.5) and shown in Fig. 5.2 for the same periodic system. The connector density that yields the LDA is simply the density itself, which has its minimum at the center of the unit cell. The exact connector spans a smaller range of values than the local density, confirming that it is an effective density, suitably averaged over a range around the local density. It is far

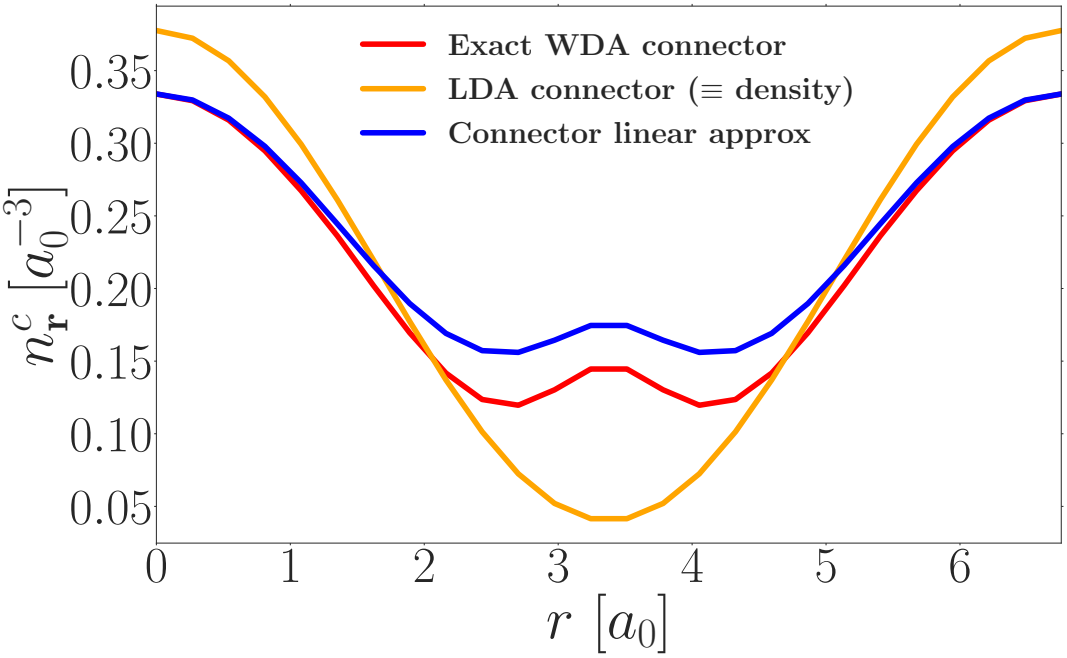

FIGURE 5.2: Target exact connector (red line), connector based on a linear expansion in the density as given by 4.5 (blue line), and the density itself, corresponding to the local density approximation connector (yellow line), for the periodic system of Fig. 5.1.

from trivial, even in this simple system: where the density is very low, the exact connector shows a bump, which is a feature that is not easy to guess. One may explain this by the fact that the system is more far-sighted in regions of low density, which mixes in more of the higher densities in the present system, and by the non-monotonous distance dependence of effective interactions, such as $f_{\mathrm{xc}}^{\mathrm{WDA}}$. This effect is very well captured by the approximate connector density, with a remaining disagreement that is much smaller than the error of the LDA.

Finally, Fig. 5.1 shows the xc potential produced by the first order connector. It gives by far the best result when compared to all approximations, illustrating the fact that the connector (4.5) takes into account a significant amount of non-locality. It shows that, by employing exactly the same linear expansion via the connector scheme, strong improvement is obtained, without additional cost.

Because the connector tends to the LDA when the density varies slowly, the improvement over LDA is especially significant when the density varies rapidly; however, some improvement is also seen in the case of more slowly varying density, i.e, when **a** is smaller, as illustrated in Fig. 5.3. The figure also shows how the connector result approaches the LDA, which in turn tends to the exact result, when the density approaches the homogeneous limit.

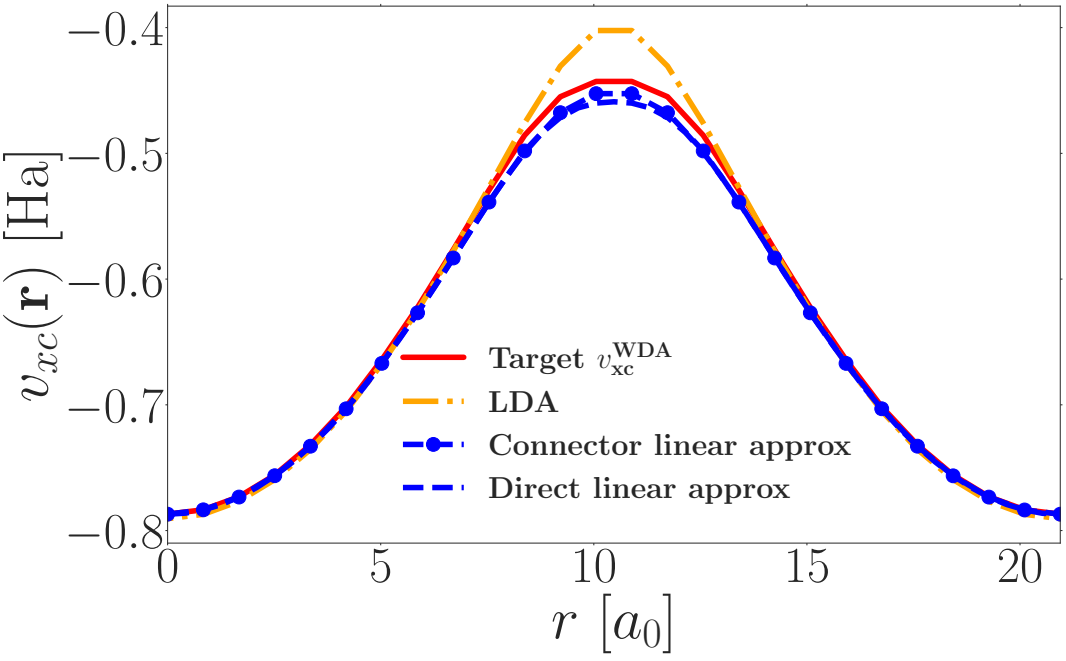

FIGURE 5.3: Comparison between the target WDA xc potential (red line) and different approximations: LDA (yellow line), direct linear approximation (blue dashed) and using the connector (blue dashed with filled cycles) for slowly varying density. In this case $n(\mathbf{r}) = A\cos(\mathbf{a}\cdot\mathbf{r}) + B$, where $a = 0.3\ a_0^{-1}$, $n_{max} = 0.3776\ a_0^{-3}$ and $n_{min} = 0.0402\ a_0^{-3}$.

5.4 Distinct connectors for exchange and correlation

In the case of the v_{xc} one is often interested in the exchange and correlation contributions separately [83, 34, 84]. Here, we benefit from the analytic expression of the target functional to address this point. Indeed, the results of the study of $v_{\mathrm{xc}}^{\mathrm{WDA}}$ might not necessarily hold for the unknown xc potential, but they can provide some useful insights into it. The exchange contribution of the WDA potential, v_x^{WDA}, is defined in this case by applying the sum rule to the exchange hole and the correct limit to the HEG. The correlation contribution, v_c^{WDA}, is the difference from the total WDA functional. Here we always use the first order connector via (4.5), replacing f_{xc} by the exchange kernel f_x^{WDA} for the exchange connector and by the correlation kernel f_c^{WDA} for the correlation connector.

In Fig. 5.4 we show the result of considering the exchange and correlation connectors separately for the WDA functional. The exchange potential (upper panel) is an order of magnitude larger than the correlation contribution; notice the scale change. The picture for the exchange is therefore pretty similar to the full xc result. The correlation contribution exhibits a distinct pattern, with the LDA being too shallow. The correlation connector accurately reproduces the target v_c^{WDA} for higher densities.

However, for very low densities the linear expansion around the LDA

yields negative connector densities, so that the connector result (curve with blue filled circles) for r in the range $[2.43, 4.32]$ is not present. This is not due to a violation of condition [A] stated in Chapter 3, which is indeed satisfied, but due to the fact that the *approximate* result of (3.11) falls outside of the allowed domain, such that (3.12) cannot be evaluated. The problem can be solved in several ways, the simplest being to modify the approximation. Indeed, the result of the linear approximation depends on the reference density of the expansion n_0. Fig. 5.4 also shows result of the direct approximation obtained by expanding around a much lower density than previously, here $n_0 = n(\mathbf{r})/6$ rather than the local density $n(\mathbf{r})$. Contrary to before, now the straightforward linear expansion of v_c^{WDA} exhibits a bump at low densities, but it is exaggerated, and moreover the results at larger densities are very poor. However, now the resulting connector density is always positive, and the connector v_c can be computed over the entire range. With respect to $n_0 = n(\mathbf{r})$, there is very little change at high densities: this again shows the strong error cancellation inherent in the connector approach and consequently makes the result very stable. Indeed, because the HEG's v_c is very steep at low densities, the connector result depends significantly on the choice of n_0. The latter is a free parameter of the linear approximation; it has been set to the local density for the purpose of comparison, but can be further optimized for the exact xc potential using exact constraints, as discussed in Ch. 4. For the present illustration, we simply highlight that the issue can be resolved by changing n_0, following the indication given by the connector density itself, which falls below the LDA.

In summary, by studying the WDA functional, we have shown that the connector theory is a suitable framework to derive a simple approximate functional that reproduces the nonlocal dependence on density for an inhomogeneous system. Using the HEG data and the linear expansion, the connector potential goes beyond the LDA. Moreover, by separating the exchange and correlation contribution, we demonstrated how critical it is to design a separate connector for each object of interest. The above results are very promising and they were the motivation for the next chapter, where we apply the expressions in the self-consistent calculation of the density for real materials without using the weighted density approximation.

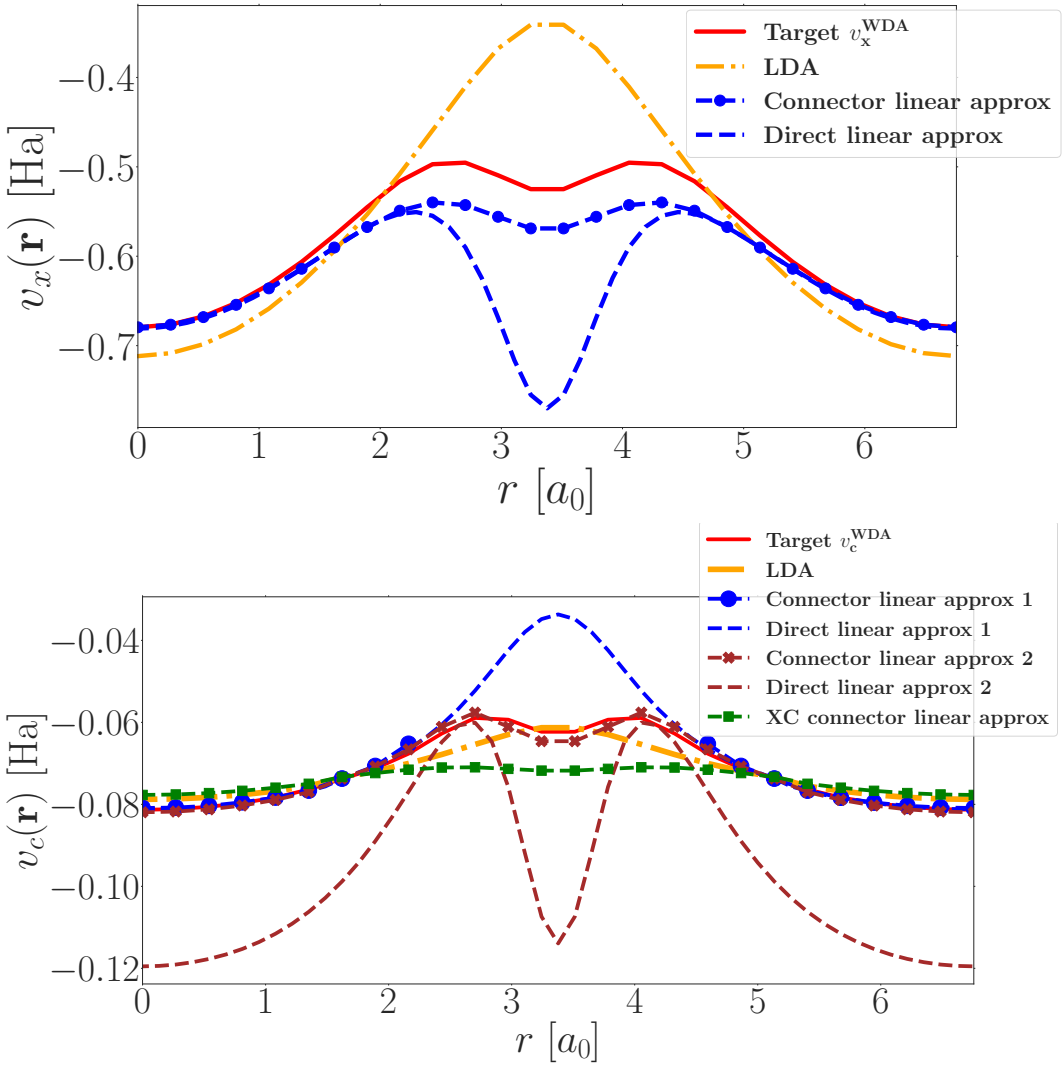

FIGURE 5.4: Comparison between the target WDA potential (red line) and different approximations: LDA (yellow line), direct linear approximation (dashed blue and brown) and using the connector (dashed blue and brown, with symbols). Exchange only (upper panel) and correlation only (bottom panel). Note that in the correlation potential the connector result is missing for r in the range [2.43, 4.32], since the connector density becomes negative. To solve this problem, it is enough to change the density n_0 around which one expands. The dashed brown curve is the result of the direct linear expansion around a density $n_0 = n(\mathbf{r})/6$, labeled "approx 2", as opposed to "approx 1" which stands for $n_0 = n(\mathbf{r})$. The brown curve with stars is the corresponding approx 2 connector result. Finally, the green curve with filled squares represents the potential $v_c(\mathbf{r}) = v_c^h(n_{\mathbf{r}}^{c,\text{approx}})$ obtained using the full xc connector, which is not consistent and therefore worsens the result.

Chapter 6

The charge density from a connector exchange correlation potential

As discussed in previous chapter, the connector has shown a very good performance in approximating non-local density functional. It describes very well the weighted density approximation (WDA) xc potential for a toy system. This promising result was the motivation to check the quality of the connector approximation for the exact xc potential. The latter is unknown and so a direct comparison is impossible. As a solution, one can look at the target quantity that is obtained from the Kohn-Sham (KS) system, i.e, the charge density. To do so, I wrote a DFT-code[1] that solves the KS equations and calculates the density. In this code I implemented the connector xc potential in order to compare the resulting density to a benchmark. The benchmark is a density obtained using Quantum Monte Carlo (QMC) method [14] which is supposed to give very accurate results. In this chapter, I discuss the results of testing the connector functional on two very different materials. One is a widely studied semiconductor, which is silicon, and the other one is an insulator, namely, sodium chloride.

The main questions that I want to answer in this chapter are :

- How does the connector compare to other popular functionals?
- What is the optimized choice of the connector free parameter n_0?
- What are the limits of using the HEG model?

The structure of this chapter is as follows. First, I remind the formula of the connector derived using linear expansion. Then, I discuss the choice of the benchmark density. Next, I carry a detailed study about using the connector xc potential to obtain the density of silicon. In this study, I try several versions of the connector and I determine the optimized one. I also check the performance of the linear expansion as an approximation to the xc potential. I finish the silicon study by comparing the quality of the connector functional with other popular DFT functionals. Finally I use the NaCl case to test the connector in a system with very localized density. I profit from this

[1] see the appendix C

case to confirm my conclusion about the best version of the connector, and to explore the limit of the model.

6.1 The unknown xc potential

So far, we have developed a connector approximation for the xc potential, using the homogeneous electron gas (HEG) as a model. The connector approximation reads

$$v_{\mathrm{xc}}(\mathbf{r},[n]) \approx v^{h}_{\mathrm{xc}}(n^{c,\mathrm{approx}}_{\mathbf{r}}), \tag{6.1}$$

where

$$n^{c,\mathrm{approx}}_{\mathbf{r}} = \frac{1}{f^{h}_{\mathrm{xc}}(n_0)} \int d\mathbf{r}' f_{\mathrm{xc}}(|\mathbf{r}-\mathbf{r}'|,n_0) n(\mathbf{r}'), \tag{6.2}$$

with n_0 the reference density around which we do the linear expansion. This connector results from a first order approximation made in both the real system and the HEG. In the real system this approximation reads

$$v_{\mathrm{xc}}(\mathbf{r},[n]) \approx v_{\mathrm{xc}}(n_0) + \int d\mathbf{r}' f_{\mathrm{xc}}(|\mathbf{r}-\mathbf{r}'|,n_0)(n(\mathbf{r}')-n_0). \tag{6.3}$$

In the following, while checking the quality of the density resulting from the connector xc potential, it will also be interesting to compare with the linear approximation results. This allows us to estimate the error cancellation obtained by the connector.

6.2 The charge density

The xc potential is difficult to judge by itself since it is not an observable. The motivation behind developing good approximation to this potential is to obtain an accurate estimation for real observables. In DFT, the first interesting observable is the electronic density. In principle, if we have the exact xc potential we get the same density for the KS system and the real one. Hence, we can check the quality of the connector xc potential, $v_{\mathrm{xc}}(n^{c,\mathrm{approx}}_{\mathbf{r}})$, by using it to calculate the density. Then we compare with a benchmark density.

In the following we will use the connector approximation for the xc potential in order to calculate the density of Si and NaCl. As a benchmark we take densities calculated by S. Chen *et al.* [14]. These densities are obtained using the *ab initio* auxiliary-field quantum Monte Carlo (AFQMC) method, which has been shown to be excellent in calculating the total energy, which is the reason why the resulting density is considered to be near-exact. We will compare the benchmark with DFT-KS densities using various approximations for the xc potential. In order to measure the error with respect to AFQMC density, $n_{\mathrm{AFQMC}}(\mathbf{r})$, we calculate the following difference for each density, $n_{\mathrm{approx}}(\mathbf{r})$, resulting from a given approximation of the xc potential

$$\Delta n(\mathbf{r}) = n_{\mathrm{approx}}(\mathbf{r}) - n_{\mathrm{AFQMC}}(\mathbf{r}), \tag{6.4}$$

and the percentage difference as

$$\Delta n_p(\mathbf{r}) = 100 \times \frac{n_{\text{approx}}(\mathbf{r}) - n_{\text{AFQMC}}(\mathbf{r})}{n_{\text{AFQMC}}(\mathbf{r})}. \tag{6.5}$$

The Mean Absolute Error (MAE) is calculated as

$$\text{MAE} = \frac{1}{V_{\text{cell}}} \int d\mathbf{r} \left|\Delta n_p(\mathbf{r})\right|, \tag{6.6}$$

with V_{cell} the volume of the unit cell.

6.3 Silicon

As a semi-conductor prototype we have studied the covalent-bond crystal silicon. The density is calculated in a basis of plane waves. To be consistent with the AFQMC study we used the same system parameters. We considered the primitive cell, which is a Face Centered Cubic (FCC) cell: it contains two Si atoms located at $(0,0,0)$ and $(\frac{1}{4},\frac{1}{4},\frac{1}{4})$. The volume of the primitive cell is a quarter of the conventional cubic one which has a lattice constant of 10.263 Bohr. To construct the KS potential, we used a Ne-core pseudopotential (the same as the AFQMC study [14]). We have then calculated the density by diagonalizing the Hamiltonian and summing the square of the wavefunctions over the four occupied valence bands and all k points. We used a plane wave cutoff of 25 Ry, and $6 \times 6 \times 6$ k-point grid.

In order to give a simple visualization of the density, as done in [14], the density is presented along line cuts, see Fig. 6.1, following the triangular route
O—$\langle 001\rangle$—O'—$\langle 110\rangle$—O''—$\langle 111\rangle$—O. The origin O is taken to be the middle point between two neighboring Si atoms, while O' and O'' are translated from O by lattice constants along the direction connecting them.

6.3.1 Density using the connector xc potential

In order to use the connector approximation of the xc potential as shown in (6.1) and (6.2), we need to specify the reference density of the expansion, n_0. The choices of n_0 can be based on physical intuitions or on some known constraint on the xc potential. In the following we compare several choices of the reference density n_0 discussed in Ch. 4, namely, the mean density, the local density, the self consistent connector and the symmetric density with an equivalent choice in the model.

6.3.1.1 The best connector

In Fig. 6.2 we show a comparison between the densities resulting from the connector approximation of v_{xc} for various choices of n_0. The LDA is added to check whether or not the non-locality of the connector functional improves the density. In table 6.1, we give the MAE of the connector approximation

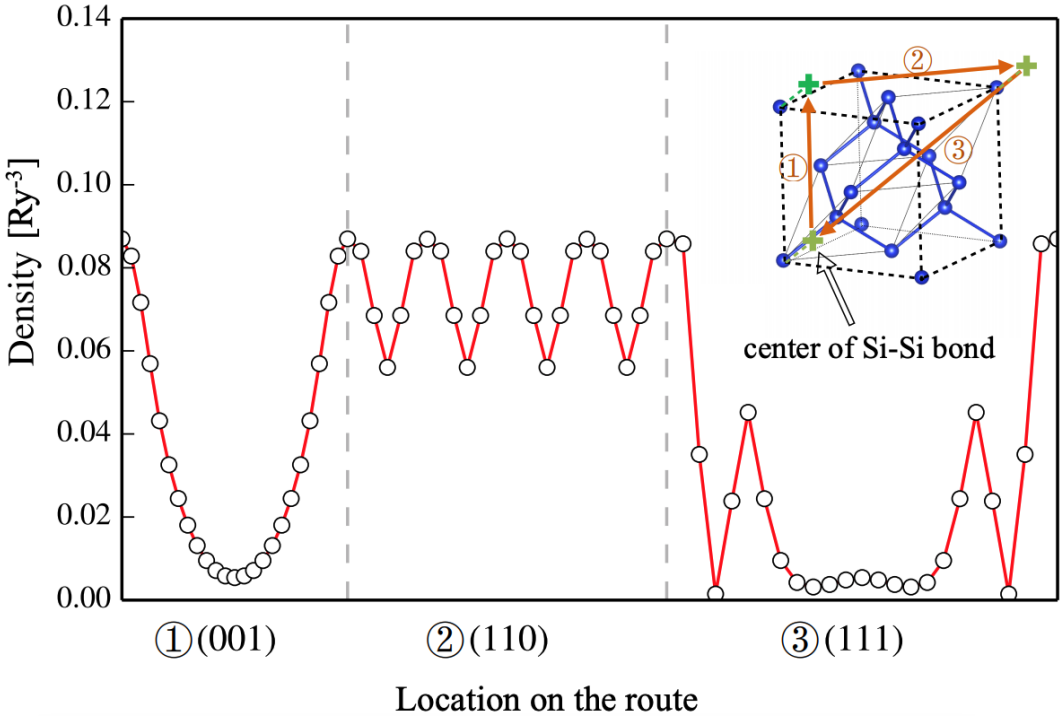

FIGURE 6.1: The benchmark charge density of silicon from AFQMC[14]. The density is plotted along the route indicated in the inset.

Choice of n_0 in connector	MAE along the route (%)	MAE in 3D grid (%)
Mean density	3.89	2.24
Local density	2.34	1.32
Self-Consistent	2.36	1.41
Symmetric	0.56	0.89

TABLE 6.1: Mean average error (MAE) of the resulting density using connector xc potential with several choices of n_0 for Si.

for several choices of the reference density n_0. For n_0 taken at the mean density, the connector does not seem optimized for this choice. Except on atoms its error is the largest. The MAE for the *connector mean* is 3.36%, along the triangular route. With n_0 being the local density the connector yields a better approximation. This was also the case for the functional studied in Ch. 5. The MAE now decreases to 2.34% and we can see a clear improvement comparing to LDA. This happens thanks to the non-locality of the connector which captures more information about the system environment. For the self consistent connector, as we can see in Fig. 6.2, it converges to the choice $n_0 = n(\mathbf{r})$. This connector is slightly better on atoms and it gives 2.36% as a MAE. Interestingly, the connectors discussed so far have a similar error in the middle region of the triangular route. They are close to the LDA and their errors show wiggles that follow the variation of the local density shown in Fig. 6.1. The reason behind this behavior might be the fact that these approximations give too much importance to the local density. If they had a sufficient non-local information about the density and its gradient, then they would take the mean density itself as a connector to plug in the v_{xc} function of the HEG. Finally, the symmetric connector seems to be the best choice. Its error is the smallest one with 0.56% as MAE. It is less than the AFQMC error bar in the majority of the middle region , where the LDA and all other connectors seem unable to describe the target.

6.3.2 Linear approximation

To design the connector discussed in previous section, we have used the linear expansion in (6.3) as an approximation for the xc potential functional. Alternatively, one can use directly this approximation as the v_{xc} of the KS system, as done in [74], and compute the corresponding density. In Fig. 6.3 we compare the density resulted from the direct linear expansion and the one obtained through the connector for two different choices for n_0: the local and the mean density. For both choices, the direct approximation yields a reasonable density which is comparable to LDA and the connector results. This is can appear surprising, since the linear expansion does not even guarantee a physical result. We also see, In Fig. 6.3, for n_0 taken at mean density and along the direction (110), where the density is large, the direct linear expansion yields the best density comparing to its corresponding connector approximation and the LDA. Along the entire route it yields 2.19% as a MAE, while for the connector, the MAE is 3.36%. This is an example where the error canceling does not happen. In the case of n_0 taken at the local density, the connector result and the linear expansion one are very similar along the triangular route. The only clear difference appears on atoms, where the connector is improving the density. The MAE using this choice of n_0 is 2.56% for the linear expansion and decreases to 2.34% for the connector.

The results of this section suggest that an optimized linear expansion for the xc potential could help to obtain a good estimation of the density. They also suggest that a higher order expansion may be a good approximation for

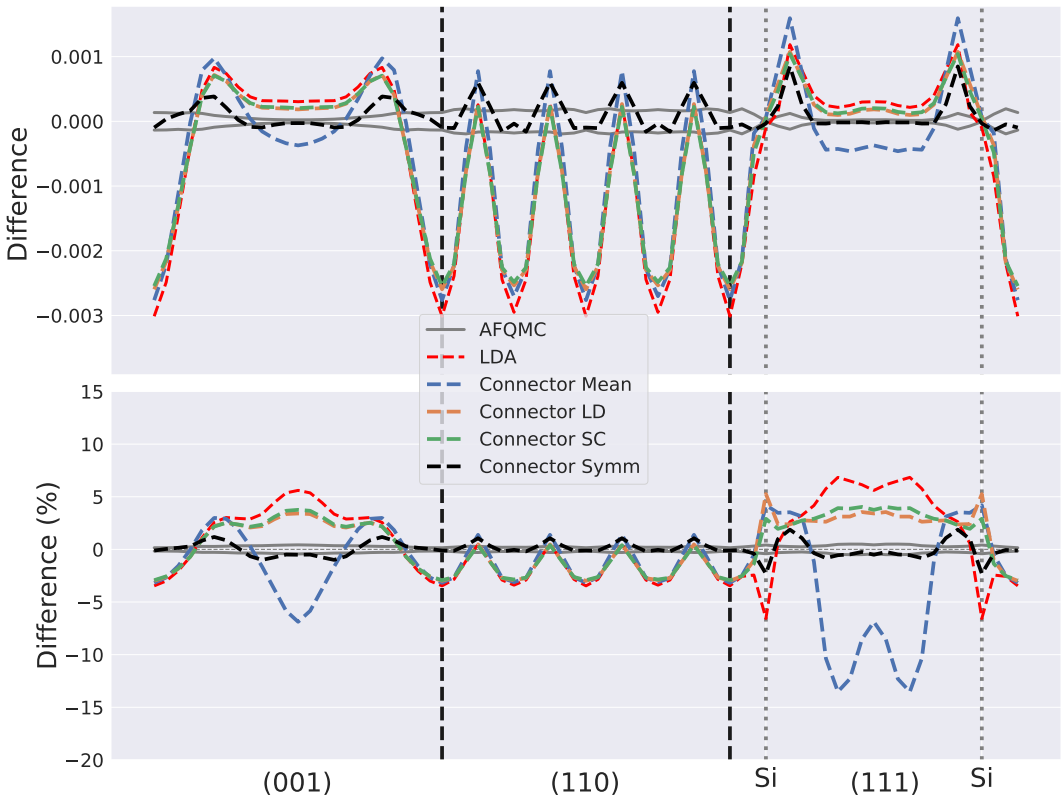

FIGURE 6.2: The upper panel shows the difference between the benchmark density and the densities resulting from approximating the xc potential using LDA or connector. The lower panel shows the corresponding percentage difference. The gray line is the error bar of AFQMC. The connector results are shown for several choices of the density n_0 in (6.2). These choices are mean density, local density (LD), self consistent (SC) connector and the Symmetric (Symm) n_0 which we have introduced in the text.

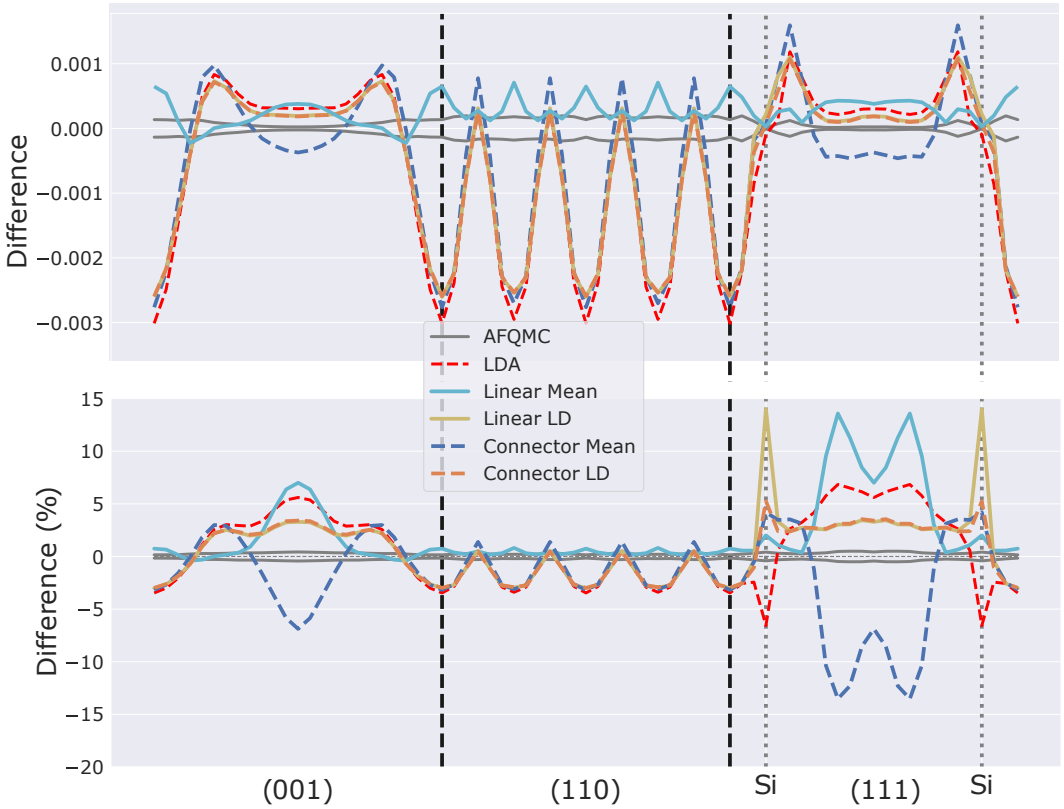

FIGURE 6.3: Similarly to Fig. 6.2, we show here a comparison between the resulting density using the connector v_{xc} and the corresponding linear approximation for two choices of n_0 : the mean and the local density.

the v_{xc}. However, in general, the connector approximations, particularly that of the symmetric connector, provide superior performance.

6.3.3 Comparison with other functionals

After selecting the connector that yields the best density, now we compare it with the densities obtained using several popular functionals for the xc potential. This functionals are: LDA; PBE, a general-gradient approximation by Perdew-Burke-Ernzerhof [44]; PBEsol, a revised version of PBE for solids [65]; PBE0, a hybrid functional between PBE and Hartree-Fock [85]; B3LYP, one of the most commonly used versions of hybrid functionals [86]. For all these functionals we use the same pseudo-potential used for AFQMC calculations.

In Fig. 6.4 we present the density differences and the percentage errors with respect to the benchmark. Along the triangular route, LDA and PBEsol yield the largest errors, but they are better than B3LYP for the entire cell as shown in table 6.2. PBE yields a better density along the route, it shows a larger error on atoms and its MAE in 3D grid is about 1%. Finally, the connector yields the most accurate density along the route. It significantly improves the LDA by capturing non-local effects, and it gives the the smallest

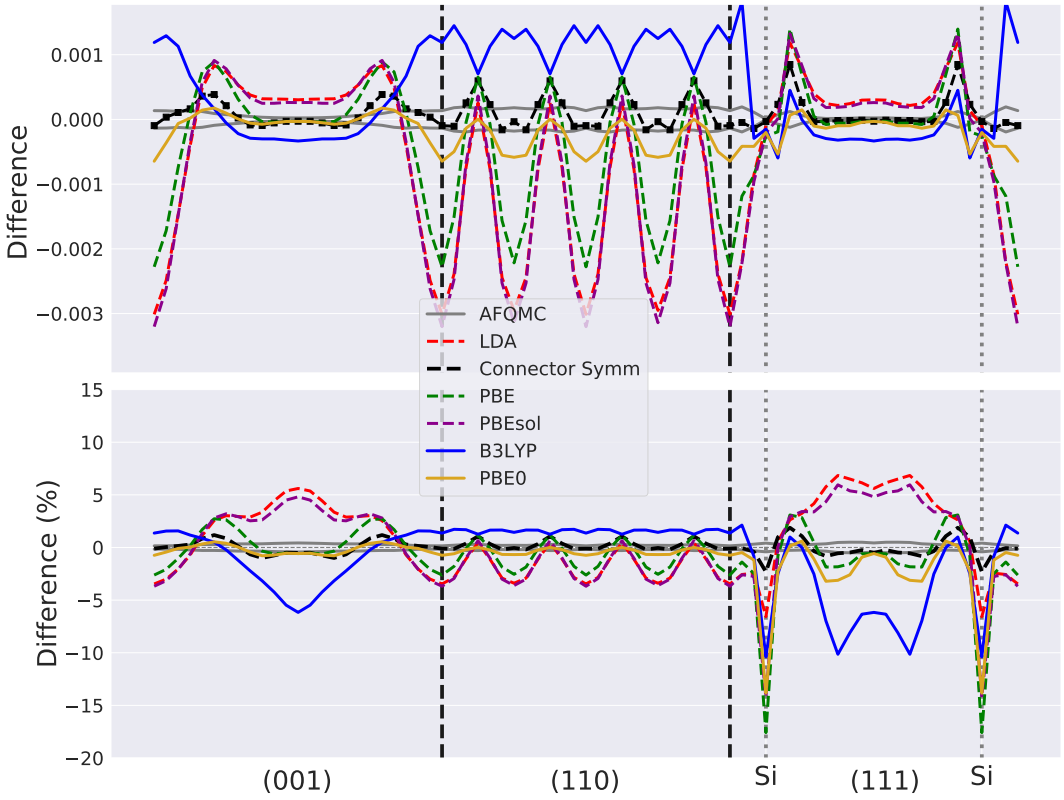

FIGURE 6.4: Similar to Fig. 6.2, a comparison between the resulting density using several functionals for the xc potential.

one among all functionals. This error becomes a little bit larger and similar to PBE0 for the entire cell.

6.4 Sodium chloride

In the previous section, we have seen that the connector performs very well for silicon. It produces a very accurate density when compared to the benchmark. This raised the question to what extent the connector good performance is transferable to other materials. The purpose of this section is to

Approximation	MAE along the route (%)	MAE in 3D grid (%)
LDA	3.10	1.93
PBE	1.87	1.07
PBEsol	3.13	1.77
B3LYP	2.74	2.17
PBE0	1.10	0.87
Connector Symm	0.56	0.89

TABLE 6.2: Mean average error of various approximated densities with respect to QMC density for bulk silicon.

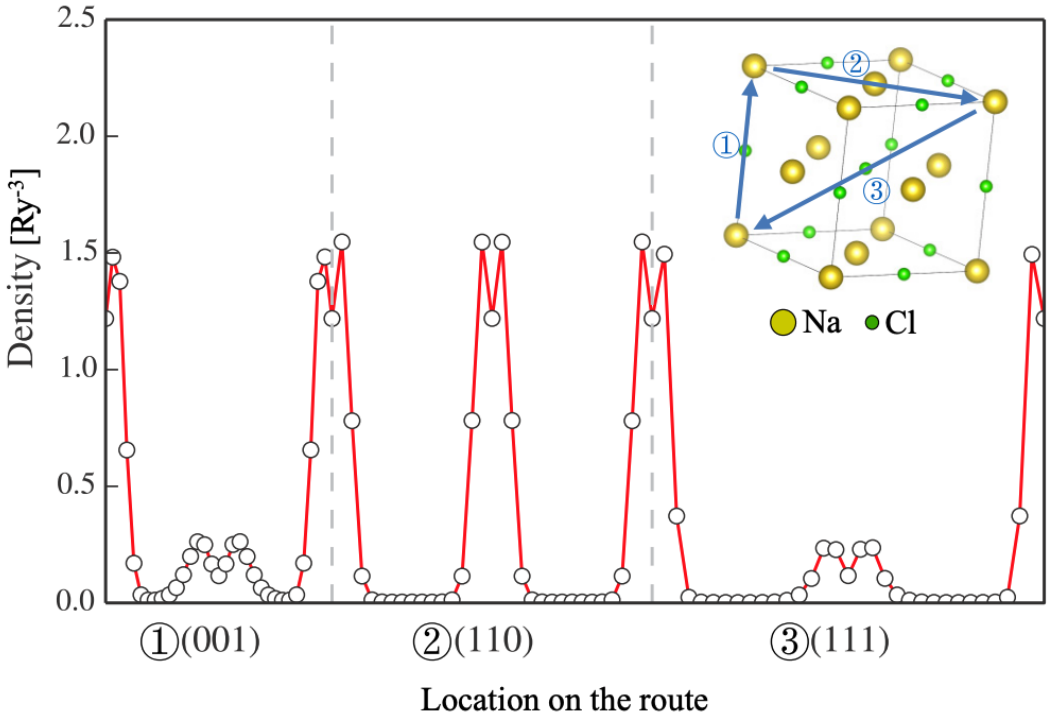

FIGURE 6.5: The benchmark charge density of sodium chloride from AFQMC [14]. The density is plotted along the route indicated in the inset.

evaluate the connector xc potential in a material that differs significantly from silicon. It is the sodium chloride, an insulating ionic crystal.

Again for the sake of consistency, the system parameters and the pseudopotential are the same as in the AFQMC study [14]. We used the primitive cell which contains one Na atom at lattice points and one Cl atom at bulk center. The volume of this cell is one quarter the FCC cubic one. The lattice constant used for the latter is 10.7563 Bohr. The plane wave cutoff is fixed to 40 Ry and we used $6 \times 6 \times 6$ k-point grid. In this case a He-core pseudopotential is used for Na and Ne-core one for Cl. This implies eight occupied valence bands. For the visualization of the density we consider the same triangular route as we did in the case of Si, but we modify the origin O to be on Na atom in this case. The AFQMC density for NaCl is displayed along the triangular route in Fig. 6.5.

6.4.1 Does the symmetric connector stay the best?

Optimizing the reference density of the expansion, n_0, can help to improve the connector v_{xc}. For silicon, we have tested several choices of n_0, the best one was the symmetric n_0 with an equivalent choice in the model. The argument of this choice was based on symmetry and bi-nearsightedness which are not limited to Si. In table 6.3, we present the MAE for the different n_0 studied in the Si case. As expected, the symmetric connectors wins over all

Choice of n_0 in connector	MAE along the route (%)	MAE in 3D grid (%)
Mean density	4.89	4.75
Local density	7.46	8.58
Self-Consistent	6.76	6.82
Symmetric	2.07	2.03

TABLE 6.3: MAE of the resulting density using connector xc potential with several choices of n_0 for NaCl.

Approximation	MAE along the route (%)	MAE in 3D grid (%)
LDA	4.47	5.13
PBE	0.86	0.81
PBEsol	2.40	2.49
B3LYP	0.67	0.61
PBE0	1.61	1.30
Connector Symm	2.07	2.03

TABLE 6.4: MAE of various approximated densities with respect to QMC density for NaCl.

other choices. This supports the generality of the argument behind that connector.

6.4.2 Comparison with other functionals

As we have already done for Si in previous section, here we carry out the same comparative study for NaCl density. In Fig 6.6 we show the error on the computed density using several DFT functionals for v_{xc} including the connector one. The best description of the benchmark density is given by B3LYP and PBE: they are very accurate along the route, except between the Na and Cl atoms along the direction (111) where the density is very low. They both yield a very small MAE as shown in table 6.4. PBE0 and connector perform better than PBEsol and LDA. Thanks to its non-locality, the connector reduces the MAE by more than a factor of two compared to LDA. The resulting density from the connector xc potential suffers more on the sodium atoms, as we see in the upper panel of Fig. 6.6. This result could be explained by the fact that NaCl density is highly localized, whereas we use a homogeneous model for the connector. This shortcoming is not a handicap for the connector in principle, since one may improve the results by choosing a model closer to the real system. The use of inhomogeneous model systems in the connector approach raises new challenges, but it is probably one of the most promising direction for future developments.

In conclusion, the connector functional of the xc potential, derived in Ch. 4 performs well when used in the self-consistent Kohn-Sham equation to calculate the charge density. It improves the LDA in a systematic way. The connector result can be improved by optimizing the reference density n_0 of the linear expansion. A symmetric n_0 in the xc kernel, in particular, produces

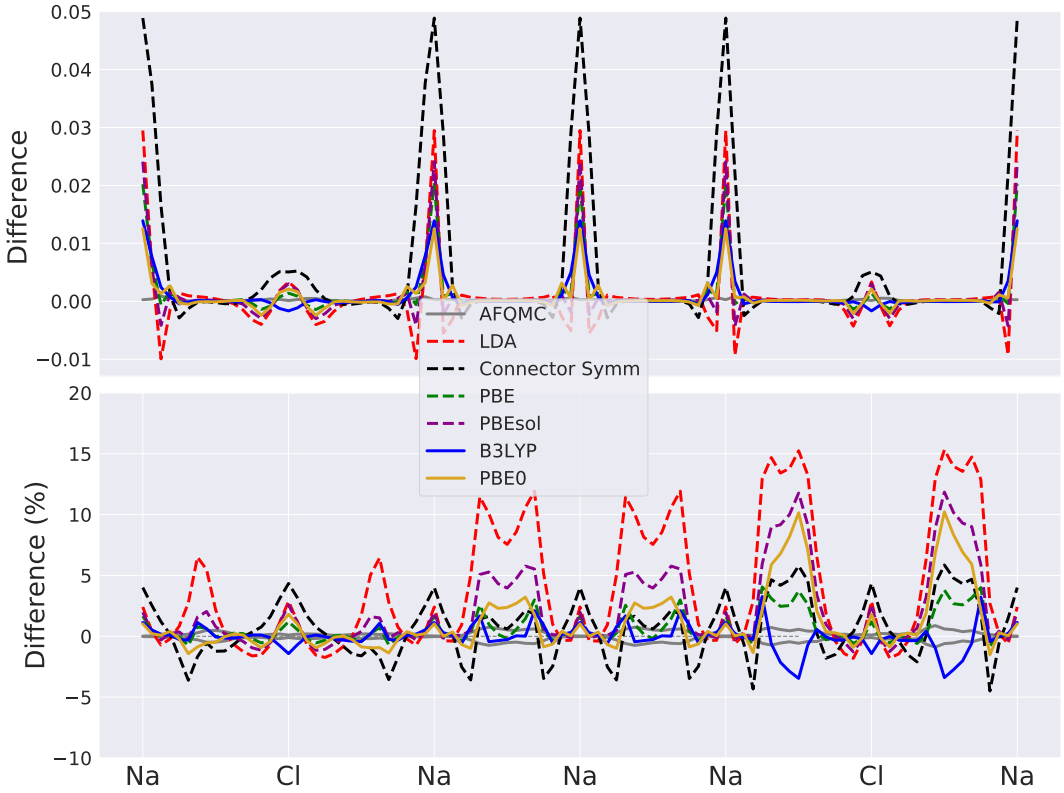

FIGURE 6.6: Same as Fig. 6.4 but for NaCl.

a very accurate density for silicon and outperforms the other connectors in NaCl. However, compared to PBE, the connector approximation does not adequately describe the density on the Na and Cl atoms, this can be due to the use of the HEG model, which is quite far from the real system with its highly localized density. On the other hand, as we will also see in the following chapter, in particular the region of the Na atoms is very delicate, and further inhomogeneous models should be considered in the future in order to disentangle different effects and uncertainties.

Chapter 7

Reverse engineering the xc potential from the density

In the previous chapter we have compared densities, but this is still a quite indirect indicator for the quality and features of the xc potential. Therefore, in the present chapter, I discuss the construction of accurate exchange correlation potentials from numerically exact densities of the simple semiconductor bulk silicon and insulating sodium chloride obtained from Auxiliary Field (AF) QMC calculations [14]. In such extended systems, to the best of our knowledge, no results for v_{xc} obtained directly from a numerically exact density are available, contrary to the situation in finite systems [87, 88, 89]. This may have several reasons: besides new technical difficulties that may arise when trying to invert the KS equations in, for example, a periodic solid, it cannot be excluded *a priori* that the high sensitivity of the potential on the density could be even worse in solids than in atoms. Moreover, while the absolute scale of the potential in a finite system can be fixed by forcing the potential to be zero at infinity, such a condition cannot be imposed in an infinite system. Finally, and most importantly, data for numerically exact densities of solids were not available in the literature.

For these reasons, many important and fundamental questions arise, in particular:

- Can one invert the KS equations in an extended system and if yes, how, and which kind of precision can be obtained? How different is the resulting v_{xc} from standard approximations such as the LDA or Perdew-Burke-Ernzerhof (PBE) generalised gradient approximation [90] (GGA)? What about the connector v_{xc} ?
- What about observables in this numerically exact KS system, and in particular, the band gap?
- How much does v_{xc} depend on details of the density? And if it depends significantly, do the resulting changes have an impact on other KS observables?

In order to answer these questions, I will first discuss how to extend a simple inversion algorithm from finite systems to solids, and then demonstrates its ability to reproduce the LDA xc potential for silicon. After performing this verification, I use the algorithm to calculate the xc potential from the

AFQMC densities of Si and NaCl, and I explain how to deal with the problem of stochastic noise in the density. Next, I calculate the numerically exact band gap of the Kohn-Sham system using the inverted xc potentials. I compare the result with the LDA and PBE band gap, and I highlight the fact that the true KS band gap is significantly smaller than the measurable photoemission gap, confirming previous estimates. Finally, I use the resulting xc potentials to determine the Kohn-Sham band structure and extract the xc energy from the total energies of Si and NaCl computed in [14]. The results can serve as a benchmark for existing approximations.

7.1 How to invert the KS problem in infinite systems

The probably simplest algorithm to obtain the KS potential from a given density has been proposed for finite systems by van Leeuwen and Baerends [91]. In its original form it was derived by solving the KS equations for the KS potential v_{KS}. The result was then translated into an iteration procedure which relates a potential $v^{\mathrm{i}+1}$ at step $i+1$ to the potential v^i at step i by the ratio of the target density n_{ref} and the density n_i at step i. As pointed out in [88], the best use of this ratio depends on the sign of the potential that is updated: for example, v may be either the usually negative total v_{KS}, or its rather positive interaction part $v_H + v_{\mathrm{xc}}$ with v_H the Hartree potential. Here we use

$$v_{\mathrm{xc}}^{i+1}(\mathbf{r}) = \frac{n_{\mathrm{ref}}(\mathbf{r}) + a}{\tilde{n}_i(\mathbf{r}) + a} v_{\mathrm{xc}}^i(\mathbf{r}) \,, \tag{7.1}$$

where a is a parameter that avoids instabilities in regions of very low density as suggested in [91], and the mixing

$$\tilde{n}_i = \alpha n_{\mathrm{i}-1} + (1-\alpha) n_i, \tag{7.2}$$

with $0 < \alpha < 1$, is introduced to smooth the convergence. This density $\tilde{n}_i$ is also used to update the Hartree potential at each iteration. (7.1) is clearly a good strategy if v_{xc} is negative, and if the density in a point $\mathbf{r}$ is determined only by the KS potential in that same point: suppose that at a given iteration, $\tilde{n}^i(\mathbf{r})$ is larger than $n_{\mathrm{ref}}(\mathbf{r})$. The algorithm then decreases the absolute value of $v_{\mathrm{xc}}(\mathbf{r})$ in that point. If the xc potential is negative, this step makes the potential more shallow, and less density will be attracted to the point at the next iteration, which pushes the solution in the good direction. Of course, it is not true that $n(\mathbf{r})$ depends only on $v_{\mathrm{xc}}(\mathbf{r})$ in the same point $\mathbf{r}$, and it has to be seen to which extent the relation is nearsighted enough to make the algorithm work in a solid.

7.1.1 Choice of the initial guess

The negative sign of the potential that is updated in (7.1) is crucial for the algorithm to work, because a positive sign would drive the result in the wrong

direction. However, contrary to the homogeneous electron gas a real system can also exhibit regions of positive v_{xc}. Moreover, in a finite system, one can impose that the potential tends to zero at large distances. In a solid, however, the zero of the potential is not defined. This fact represents both an advantage and a drawback: on the upside, it allows us to introduce a rigid negative shift in the initial guess of the potential such that it remains negative throughout the iteration. This shift is arbitrary within reasonable limits: if it is too small, positive regions may appear and be an obstacle for convergence. If it is too large, the algorithm becomes unstable, because also the shift is multiplied at every step by the density ratio. Reasonable values lie within the maximum amplitude of the potential. On the downside, iteration of (7.1) yields v_{xc} only up to a constant. This is not due to our introduction of a shift, but to the fact that the density does not contain information about the absolute value of the potential. This problem can therefore not be overcome. The resulting potential can, however, be used to calculate a well defined density, xc energy and KS observables such as (besides the meaningless constant shift) the KS band structure.

For the results shown in the following, we use as initial guess $0.3 \times v_{\mathrm{xc}}^{\mathrm{LDA}}$ with a rigid downwards shift of 0.2 a.u. for silicon and 0.4 a.u. for NaCl.

7.1.2 Reproducing the LDA xc potential

To illustrate the reliability of the procedure it is instructive to examine a case where the density-potential relation is well known; here, we choose the LDA. This means that in (7.1), $n_{\mathrm{ref}} = n_{\mathrm{LDA}}$ is the density obtained in a standard LDA Kohn-Sham self-consistent calculation with xc potential $v_{\mathrm{xc}}^{\mathrm{LDA}}$ at convergence. Ideally, for $i \to \infty$ we should find $v_{\mathrm{xc}}^{\mathrm{LDA,i}} \to v_{\mathrm{xc}}^{\mathrm{LDA}}$ and $n_i \to n_{\mathrm{LDA}}$. Fig. 7.1 and 7.2 show results for silicon.

In Fig. 7.1 the absolute value of the maximum (over the unit cell) relative error of the density compared to the reference LDA one

$$\Delta_i = \max_{\mathbf{r}} \left| \frac{n_i(\mathbf{r})}{n_{\mathrm{LDA}}(\mathbf{r})} - 1 \right| \tag{7.3}$$

is shown as a function of the number of iterations. It decreases smoothly and very fast. The same is true for the mean (of absolute values, over the unit cell) relative error, given in the inset. In Fig. 7.2 snapshots for the errors on density and v_{xc} are presented. The upper panel gives the percentage error of the density $(n_i(\mathbf{r})/n_{\mathrm{LDA}}(\mathbf{r}) - 1) \times 100\,\%$ along a path through the unit cell (the same as in Ref. [14]) at $i = 500$ iterations, multiplied by 10^4 in order to make it visible. It is largest, with a maximum of 6.55×10^{-4} %, in places where the LDA density, shown by the thin magenta line in the upper panel (scale on the right side), is low. The percentage error of the potential is shown in the bottom panel. Because of the arbitrary shift, only a comparison of the variations of the potential is pertinent. Indeed, during the iterations the average potential continuously moves upwards. The figure has been obtained by re-aligning at the end of the iterations the average potentials. This requires a

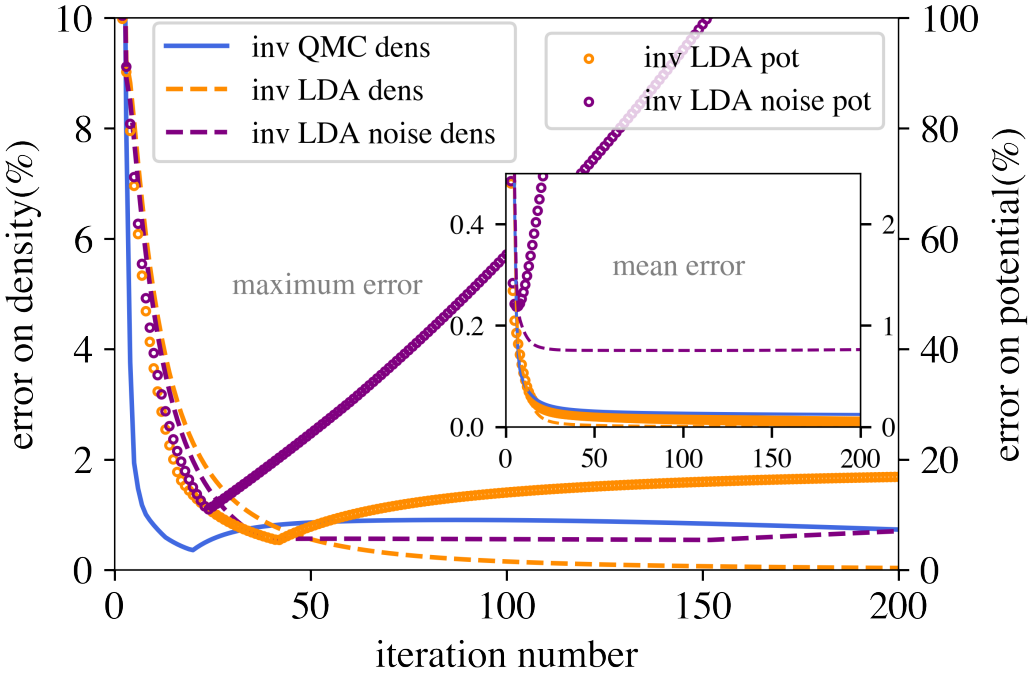

FIGURE 7.1: Errors of the iteration procedure as a function of number of iterations i. The curves in the main panel show the maximum (over the unit cell) relative error of the density versus the iteration number for the inverted LDA, inverted noisy LDA and QMC xc potentials. Each inverted density is compared to its corresponding reference result. Symbols give the maximum (over the unit cell) relative error of the xc potential for the inverted LDA and inverted noisy LDA. In these cases the error is defined with respect to v_{xc} of KS LDA, since the xc potential that yields the noisy density is unknown. In the inset: Curves show the mean (over the unit cell) relative error of the density versus the iteration number for the inverted LDA, noisy LDA and QMC xc potentials. Symbols are for the inverted LDA and inverted noisy LDA potentials. For all calculations, the starting v_{xc} is 30% LDA with a shift of -0.2 a.u..

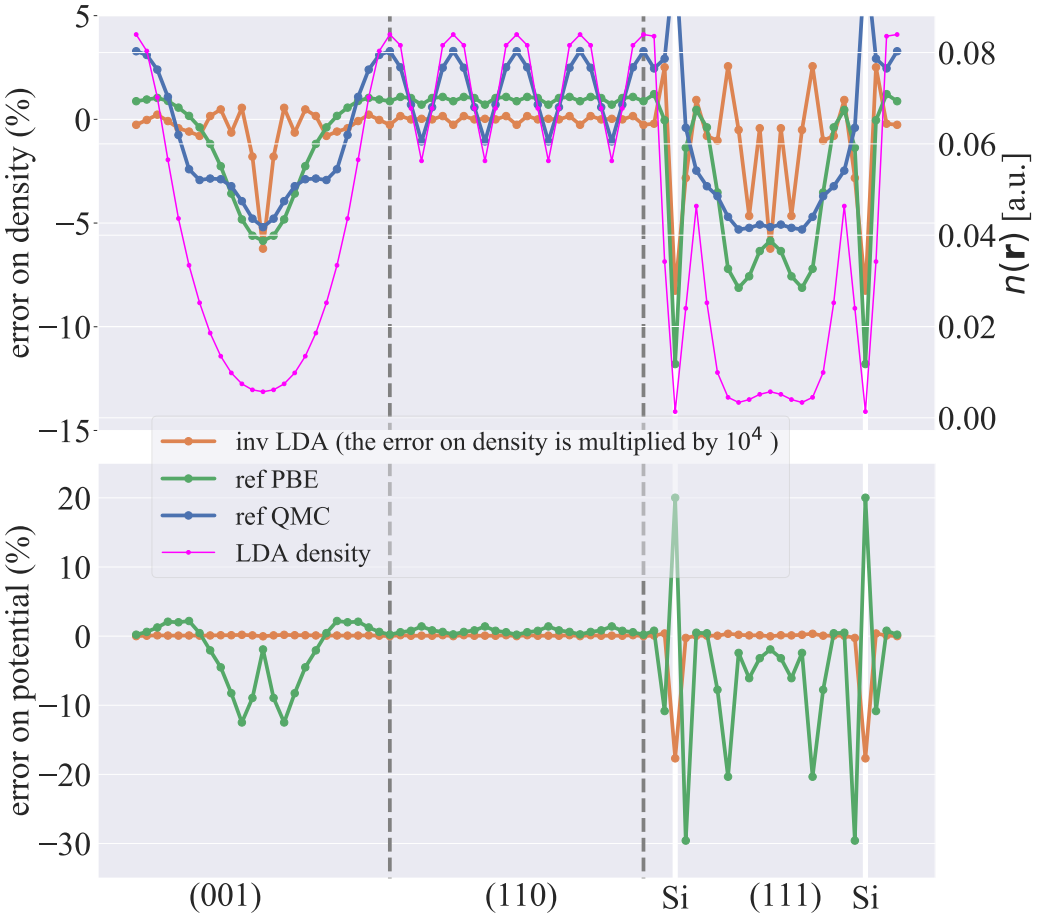

FIGURE 7.2: Density and xc potential of bulk silicon along a path across the unit cell. The position of atoms are indicated by a white vertical line. For the LDA, the xc potential is obtained from a self-consistent KS calculation ($v_{\mathrm{xc}}^{\mathrm{LDA}}$), or using the iterative procedure, after i iterations, with the KS LDA density n_{LDA} as reference density n_{ref} ($v_{\mathrm{xc}}^{\mathrm{LDA,i}}$). The density $n^{\mathrm{LDA,i}}$ is then recalculated using $v_{\mathrm{xc}}^{\mathrm{LDA,i}}$ in the KS equation. Upper panel: orange, relative error (in percent) of the density from the iteration procedure compared to the reference LDA density, defined as $(n^{\mathrm{LDA,i}}(\mathbf{r})/n_{\mathrm{LDA}}(\mathbf{r}) - 1) \times 100\,\%$ after $i = 500$ iterations, where the maximum relative error of the density over the unit cell is 6.55×10^{-4}%. The error is multiplied by 10^4 in order to make it visible on the scale of the figure. For comparison, in green the unscaled relative difference $(n_{\mathrm{PBE}}(\mathbf{r})/n_{\mathrm{LDA}}(\mathbf{r}) - 1) \times 100\,\%$ of the PBE and LDA self-consistent densities as well as in blue, the unscaled relative difference $(n_{\mathrm{QMC}}(\mathbf{r})/n_{\mathrm{LDA}}(\mathbf{r}) - 1) \times 100\,\%$ of the QMC and the self-consistent LDA densities. Thin magenta line, LDA density (scale on right side). Lower panel: relative difference of $v_{\mathrm{xc}}^{\mathrm{LDA,i=500}}$ with respect to $v_{\mathrm{xc}}^{\mathrm{LDA}}$, and, for comparison, the relative difference of the self-consistent PBE potential $v_{\mathrm{xc}}^{\mathrm{PBE}}$ with respect to $v_{\mathrm{xc}}^{\mathrm{LDA}}$ in green. All relative differences of potentials are given in percent and unscaled.

downwards shift of the iterative potential of 0.06 a.u.. Again, the maximum error is found in places of lower density, here in particular on the atoms. Note that, contrary to the case of the density, the error of the potential has not been scaled. Indeed, the relative error is significantly larger for the potential than for the density. This can also be appreciated in Fig. 7.1, where the open circles give the maximum and mean absolute errors on the xc potential as a function of iterations. In order to illustrate that the remaining errors are small enough to make discussions meaningful, the errors in Fig. 7.2 are compared to the difference between two different functionals, here, between PBE and LDA. The top panel contains the relative difference $(n_{\mathrm{PBE}}(\mathbf{r})/n_{\mathrm{LDA}}(\mathbf{r})-1)\times 100\,\%$ of the PBE and LDA self-consistent densities; note that this difference is *not* scaled, and therefore more than 10^4 times larger than the inversion error. The relative difference $(v_{\mathrm{xc}}^{\mathrm{PBE}}(\mathbf{r})/v_{\mathrm{xc}}^{\mathrm{LDA}}(\mathbf{r})-1)$ of the KS PBE and LDA xc potentials can be found in the bottom panel. Differences can be seen throughout the path, although regions of lower density show larger differences. These differences are, though slightly larger, of the same order as the differences in the density. Except for the atoms, they are, like in the case of the density, much larger than the error of the inversion. This demonstrates that the inversion yields meaningful results, with an error bar that is much smaller than the differences we wish to discuss.

7.2 Exchange correlation potential from QMC densities

Given the findings of the previous section, we can now examine the results obtained by applying the algorithm with the very same choices in order to obtain the xc potential from the QMC densities for Si and NaCl.

7.2.1 Silicon

For silicon, the maximum relative error of the density, $\tilde{n}_i$, as a function of the number of iterations i is given by the blue curve in Fig. 7.1. Interestingly, it shows an overall decrease, but with a pronounced minimum at $i=20$. At this point, it has decreased to 0.38 %. The minimum is followed by a modest increase, after which the error decreases again monotonously. In correspondence to the minimum, the mean relative error in the inset, instead, reaches a plateau of about 0.02 %, and a higher precision cannot be reached. The upper panel of Fig. 7.3 shows the local relative error on the density after 20 iterations, $(n^{\mathrm{QMC,i=20}}(\mathbf{r})/n_{\mathrm{QMC}}(\mathbf{r})-1)\times 100\,\%$, along the same path as in Fig. 7.2. The result stays well within the stochastic error bar of the QMC calculation. For comparison, we also show the unscaled deviations of the reference LDA, PBE and Connector[1] densities, i.e., $(n_{\mathrm{LDA}}(\mathbf{r})/n_{\mathrm{QMC}}(\mathbf{r})-1)\times 100\,\%$, $(n_{\mathrm{PBE}}(\mathbf{r})/n_{\mathrm{QMC}}(\mathbf{r})-1)\times 100\,\%$, and $(n_{\mathrm{connector}}(\mathbf{r})/n_{\mathrm{QMC}}(\mathbf{r})-1)\times 100\,\%$. As

[1] the Connector density is th density resulting from the self-consistent KS calculation using $v_{\mathrm{xc}}^{\mathrm{connector}} \equiv v_{\mathrm{xc}}^{h}(n_{\mathbf{r}}^{c,\mathrm{approx}})$ with $n_{\mathbf{r}}^{c,\mathrm{approx}}$ given by (4.7).

also shown in Ref. [14], differences between LDA, PBE and the QMC densities are largest on the atoms and also in other regions of low density, but can still be significant in regions of higher density above the diagonal of a face (second segment of the path), where LDA and PBE are very similar, in contrast to the Connector, which is more similar to the QMC result. Most importantly, the differences between different densities are much larger than the error due to the inversion of the QMC density: while the mean relative error at $i = 20$ is 0.04%, the mean relative differences between the approximate and QMC densities are: 1.93 % for LDA, 1.07 % for PBE and 0.89% for Connector. The inversion error is, however, larger than in the case of the inverted LDA, by about a factor 500 for the maximum relative error and 10^3 for the mean average error. The xc potentials are compared in the middle panel of Fig. 7.3. All three potentials have a similar shape. However, there are differences, and they are largest between QMC on one side, and LDA ,PBE, and Connector on the other side. In other words, our numerically determined and supposedly most accurate KS xc potential turns out to be similar, but still significantly different, from other approximations. This becomes clearer in the bottom panel, where the relative differences of LDA, PBE and Connector with respect to the QMC xc potential (aligned at their average value) are shown: these differences are significant, and they are similar for LDA and PBE along most of the path. The mean relative difference with respect to the QMC result for potentials is 3.90 % for the LDA, 3.88 % for the PBE, and 2.36 % for the Connector, of similar order, though larger, than the mean relative difference of the densities. This result is stable: the figure also shows the QMC result obtained at $i = 10$, where the maximum and mean absolute errors on the density are 0.90 % and 0.09 %, respectively. The differences with respect to the potential obtained at $i = 10$ can hardly be seen.

Although we have reached sufficient precision on the density, which lies within the QMC error bar, and the xc potential, which shows significant and stable differences with respect to common functionals, one may want to continue the iterations, since Fig. 7.1 shows that the maximum error of the QMC inversion could be decreased further. However, the fact that a plateau is reached in the mean relative error, as the inset in Fig. 7.1 shows, anticipates that one might encounter problems when doing so. The blue curve in the upper panel of Fig. 7.4 shows the density from the QMC inversion at $i = 500$, where the maximum error has decreased from 0.38% to 0.21 %. Indeed, the error is now further away from the QMC error bar in the most critical points along the path, with respect to the $i = 20$ result shown in Fig. 7.2. This, however, merely corresponds to a redistribution of the error, since the mean absolute error has changed from 0.04 % at $i = 20$ to 0.02 % at $i = 500$. Most strikingly, the xc potential obtained from the QMC inversion, shown in the bottom panel of Fig. 7.4, is no longer smooth. It develops spikes that become even more pronounced when one iterates further, while still decreasing the maximum relative error on the density.

Visibly, the algorithm does not succeed in improving the result any further and introduces unexpected features when trying to do so. Difficulties with the inversion procedure have also been reported for finite systems, and

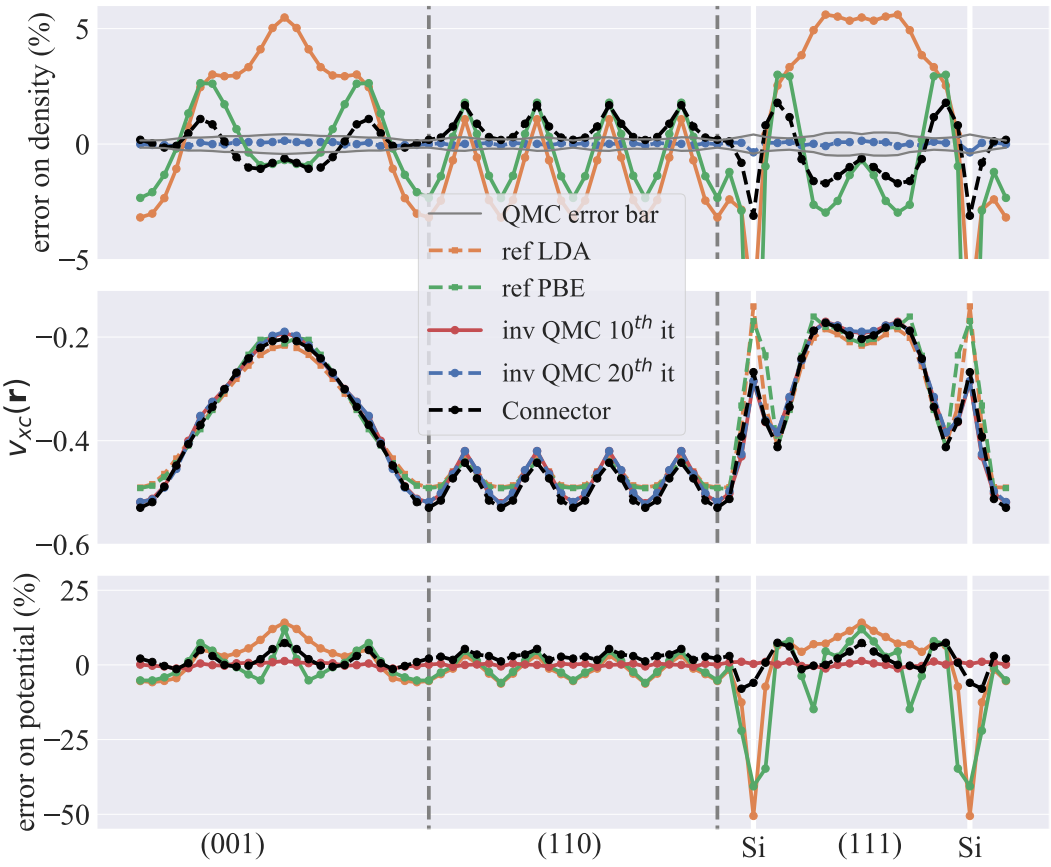

FIGURE 7.3: Density and exchange correlation potential of bulk silicon along a path across the unit cell. The position of atoms are indicated by white vertical lines. For the LDA, PBE, and Connector, density and potential are obtained from a self-consistent KS calculation. For the QMC, the iterative procedure with the QMC density as reference density $n_{\text{ref=n}_{\text{QMC}}}$ has been carried out. The iterative procedure starts at 0.3 $v_{\text{xc}}^{\text{LDA}}$. The initial potential is shifted by -0.2 a.u.. The potential $v_{\text{xc}}^{\text{QMC,i}}$ is obtained after $i = 20$ iterations. The density $n^{\text{QMC,20}}$ is then recalculated using $v_{\text{xc}}^{\text{QMC,20}}$ in the KS equation. The maximum error on the density at $i = 20$ compared to the reference n_{QMC} is 0.38 %, and the mean absolute error is 0.04%. Top panel: in blue, relative error in percent of the density $n^{\text{QMC,20}}(\mathbf{r})$ with respect to the reference QMC density $n_{\text{QMC}}(\mathbf{r})$. For comparison, the relative differences (in percent) with respect to $n_{\text{QMC}}(\mathbf{r})$ of the self-consistent LDA (orange), PBE (green), and Connector (black) densities are also shown. In grey, the stochastic error bar of QMC. Middle panel: $v_{\text{xc}}^{\text{QMC,20}}$ (blue), and, for comparison, $v_{\text{xc}}^{\text{LDA}}$ (orange), $v_{\text{xc}}^{\text{PBE}}$ (green), and $v_{\text{xc}}^{\text{connector}}$ (black), as well as $v_{\text{xc}}^{\text{QMC,10}}$ (red). The average potentials are aligned. Bottom panel: relative difference (in percent) of LDA (orange), PBE (green), Connector (black), and QMC at i=10, xc potentials, respectively, with respect to $v_{\text{xc}}^{\text{QMC,20}}(\mathbf{r})$.

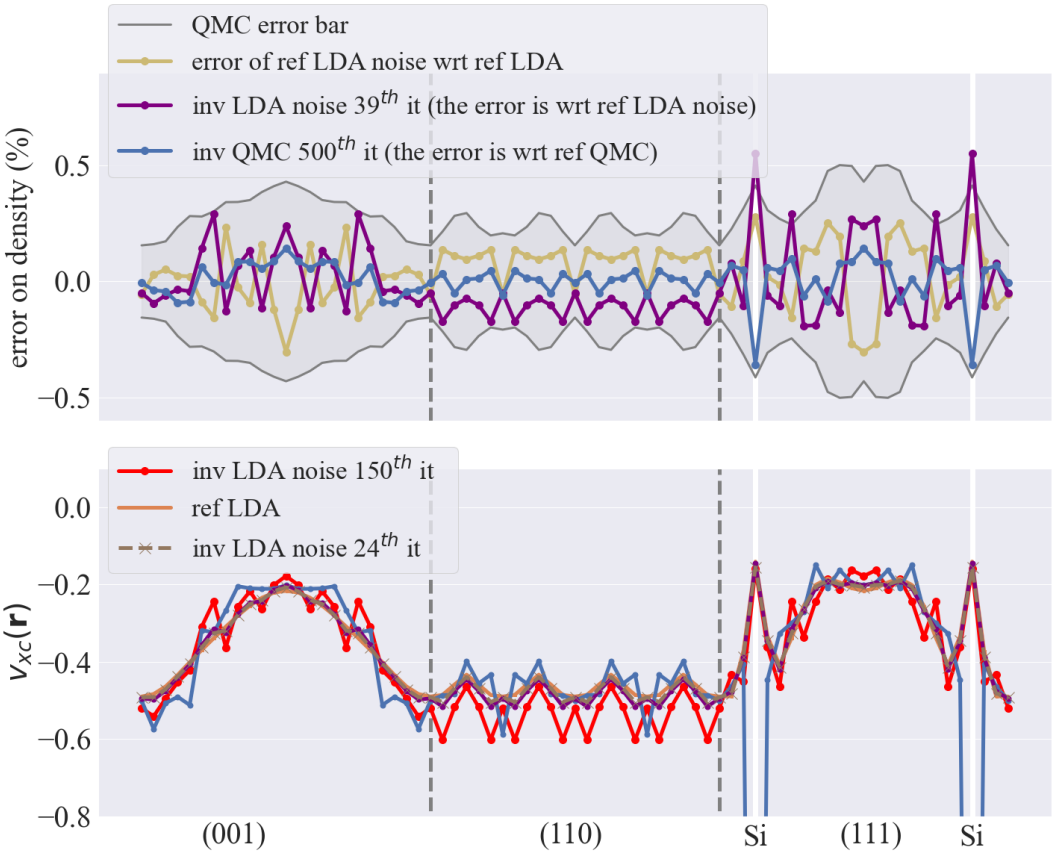

FIGURE 7.4: Density and exchange correlation potential of bulk silicon along a path across the unit cell. The position of atoms are indicated by white vertical lines. Top panel: For the density, relation between noise and errors of the iterative procedure. The yellow curve is $(n^{\mathrm{LDA+noise}}(\mathbf{r})/n^{\mathrm{LDA}}(\mathbf{r})-1)$ in percent, where $n^{\mathrm{LDA+noise}}(\mathbf{r})$ is the LDA density from the KS calculation decorated with a multiplicative gaussian noise. The noise lies within the stochastic error bar of the QMC calculation (grey lines). The red curve uses $n^{\mathrm{LDA+noise}}(\mathbf{r})$ as reference density, from which the xc potential is obtained after $i = 150$ iterations ($v_{\mathrm{xc}}^{\mathrm{LDA+noise,150}}$), where the maximum relative error is 0.54 %. The density $n^{\mathrm{LDA+noise,150}}$ is then recalculated using $v_{\mathrm{xc}}^{\mathrm{LDA+noise,150}}$ in the KS equation. The iterative procedure starts at 0.3 $v_{\mathrm{xc}}^{\mathrm{LDA}}$. The initial potential is shifted by -0.2 a.u.. The curve shows $(n^{\mathrm{LDA+noise,150}}(\mathbf{r})/n^{\mathrm{LDA+noise}}(\mathbf{r})-1)$ in percent. For comparison, the same result but for $i = 39$ is shown (in purple), where the noisy LDA maximum absolute relative error on the density has its first minimum, which is 0.56 %, and the mean absolute relative error is 0.15 %. The blue curve is $(n^{\mathrm{QMC,500}}(\mathbf{r})/n^{\mathrm{QMC}}(\mathbf{r})-1)$, the QMC error at 500 iterations (with a maximum absolute relative error of 0.21 % and a mean absolute relative error 0.02%). Bottom panel: exchange-correlation potential. The orange curve gives the LDA potential calculated with the clean LDA density. In red, potential obtained by inversion with the noisy LDA density as reference, at $i = 150$. In purple and brown, same but at $i = 39$ and $i = 24$, respectively. In blue, $v_{\mathrm{xc}}^{\mathrm{QMC,500}}(\mathbf{r})$.

they have been attributed to the finite basis set which may introduce an inconsistency between density and external potential [92, 87, 93, 94, 95].

7.2.2 Simulating the QMC stochastic noise

As we have verified above, the results of the inversion are sufficiently well converged, but another problem arises: the QMC density has stochastic noise. In order to show that this small noise may be responsible for the observed behavior, Fig. 7.4 shows results for the inversion of the LDA system, but where the LDA density has been decorated with a multiplicative gaussian noise within the QMC stochastic error bar. To appreciate what this means, the yellow curve in the upper panel gives the relative difference of the noisy LDA density with respect to the clean one. The error of the inversion of the noisy LDA data is displayed in Fig. 7.1 (purple curve). It behaves similarly to the QMC inversion error: the maximum absolute relative error decreases rapidly and reaches a minimum, from whereon a slight increase followed by a decrease is noted. The mean absolute relative error, instead, reaches a plateau. The inversion error on the density is given by the purple curve in the upper panel of Fig. 7.4, representing $(n^{\mathrm{LDA+noise,i=39}}(\mathbf{r})/n^{\mathrm{LDA+noise}}(\mathbf{r})-1)$ in percent. The relative error is of similar magnitude as the noise itself, as in the QMC case. The bottom panel shows xc potentials: the red curve is the xc potential resulting from inversion of the noisy LDA data at $i = 150$. It has spikes that are of the same order as those of $v_{\mathrm{xc}}^{\mathrm{QMC,500}}$ and that are in percentage orders of magnitude larger than the noise of the density, again as in the case of $v_{\mathrm{xc}}^{\mathrm{QMC,500}}$. With such an error bar, one would not be able to distinguish the LDA and QMC potentials. By the way of contrast, the xc potential resulting from the noisy LDA data but at only $i = 39$ iterations, where the maximum absolute relative error on the density has its minimum, shows only very small spikes. The result is stable in the range of iterations preceding that minimum: the figure also shows the result for $i = 24$, with a virtually indistinguishable potential. Moreover, this potential is close to the clean LDA potential, given by the orange curve. In this range of iterations, the remaining difference may reflect the difference between noisy and clean densities, and we can consider the resulting potential to be reliable. The spikes that develop by iterating further, instead, will increasingly also be triggered by the fact that the noisy density and the KS LDA hamiltonian are not completely consistent, which means that the ultimately converged result cannot be found.

The observations concerning the behavior of the noisy LDA are strictly analogous to our QMC-based results. This gives strong evidence for the fact that the inversion problem of the QMC data after a certain number of iterations is indeed due to the stochastic noise of the QMC. Moreover, it suggests that a sufficiently reliable xc potential is obtained by taking the result in the range where a stable and relatively smooth potential is obtained, and before the mean error on the density stops to decrease. In the present case, this confirms the choice $i = 20$, for which the QMC xc potential is given in Fig. 7.3. In

other words, this xc potential is, to the best of our knowledge, today's most precise estimate for the true xc potential of bulk silicon.

7.2.3 Sodium Chloride

In Fig. 7.5 we show the errors as a function of the number of iterations, for sodium chloride. The errors of the inverted QMC density reflect the same trends as the silicon case. They decrease rapidly before reaching a plateau around the iteration $i = 150$, with a maximum absolute error of 0.32% and a mean absolute error of 0.04%. The errors then decrease slightly, reaching 0.29% and 0.03% for the maximum and the mean absolute error, respectively, at $i = 200$. Contrary to the case of Si, the stochastic QMC noise does not lead to the appearance of spikes in the xc potential, as illustrated in Fig. 7.6. This could be because the noise is very small on the Na and Cl atoms where the density is extremely significant. In order to investigate this further, the LDA decorated with a Gaussian noise of the same magnitude as the QMC, is also shown in Fig. 7.5. Its xc potential does not have any significant spikes, at least until $i = 200$, the errors of this potential as function of the iteration number are plotted in 7.5 with open circles. Similarly to Fig. 7.3 for silicon, in Fig. 7.7 we show the error on the density and the xc potential along a path for NaCl. The QMC-derived xc potential differs from the LDA, PBE, and Connector especially on the sodium atoms, where the density shows a rapid oscillation. At first sight, however, and as in the case of silicon, it is difficult to detect important differences between the approximate and the QMC-derived potentials. While it is exciting to see the numerically exact xc potential for real semiconductors and insulators, in order to gain more insight and elucidate several general fundamental points, it is useful to switch to a representation that highlights the essence of the difference.

7.3 Non-locality of the KS exchange correlation functional

In the LDA, $v_{\mathrm{xc}}(\mathbf{r})$ is a monotonic function of $n(\mathbf{r})$. The exact KS potential is a functional of the density everywhere, which means that the potential can take different values in different points $\mathbf{r}$ where the density, instead, is the same. This expresses the fact that $v_{\mathrm{xc}}(\mathbf{r})$ depends not just on the local density, but also on the environment. Scattering of the map $n(\mathbf{r}) \rightarrow v_{\mathrm{xc}}(\mathbf{r})$ therefore exhibits the non-locality of a potential. One could also imagine some particularly simple systems, where in a given density range only one kind of environment exists. In that case the potential might remain a function $v_{\mathrm{xc}}(n(\mathbf{r}))$, but it could be different from $v^h_{\mathrm{xc}}(n)$ of the homogeneous electron gas, and hence the LDA, due to the influence of the environment. This is therefore also a possible consequence of non-locality of the true functional. In the general case, one would expect several curves reflecting several kinds of environment, maybe superposed by some scattering of the results.

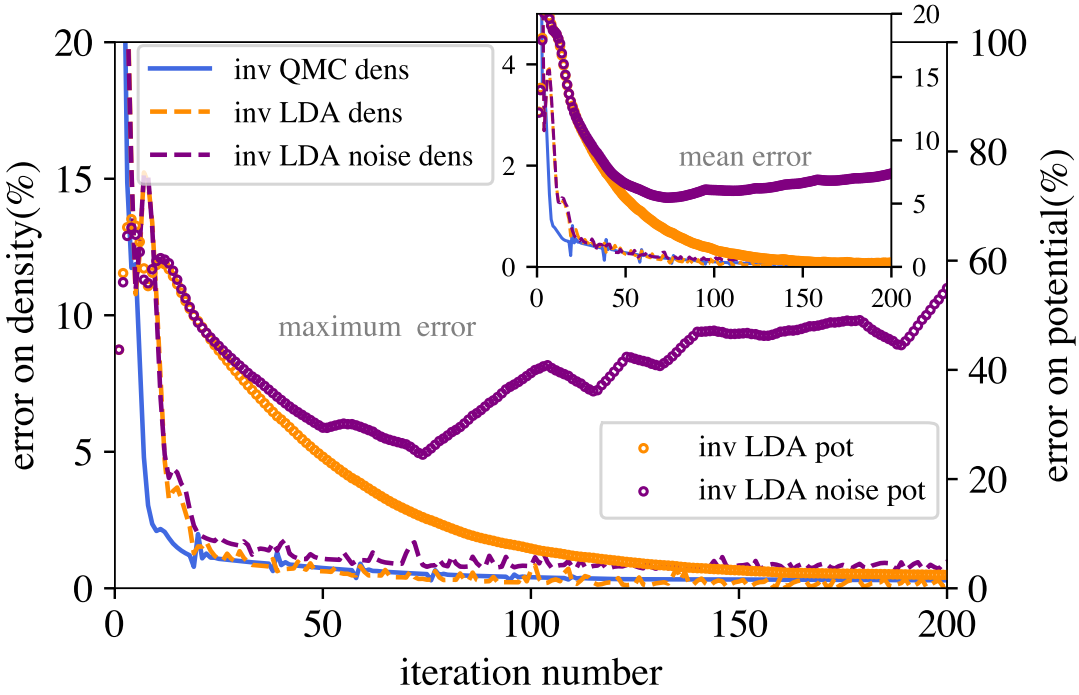

FIGURE 7.5: Same as Fig. 7.1, but for NaCl. For these calculations, the starting v_{xc} is 30% LDA with a shift of -0.4 a.u.. The shift has been changed compared to silicon case in order to ensure the negativity of the potential.

Fig. 7.8 and 7.9 show our results for the map $n(\mathbf{r}) \rightarrow v_{xc}(\mathbf{r})$ in silicon and NaCl, respectively. The reference LDA result simply reproduces the universal function $v_{xc}(n)$ of the homogeneous electron gas. In silicon, the PBE and Connector results are also dominated by a simple monotonic function, but they are steeper than the LDA. Moreover, they are slightly scattered, and a new branch appears at low densities. The points on the new branch stem from data close to the atoms, where the potential is rapidly varying and the LDA breaks down. As expected, inversion of the noisy LDA data leads to a more scattered potential, shown in the inset for $i = 24$ and $i = 39$. However, the result is essentially a scattered version of the clean LDA result, slightly blurred according to the number of iterations, and no additional features are caused by the noise. The QMC xc potential is blurred similarly to the noisy LDA result, and we can therefore not discern to which extent some scattering around a function is an intrinsic feature of the exact KS potential. However, similarly to the PBE and Connector, one can identify a dominant curve, and with respect to the LDA, two main changes are seen: the curve is steeper than the LDA one, and near the atoms an additional branch appears. The change in slope of the main branch with respect to the LDA goes in the same direction as in the PBE result, and it is more pronounced as the Connector result suggests. Also the branching happens in a similar region as in the case of PBE and Connector. It departs in the same direction as the Connector contrary to PBE which goes in the wrong direction. We have carefully examined

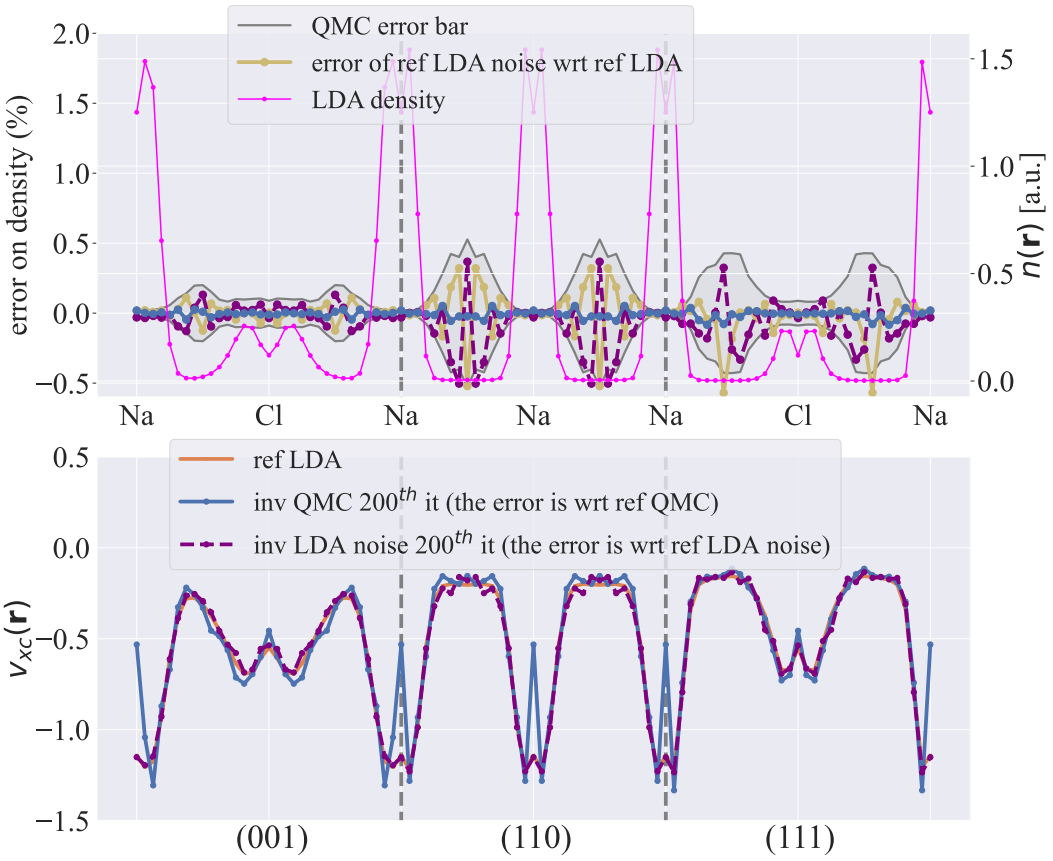

FIGURE 7.6: Influence of the noise on the inverted xc potential for NaCl, similar to Fig. 7.4. Here we show the error on density (upper panel) and the xc potential (lower panel) from the last iteration for both QMC and noisy LDA. The yellow curve is $(n^{\mathrm{LDA+noise}}(\mathbf{r})/n^{\mathrm{LDA}}(\mathbf{r}) - 1)$ in percent, where $n^{\mathrm{LDA+noise}}(\mathbf{r})$ is the LDA density from the KS calculation decorated with a multiplicative gaussian noise. For all iterations, neither $v_{\mathrm{xc}}^{\mathrm{QMC}}$ nor $v_{\mathrm{xc}}^{\mathrm{LDA+noise}}$ develop significant spikes as in the case of silicon. Nevertheless, the influence of the noise on the noisy LDA is slightly visible between atoms. In the same regions the QMC-derived potential shows a similar spikes.

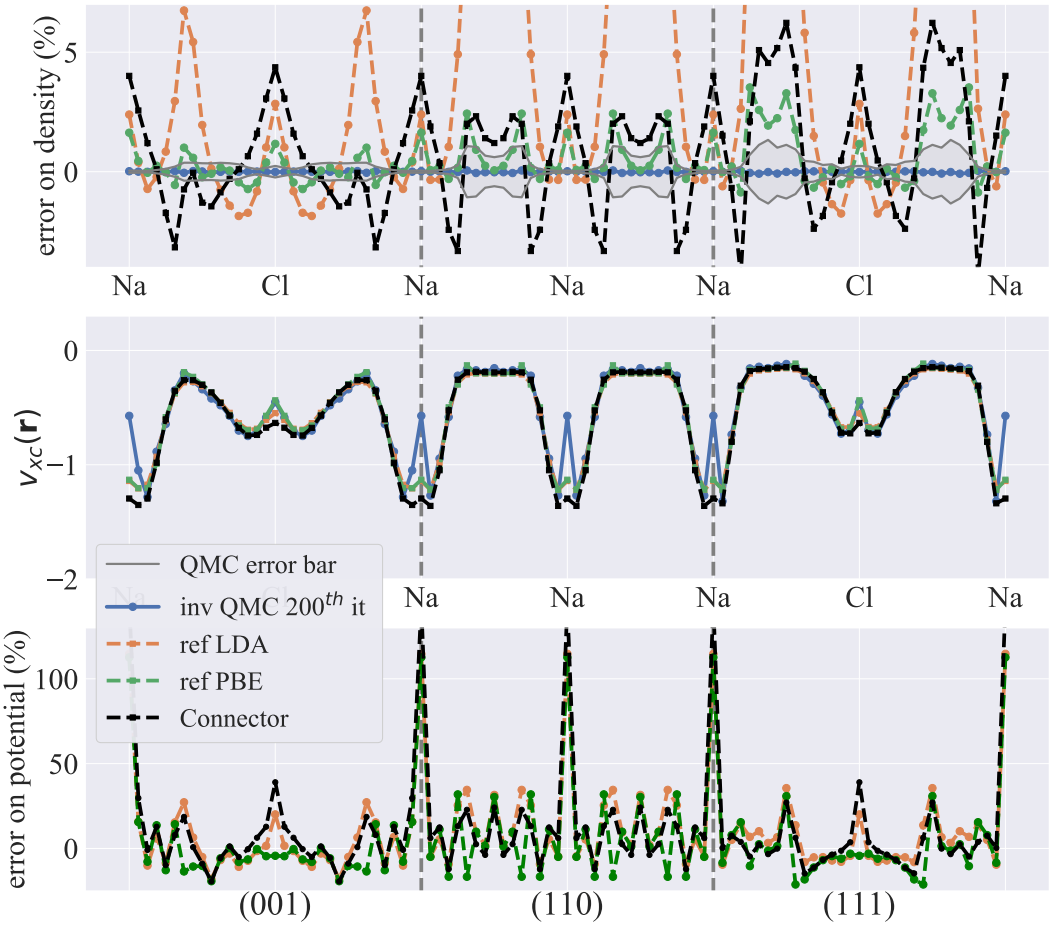

FIGURE 7.7: Density and exchange correlation potential of sodium chloride along a path across the unit cell, similar to Fig. 7.3. Here, the iterative procedure starts at 0.3 v_{xc}^{LDA}. The initial potential is shifted by -0.4 a.u.. The potential $v_{xc}^{QMC,i}$ is obtained after $i = 200$ iterations. The density $n^{QMC,200}$ is then recalculated using $v_{xc}^{QMC,200}$ in the KS equation. The maximum error on the density at $i = 200$ compared to the reference n_{QMC} is 0.29 %, and the mean absolute error is 0.03%.

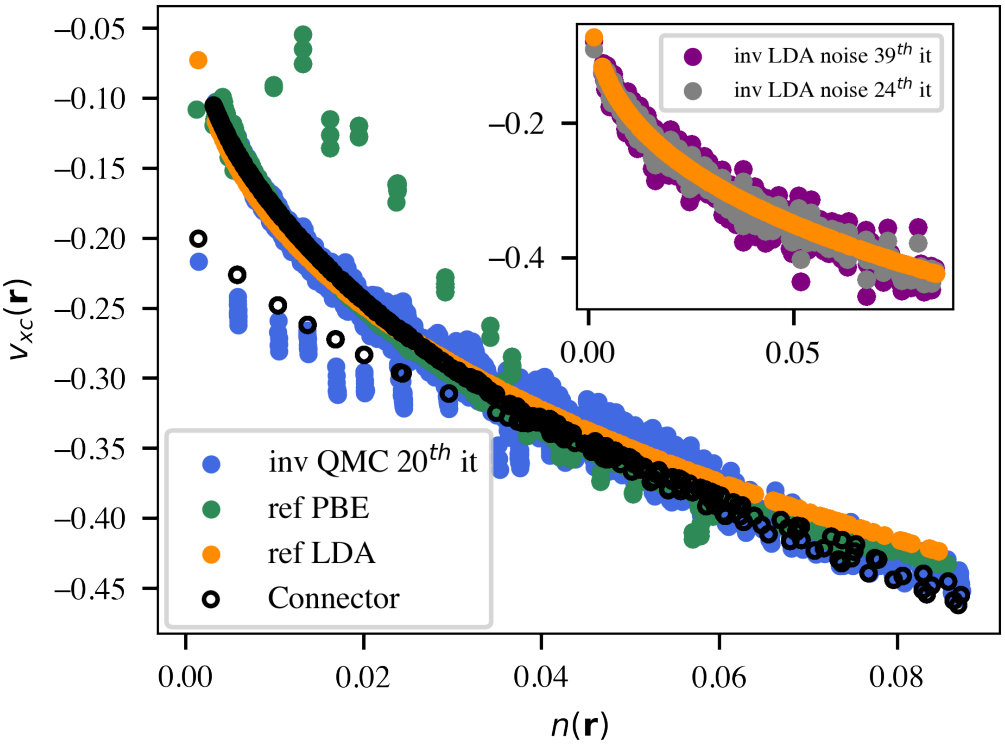

FIGURE 7.8: Map of the xc potential versus the local density in silicon. Results of the inversion of noisy LDA and QMC are compared to clean LDA, PBE, and Connector potentials. Each v_{xc} is plotted against its own density. The main panel shows KS LDA, PBE and Connector potentials compared to the QMC inversion result at 20 (minimum of maximum absolute relative error of the density) iterations. In the inset, KS LDA is compared to the inversion of noisy LDA at 24 (smooth potential) and 39 (minimum of maximum relative error of the density) iterations.

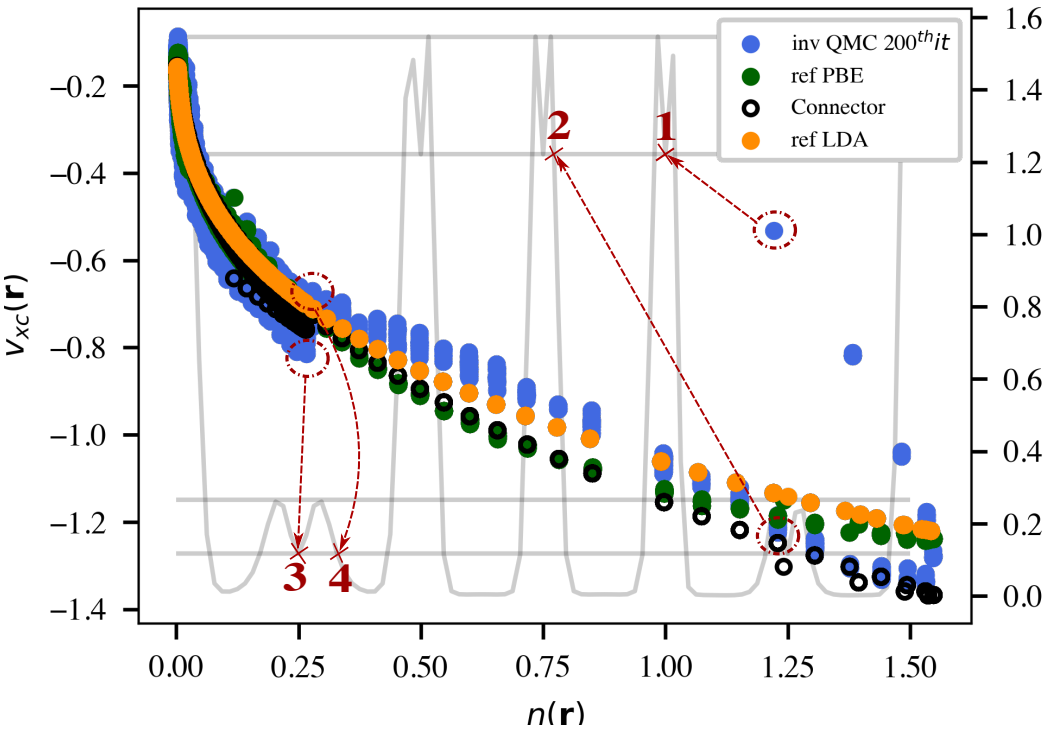

FIGURE 7.9: Map of the xc potential versus the local density in NaCl. The result of the inversion of the QMC density is compared to LDA and PBE potentials. Each v_{xc} is plotted against its own density. The main panel shows KS LDA, PBE and Connector potentials compared to the QMC inversion result at the 200^th iteration. In the background, density of NaCl along the path (scale on right side). Numbers indicates the regions to which the data points belong. Data point 1 corresponds to the potential on a Na atom, while data point 2 which has the same density corresponds to the potential in an environment very close to the atom. Similarly, data point 3 from the lower branch corresponds to the potential on a Cl atom, while the data point 4 corresponds to the potential in the vicinity of this atom.

the branch results. The QMC branch is stable as a function of the iterations, which suggests that it is reliable. Interestingly, the correction of the main branch with respect to the LDA $v_{\rm xc}^{\rm LDA}$ may be translated in different ways, in particular: $v_{\rm xc}^{\rm corr}(\mathbf{r}) = F_e(n(\mathbf{r}))v_{\rm xc}^{\rm LDA}(n(\mathbf{r}))$ with a correction factor F_e that depends on the local density and that is determined by the environment e, or $v_{\rm xc}^{\rm corr}(\mathbf{r}) = v_{\rm xc}^{\rm LDA}(\mathcal{F}_e(n(\mathbf{r}))n(\mathbf{r}))$, where $\mathcal{F}_e$ stretches the density axis. Such correction factors are reflected in the GGAs, where the environment-dependence is obtained through the gradient, as we can see in (2.62).

The QMC map for NaCl in Fig. 7.9 looks different, but it suggests a similar interpretation: we find a main branch that corresponds to a slightly modified LDA, an additional branch at low densities and another additional branch at high density. In background, the figure also shows the density along the path. Numbers indicate to which place selected data points correspond. For example, data point 1 on the additional high-density branch corresponds to the potential on the sodium atom, where the density is very quickly varying, which explains why the LDA completely fails. Data point 2, instead, corresponds to a place with similar density but located in a more gentle environment, although the gradient of the density is still significant. As expected, here we are on the main branch, which is however modified with respect to the LDA. Both PBE and Connector yield an extra branch at low density near the Cl atom (data point 3 and 4). It is not clear in the map which one is more accurate, however Fig. 7.7 may suggest that PBE describes better the environment in this regime, since it yields a smaller error on the density in these regions. In the high-density regime, the Connector overestimates the potential. This is due to the high densities of the surrounding points, as one can see from the sketch of the density. In fact, the Connector takes a weighted average of this environment, and so it misses the reduction of the density on the Na atom (data point 1). Instead, PBE better captures this information. This is likely due to its explicit dependence on the gradient of the density. In the main branch PBE and Connector show a similar performance.

More QMC results for different materials presented as maps such as the one in Fig. 7.8 may give precious insight about the most efficient way to introduce a correction factor, e.g., F versus $\mathcal{F}$, and about the most important features distinguishing different environments.

7.4 Significance of the Kohn-Sham potential

The iteration procedure for inverting the xc potential of silicon reveals a striking observation: very different $v_{\rm xc}(\mathbf{r})$ can yield very similar densities[2]. In particular, the extremely spiky potentials obtained at higher iterations in the inversion of the noisy densities still correspond to a very small error in the density, of the order of, or smaller than, the noise itself. This raises the question what will happen to other KS observables: even though, as discussed above, these do not by themselves have direct physical meaning in an exact sense, they can still be seen as an approximation to the physical quantities

[2] a similar observation for finite systems has been pointed out in Ref. [89].

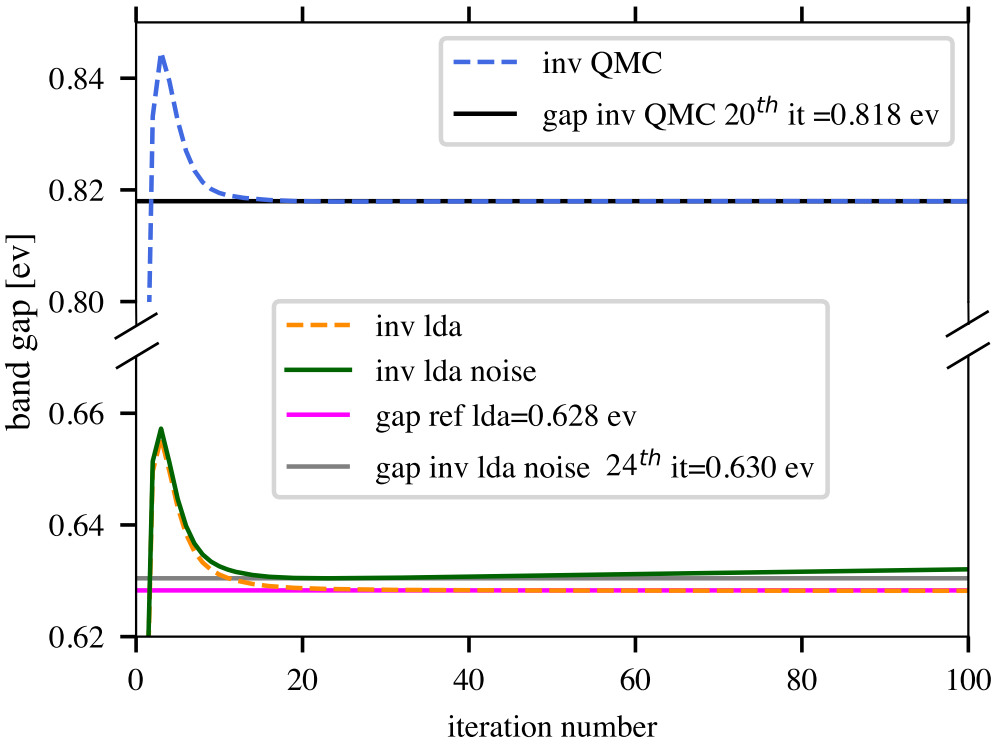

FIGURE 7.10: Band gap of silicon: convergence with number of iterations for QMC (upper panel) and clean and noisy LDA (lower panel). Horizontal lines are the KS gap for the clean LDA, and estimated best result from iterative procedure for noisy LDA and QMC. Note the change in scale.

[96, 97], and they are frequently used as starting points for calculations in a more appropriate framework, such as many-body perturbation theory [1]. We therefore show in Fig. 7.10 the KS band gap of silicon as a function of the number i of iterations at which the KS potential and corresponding density were calculated. The result converges very rapidly with i and remains stable even after the potential has developed huge spikes. The same good convergence property is found for NaCl, as shown in Fig. 7.11. This means that very different xc potentials can yield not only very similar densities, but also very similar KS observables more in general. Moreover, Fig. 7.10 shows that the gaps corresponding to clean and noisy LDA densities are almost indistinguishable, i.e., the noise does not affect KS observables. It confirms the statement, mostly based on findings from finite systems, that examining the xc potential alone is not sufficiently meaningful [98]. It also suggests that an effort is needed to distinguish in the KS potential crucial features, which must be contained in good functionals, from others that may be quantitatively strong in the potential, but insignificant for its effects.

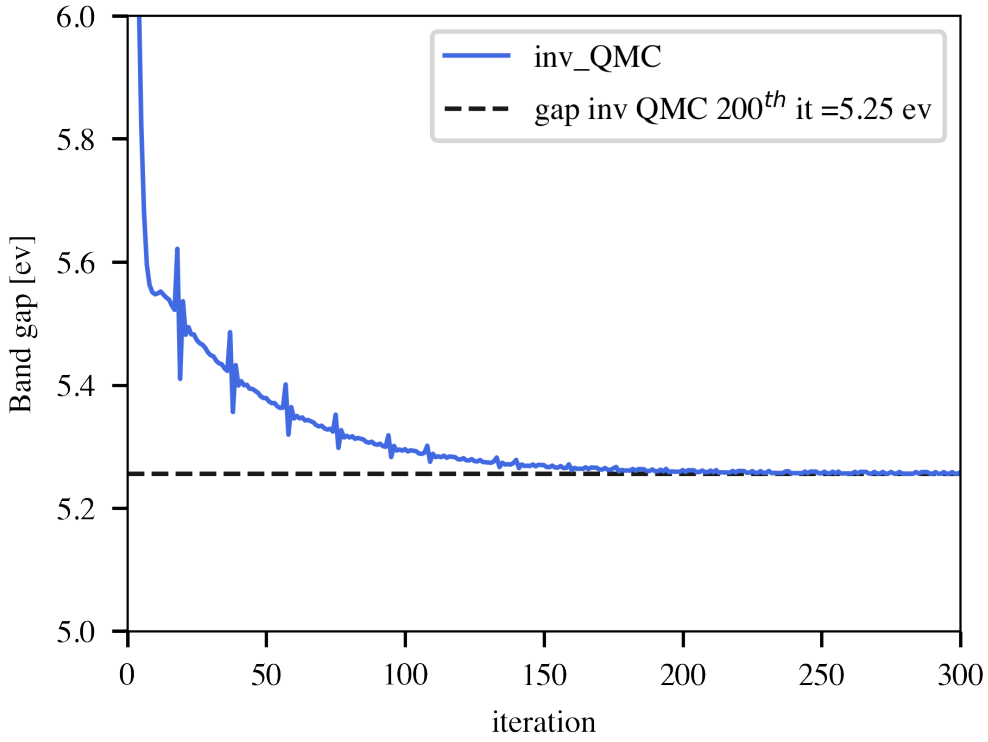

FIGURE 7.11: Band gap of NaCl: convergence with number of iterations for QMC. Horizontal line is the converged KS gap iterative procedure.

7.4.1 Kohn-Sham band gap

The study of the KS band gap is interesting by itself, since there is long-standing debate concerning the difference between observables in the real and in the Kohn-Sham auxiliary system. In absence of knowledge of the exact Kohn-Sham potential, it was not possible to discriminate between the discrepancies due to approximations of the functional, and discrepancies due to the difference between the (even exact) Kohn-Sham system itself and the real material. Precious hints were already given by work on model systems; for example, Knorr and Godby [99] determined the xc potential by inversion from the density of a finite one-dimensional model semiconducting wire that was then extrapolated to infinite length. Most of the band gap error was shown to be due to the fact that the exact KS eigenvalue gap differs from the fundamental electron addition and removal gap, and not to approximations. Indeed, the KS eigenvalue gap calculated at fixed particle number disregards the derivative discontinuity of the exact xc potential upon change of particle number [100, 101, 102]. Since the numerically exact density and/or xc potential can be obtained only for very few systems, several studies used the link between the xc potential and the self-energy given by the Sham-Schlüter equation [101] in order to extract v_{xc} from the self-energy. These include work on a two-plane wave model [101, 103], the surface barrier for semi-infinite jellium [54], and the study of several real semiconductors and insulators [104, 105, 106, 107, 108, 109]. These studies confirmed that the error inherent in using Kohn-Sham eigenvalues instead of true electron addition and removal energies is significant. However, the approaches used to determine the potential involved themselves approximations whose quantitative impact on the findings are not known: first, the Sham-Schlüter equation was linearized in all studies. Second, the self-energy itself was approximated in many-body perturbation theory, mostly on the GW level. With the present study, we finally do have a numerically exact Kohn-Sham potential at hand for real materials, and we can therefore draw definite conclusions concerning the band gap, of standard semiconductors and insulators.

Results for the converged band gap of silicon and NaCl are shown in Table 7.1. For silicon, our numerically exact minimum indirect KS band gap is 0.82 eV, about 30 % larger than the KS gap of 0.63 eV calculated in LDA, and significantly smaller than the experimental gap of 1.17 eV. The Connector and PBE gaps of 0.86 eV and 0.80 eV, respectively, are close to the QMC-derived value of 0.82 eV. In NaCl, the situation is similar, with the QMC-derived gap about 14% greater than the LDA one, 7% larger than the Connector, and just 3% larger than the PBE gap. Our QMC derived KS gaps confirm the conclusion of Ref.[104, 105] and thus definitely highlight the fact that a good KS potential will not yield a "good" band gap. Overall, the band gap is an excellent illustration for the fact that the exact Kohn-Sham system is an auxiliary system designed to use the exact density, but not other observables.

TABLE 7.1: Exact KS band gaps

v_{xc}	KS gap Si (ev)	KS gap NaCl
AFQMC	0.82	5.25
PBE	0.80	5.08
Connector	0.86	4.87
LDA	0.63	4.59

7.4.2 Exchange correlation energy

So far, we have obtained numerically exact xc potentials for silicon and sodium chloride. Here, we use these results together with the total energy calculated by Chen *et al.* [14] to give benchmarks for the xc energy of Si and NaCl.

From the total energy, E_{tot}, the xc energy, E_{xc}, can be extracted as follows

$$E_{\text{xc}} = E_{\text{tot}} - \left\{ \sum_{i}^{N/2} \epsilon_i - E_{\text{Hartree}} - \int d\mathbf{r} n(\mathbf{r}) v_{\text{xc}}(\mathbf{r}) + E_{\text{Ewald}} + E_{\text{PspCore}} \right\}, \tag{7.4}$$

where ϵ_i are KS eigenvalues, and E_{Ewald} contains the resulting energy from the ion-ion interaction as well as the interaction of the average electron density with the ions and with itself. The term E_{PspCore} is a contribution due to the non-Coulombic part of the local pseudopotential.

The xc energy of Si and NaCl is plotted in Fig. 7.12 as a function of the number of iterations at which the xc potential and corresponding density were calculated. In the case of silicon, the result converges very rapidly, and the value of the xc energy resulting from the use of the smooth potential at the 20^{th} iteration remains stable, even after the potential develops enormous spikes. This confirms our prior observation regarding the KS band gap, namely that extremely very different xc potentials can yield very similar observables. The same good convergence property is found for NaCl. In this case, we take the xc energy from the last iteration, because the xc potential does not develop spikes when the number of iterations increases, which means that we can trust the inverted xc potential even after large number of iteration.

7.5 Conclusion

In conclusion, we have constructed accurate xc potentials for Si and NaCl using a simple algorithm that involves working with the xc potential alone and imposing a shift that ensures the potential is always negative. Using the resulting potentials we calculated the band gap of the corresponding Kohn-Sham system and the xc energy of Si and NaCl. In the case of silicon, we showed that the stochastic noise of the QMC data may limit the precision that can be reached for the xc potential in itself. The reasons may be that

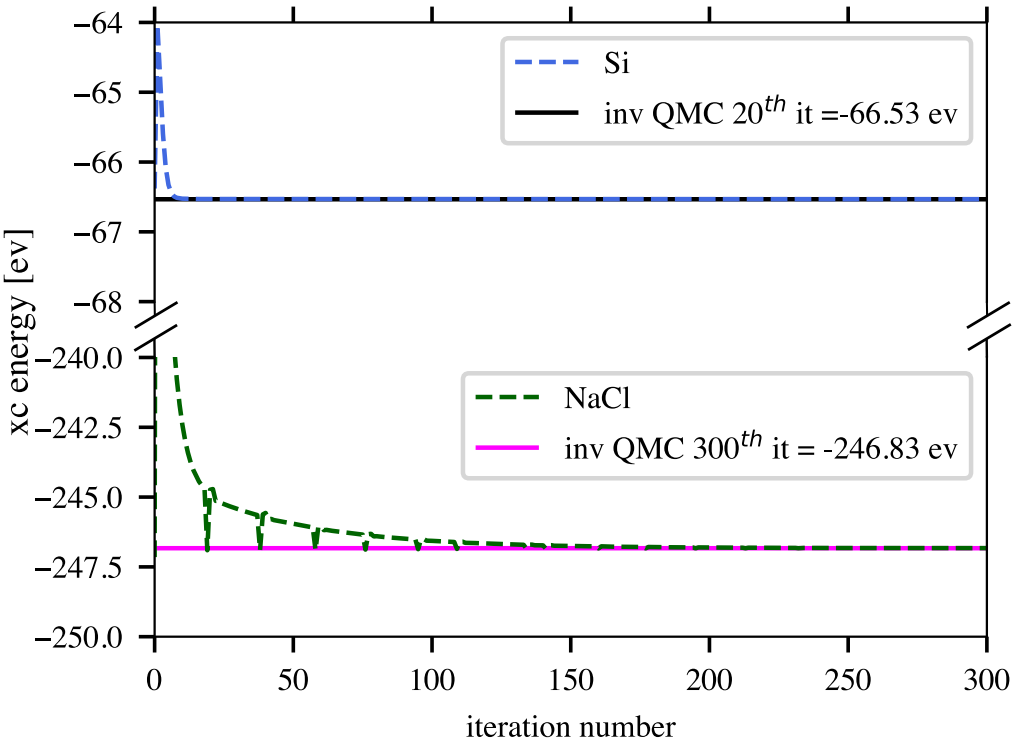

FIGURE 7.12: Exchange correlation energy : convergence with number of iterations for Si (upper panel) and NaCl (lower panel). Horizontal lines are the xc energy that we used in the rest of the thesis. Note the change in scale.

noisy data reflect a more non-local dependence of the density on the potential, which is not included in the algorithm, or that the noise makes the density inconsistent with the external potential. Whereas the calculation of the xc potential is delicate and suffers from noise, KS band gap, charge density and xc energy do not, and can be determined with high precision. This means that the noise does not affect observables in general. We have also shown that the exact KS band structure and band gaps are slightly larger than the LDA ones for the systems studied here, and significantly smaller than the measurable quasi-particle gaps, such definitely confirming a prior hypothesis. For both NaCl and Si, The exact (from QMC) xc potential can be described as an ensemble of multiple simple functions of the local density. Which of these functions is appropriate depends on the environment, which means, the non-locality is taken into account through an environment-dependence of the function to choose. In the case of silicon, the connector xc potential is capable of recovering the majority of the environment-dependence of the simple functions. PBE, on the other hand, works better with NaCl, but it underestimates this dependence.

Chapter 8

Approximating the exchange correlation energy

The results of the connector xc potential for the density of silicon and sodium chloride in Ch. 6, confirm that connector theory is a promising strategy for developing new simple functionals capable of outperforming the LDA and many other functionals. In this chapter, we will first examine whether we can construct a functional for the xc energy using the connector xc potential. Then, we will discuss another connector designed specifically for the xc energy density, $\epsilon_{\rm xc}(\mathbf{r})$. Here, we also use silicon and sodium chloride to evaluate the approximations. The benchmark xc energies are extracted from total energies computed using QMC [14]. In order to do so, we make use of the inverted xc potentials calculated in the previous chapter, which yield the QMC densities.

8.1 Energy from the exchange correlation potential

The xc potential is the functional derivative of the xc energy functional, so one can think about a functional integration of the connector xc potential in order to obtain the corresponding energy functional [110]. Nevertheless, we want to avoid this complicated scheme since it is an ill defined problem and very heavy numerically. Instead, in the following we will express the xc energy explicitly in terms of the xc potential, so that we can profit from the accurate approximation of the latter to estimate the xc energy. In principle, the xc energy functional can be written as

$$E_{\rm xc}[n] = \int d\mathbf{r}' n(\mathbf{r}')\epsilon_{\rm xc}([n],\mathbf{r}'). \tag{8.1}$$

By taking the functional derivative of this equation we get

$$v_{\rm xc}([n],\mathbf{r}) = \epsilon_{\rm xc}([n],\mathbf{r}) + \int d\mathbf{r}' n(\mathbf{r}')\frac{\delta\epsilon_{\rm xc}([n],\mathbf{r}')}{\delta n(\mathbf{r})}, \tag{8.2}$$

or

$$\epsilon_{\rm xc}([n],\mathbf{r}) = v_{\rm xc}([n],\mathbf{r}) - \int d\mathbf{r}' n(\mathbf{r}')\frac{\delta\epsilon_{\rm xc}([n],\mathbf{r}')}{\delta n(\mathbf{r})}. \tag{8.3}$$

Hence, we can write the xc energy using the xc potential term explicitly as

$$E_{\mathrm{xc}}[n] = \int d\mathbf{r} n(\mathbf{r}) v_{\mathrm{xc}}([n], \mathbf{r}) - \int d\mathbf{r} d\mathbf{r}' n(\mathbf{r}) n(\mathbf{r}') \frac{\delta \epsilon_{\mathrm{xc}}([n], \mathbf{r}')}{\delta n(\mathbf{r})}. \tag{8.4}$$

From this equation we see that we need two ingredients to construct the xc energy function: the xc potential and the functional derivative of the xc energy density, $\frac{\delta \epsilon_{\mathrm{xc}}([n],\mathbf{r}')}{\delta n(\mathbf{r})}$. For the first term, we aim to use the connector xc potential (6.2) in order to examine its utility in improving the energy. However, because we lack a similar connector approximation for the second term, we will approximate it using well-known functionals such as LDA and PBE. Before we discuss the approximate xc energy for Si and NaCl, let us first consider the contribution of each term in (8.4), as this allows us to determine what is the dominant term, whose approximation is more significant for the xc energy.

8.1.1 Dominant term of the exchange correlation energy

The exchange correlation energy in (8.4) can be divided into two terms:

$$E_v = \int d\mathbf{r} n(\mathbf{r}) v_{\mathrm{xc}}([n], \mathbf{r}), \tag{8.5}$$

and

$$E_{\delta\epsilon} = - \int d\mathbf{r} d\mathbf{r}' n(\mathbf{r}) n(\mathbf{r}') \frac{\delta \epsilon_{\mathrm{xc}}([n], \mathbf{r}')}{\delta n(\mathbf{r})}. \tag{8.6}$$

We estimated these terms for three materials: silicon, sodium chloride, and solid helium, using various approximations. The data, summarized in table 8.1, show that E_v is always the part that contributes the most to the total xc energy, with an absolute value more than four times that of $E_{\delta\epsilon}$. This is interesting because we can readily estimate this term using the connector xc potential, allowing us to investigate the transferability of the connector approximation quality from the potential to a new observable, the xc energy. It is worth noting that in an extended system, the inverted potential is defined up to a constant, and therefore comparing the LDA or PBE estimation of each term separately to the QMC one is not necessary significant. However, the sum of E_v and $E_{\delta\epsilon}$, i.e., the xc energy, is well defined.

8.1.2 Results and comparison with other approximations

In table 8.2 we benchmark the xc energy of silicon and sodium chloride resulting from using LDA, PBE and the connector approximation. The latter consists of two parts: first, E_v that is calculated using the connector (4.7) for the xc potential. The remaining part, $E_{\delta\epsilon}$, is calculated using LDA or PBE. For silicon, the results indicate that using the connector v_{xc} for the xc energy yields an improvement over both the LDA and PBE. The optimal result is found by coupling $E_v^{\mathrm{connector}}$ and $E_{\delta\epsilon}^{\mathrm{PBE}}$; this approximation reduces the PBE

	Si		NaCl		He	
	E_v (eV)	$E_{\delta\epsilon}$ (eV)	E_v (eV)	$E_{\delta\epsilon}$ (eV)	E_v (eV)	$E_{\delta\epsilon}$ (eV)
LDA	-85.09	19.83	-314.20	75.73	-28.93	6.78
PBE	-86.98	21.22	-320.17	73.62	-32.20	7.34
QMC	-85.68	19.15	-323.69	76.86	–	–

TABLE 8.1: Comparison of the term (8.5) and (8.6) of the exchange correlation energy for bulk silicon, sodium chloride and solid helium. The results show that E_v is always the largest term, regardless the approximate functional. The QMC results are obtained using the inverted xc potential discussed in the previous chapter.

	Si	NaCl
LDA	-62.26	-238.47
PBE	-65.76	-246.55
Connector (with LDA)	-67.56	-242.32
Connector (with PBE)	-66.17	-244.43
QMC	-66.53	-246.83

TABLE 8.2: Exchange correlation energy in (eV) for Si and NaCl using several approximations. The connector with LDA (PBE) means that we use the connector xc potential for the term E_v and the LDA (PBE) for $E_{\delta\epsilon}$.

error by a factor of two. The same trend is observed for NaCl, however in this case the PBE is the most accurate functional. This is expected since the PBE xc potential is more accurate for NaCl, as we have shown in Ch. 6, when we compared the densities.

Note that taking E_v and $E_{\delta\epsilon}$ from distinct functionals is consistent here, because the LDA, PBE and connector xc potentials all tend to zero when the density becomes infinitesimally small. That is to say that they are not defined up to a constant as the inverted xc potential from the QMC density.

8.2 Connector for the exchange correlation energy

According to the connector scheme discussed in Ch. 3, the connector is in principle different for each object of interest. So there is no optimal density of a HEG for simulating a given material; rather, there is an optimal density of a HEG for simulating a given observable, possibly in a given point and/or at a given frequency. For instance, in Ch. 4, we have discussed an approximate connector that yields a good[1] approximation of the xc potential as shown in Ch. 6. This does not imply that the same connector will also yield a good approximation to the xc energy density, ϵ_{xc} and so to the total energy.

[1] in the sense that a good v_{xc} is the one that yields a good density compared to a benchmark.

Notably, this does not mean that $v_{\mathrm{xc}}(\mathbf{r}) = v^h_{\mathrm{xc}}(n^c_{\mathbf{r},\mathrm{xc}})$ is functional derivative of

$$E^c_{\mathrm{xc}}[n] \equiv \int d\mathbf{r} n(\mathbf{r}) \epsilon_{\mathrm{xc}}(n^c_{\mathbf{r},\mathrm{xc}}) \ : \tag{8.7}$$

the functional derivative of the such defined $E^c_{\mathrm{xc}}[n]$ yields

$$\begin{aligned} \frac{\delta E^c_{\mathrm{xc}}[n]}{\delta n(\mathbf{r})} &= \int d\mathbf{r}' \frac{\delta \left(n(\mathbf{r}') \epsilon_{\mathrm{xc}}(n^c_{\mathbf{r}',\mathrm{xc}}) \right)}{\delta n(\mathbf{r})} \\ &= \int d\mathbf{r}' \Bigg[\delta(\mathbf{r} - \mathbf{r}') \epsilon_{\mathrm{xc}}(n^c_{\mathbf{r}',\mathrm{xc}}) \\ &\quad + n(\mathbf{r}') \frac{d\epsilon_{\mathrm{xc}}(n^c_{\mathbf{r}',\mathrm{xc}})}{dn^c_{\mathbf{r}',\mathrm{xc}}} \frac{\delta n^c_{\mathbf{r}',\mathrm{xc}}}{\delta n(\mathbf{r})} \Bigg] \\ &= \epsilon_{\mathrm{xc}}(n^c_{\mathbf{r},\mathrm{xc}}) + \int d\mathbf{r}' n(\mathbf{r}') \frac{d\epsilon_{\mathrm{xc}}(n^c_{\mathbf{r}',\mathrm{xc}})}{dn^c_{\mathbf{r}',\mathrm{xc}}} \frac{\delta n^c_{\mathbf{r}',\mathrm{xc}}}{\delta n(\mathbf{r})} \end{aligned} \tag{8.8}$$

while the connector xc potential using the same connector, n^c_{xc}, would read

$$v^c_{\mathrm{xc}}(\mathbf{r}) = \epsilon_{\mathrm{xc}}(n^c_{\mathbf{r},\mathrm{xc}}) + n^c_{\mathbf{r},\mathrm{xc}} \frac{d\epsilon_{\mathrm{xc}}(n^c_{\mathbf{r},\mathrm{xc}})}{dn^c_{\mathbf{r},\mathrm{xc}}} \, . \tag{8.9}$$

In order for the two $v^c_{\mathrm{xc}}(\mathbf{r})$ to be the same, the following relation should hold:

$$\int d\mathbf{r}' n(\mathbf{r}') \frac{d\epsilon_{\mathrm{xc}}(n^c_{\mathbf{r}',\mathrm{xc}})}{dn^c_{\mathbf{r}',\mathrm{xc}}} \frac{\delta n^c_{\mathbf{r}',\mathrm{xc}}}{\delta n(\mathbf{r})} = n^c_{\mathbf{r},\mathrm{xc}} \frac{d\epsilon_{\mathrm{xc}}(n^c_{\mathbf{r},\mathrm{xc}})}{dn^c_{\mathbf{r},\mathrm{xc}}} \, . \tag{8.10}$$

This is possible in some circumstances; for example, the first-order connector outlined in (4.5) has a free variable, namely the density at which the derivative is taken, which can be chosen to satisfy the relation. Whether this is a reasonable technique for improving energy and/or potential approximations remains an open question.

A more natural technique to approximate the xc energy is to design a different connector for the xc energy density. If we consider the first-order connector for ϵ_{xc}, we obtain

$$n^{c,\mathrm{approx}}_{\mathbf{r},\epsilon} = \frac{\int d\mathbf{r}' f_\epsilon(\mathbf{r} - \mathbf{r}'; n_0) n(\mathbf{r}')}{f^h_\epsilon(n_0)} \tag{8.11}$$

where, in analogy to f_{xc}, we define $f_\epsilon \equiv \delta\epsilon_{\mathrm{xc}}/\delta n$. To determine this quantity, let us take the functional derivative of (8.3), this yields

$$f_\epsilon([n], \mathbf{r}, \mathbf{r}') = f_{\mathrm{xc}}([n], \mathbf{r}, \mathbf{r}') - f_\epsilon([n], \mathbf{r}, \mathbf{r}') - \int d\mathbf{r}'' n(\mathbf{r}'') \frac{\delta^2 \epsilon_{\mathrm{xc}}([n], \mathbf{r}'')}{\delta n(\mathbf{r}) \delta n(\mathbf{r}')}. \tag{8.12}$$

Now we approximate the second derivative of $\epsilon_{\rm xc}$ using that of the LDA, and we evaluate the derivative at n_0 , i.e. :

$$\left.\frac{\delta^2\epsilon_{\rm xc}([n],\mathbf{r}'')}{\delta n(\mathbf{r})\delta n(\mathbf{r}')}\right|_{n_0} \approx \left.\frac{d^2\epsilon_{\rm xc}(n(\mathbf{r}''))}{dn(\mathbf{r}'')^2}\right|_{n(\mathbf{r}'')=n_0} \delta(\mathbf{r}'-\mathbf{r}'')\delta(\mathbf{r}-\mathbf{r}''), \tag{8.13}$$

which yields

$$f_\epsilon([\mathbf{r}-\mathbf{r}'|,n_0) = \frac{1}{2}\left(f_{\rm xc}(n_0,|\mathbf{r}-\mathbf{r}'|) - n_0\frac{d^2\epsilon_{\rm xc}(n_0)}{dn_0^2}\delta(\mathbf{r}-\mathbf{r}')\right). \tag{8.14}$$

If we use this in (8.11), we get

$$n_\epsilon^{c,\rm approx}(\mathbf{r}) = \frac{1}{2}\left(\frac{f_{\rm xc}^h(n_0)n_{\rm xc}^{c,\rm approx}(\mathbf{r}) - n_0\frac{d^2\epsilon_{\rm xc}(n_0)}{dn_0^2}n(\mathbf{r})}{\frac{d\epsilon_{\rm xc}(n_0)}{dn_0}}\right), \tag{8.15}$$

where $n_{\rm xc}^{c,\rm approx}(\mathbf{r})$ is the first order connector of the xc potential. By using $n_\epsilon^{c,\rm approx}(\mathbf{r})$ in (8.7) we get an approximate functional for the xc energy, $E_{\rm xc}^c[n]$.

In table 8.3, we present the error on the xc energy of various density functionals for Si and NaCl. To focus on the functionals' quality, we use the same densities for all of them, namely the QMC densities calculated in [14]. It was observed in this reference that the total energy is not particularly sensitive to the density's quality, but rather to the functional used. For both materials, the accuracy of the connector approximations depends to some extent on the reference density n_0. A straight-forward use of the connector $n_{\rm xc}^{c,\rm approx}$, which was designed initially for the xc potential, in 8.7 yields a similar estimation of the xc energy as other functionals, namely, LDA and PBE. However, the connector functional designed especially for this purpose is systematically better than $n_{\rm xc}^c$ for the two materials. In the case of silicon, the connector $n_\epsilon^{c,\rm approx}$ with a symmetric choice for n_0 improves the xc energy by about a factor of ten compared to LDA and PBE; a similar performance can be obtained using $n_{\rm xc}^{c,\rm approx}$ with n_0 equal to the local density. However, the error of the latter becomes larger in the case of NaCl. In this case, we also observe that $n_\epsilon^{c,\rm approx}$ becomes nonphysical, i.e., it yields negative values if we use the local density or the symmetric choice for n_0. The reason is an overshooting of the linear expansion around small densities. To cure this issue, we used rather the mean density for n_0 in all terms of (8.15) except for $n_{\rm xc}^{c,\rm approx}$ where we keep the original n_0. For NaCl, the resulting xc energy from this connector can reach almost the same accuracy as the PBE, which gives the closest density and xc energy to QMC results for this material. For silicon, a significant improvement is obtained. To conclude, the results shown in 8.3 are favorable to the connector approximation constructed for the xc energy. This approximation is a functional of the density, which means that it can be tested and used for any system. It can be also used to derive a new functional for the xc potential.

More generally, starting with a connector $n_{\mathbf{r}}^c$ for $\epsilon_{\rm xc}$, one may obtain $v_{\rm xc}$

		error on E_{xc} (%)	
		Si	NaCl
LDA		1.90	3.38
PBE		1.15	0.11
Connector $n_{xc}^{c,approx}$ with n_0 =	mean density	1.61	3.13
	local density	0.22	1.15
	symmetric	0.52	1.84
Connector $n_{\epsilon}^{c,approx}$ with n_0 =	mean density	1.67	2.99
	local density	0.67 | 0.80*	0.21*
	symmetric	0.18 | 0.31*	0.16*

TABLE 8.3: The error of the xc energy of Si and NaCl using various approximate functionals. We use the QMC density in all functionals. For NaCl, the connector $n_{\epsilon}^{c,approx}(\mathbf{r})$ becomes negatives if we take n_0 at the local density or the symmetric choice described in Sec. 4.3.1.3. To solve this problem, we changed the density n_0 to the mean density in all terms of (8.15) except the $n_{xc}^{c,approx}(\mathbf{r})$ term. The resulting values of this treatment are highlighted by the symbol: *. The equivalent results for Si are given for the sake of comparison.

as the functional derivative of the connector approximation E_{xc}^{c}, as done in (8.8), because the connector approach generates $n_{\mathbf{r}}^{c}$ as a density functional. The resulting v_{xc}^{c} can be written as

$$\begin{aligned} v_{xc}^{c}(\mathbf{r}) &= \epsilon_{xc}(n_{\mathbf{r},\epsilon}^{c}) + \int d\mathbf{r}' n(\mathbf{r}') \frac{f_{\epsilon}^{h}(n_{\mathbf{r}',\epsilon}^{c})}{f_{\epsilon}^{h}(n_0)} f_{\epsilon}(\mathbf{r}-\mathbf{r}';n_0) \\ &= v_{xc}^{h}(n_{\mathbf{r},\epsilon}^{c}) - n_{\mathbf{r},\epsilon}^{c} \frac{d\epsilon_{xc}(n_{\mathbf{r},\epsilon}^{c})}{dn_{\mathbf{r},\epsilon}^{c}} \\ &+ \int d\mathbf{r}' n(\mathbf{r}') \frac{f_{\epsilon}^{h}(n_{\mathbf{r}',\epsilon}^{c})}{f_{\epsilon}^{h}(n_0)} f_{\epsilon}(\mathbf{r}-\mathbf{r}';n_0)\,, \end{aligned} \tag{8.16}$$

if we neglect the dependence of n_0 on the density $n(\mathbf{r})$. This $v_{xc}^{c}(\mathbf{r})$ will in general be different from (8.9). The consistent connector density that represents the $v_{xc}^{c}(\mathbf{r})$ in (8.16), instead, is obtained by inverting the HEG and reads

$$\begin{aligned} n_{\mathbf{r},xc}^{c} &= v_{xc}^{h,-1}\Big(v_{xc}^{h}(n_{\mathbf{r},\epsilon}^{c}) - n_{\mathbf{r},\epsilon}^{c} f_{\epsilon}^{h}(n_{\mathbf{r},\epsilon}^{c}) \\ &\quad + \int d\mathbf{r}' n(\mathbf{r}') \frac{f_{\epsilon}^{h}(n_{\mathbf{r}',\epsilon}^{c})}{f_{\epsilon}^{h}(n_0)} f_{\epsilon}(\mathbf{r}-\mathbf{r}';n_0) \Big)\,. \end{aligned} \tag{8.17}$$

The two connector densities fulfill $n_{\mathbf{r},xc}^{c} \approx n_{\mathbf{r},\epsilon}^{c}$ only under special conditions, for example, if we had $n_{\mathbf{r}',\epsilon}^{c} \approx n_{\mathbf{r},\epsilon}^{c}$ in the integral.

In conclusion, we have shown two promising ways to use the connector for the xc energy: either by using the connector, n_{xc}^{c}, from the v_{xc} or from the extra connector for ϵ_{xc}. Here we have explored only the first order approximation, and the results are good enough to motivate further work in this

direction.

Chapter 9

Charge density as functional of the potential

In this chapter I discuss an example of application of the connector theory for real materials other than the development of a density functional. In DFT, the ground state density can be calculated in principle by minimization of the total energy functional. However, because the density functional for kinetic energy is unknown, in practice one calculates orbitals using the Kohn-Sham Hamiltonian. In this chapter, we will show that the connector theory enables us to take a different route, namely, to derive an explicit expression for the density as functional of the KS potential. This functional requires only knowledge of the KS potential and the input from the HEG, without the need for the KS orbitals. So, the first step to proceed is to generate a KS potential and construct the independent particles Hamiltonian. The resulting density from this Hamiltonian represents the target density in this case. Then, using the connector scheme we build a potential functional for that density that takes the KS potential as input to calculate an approximation for the density. Finally, we compare the connector results and other approximations against the target density. As we will see, the findings suggest that the resulting functional can be useful in some real applications. In particular, the connector functional yields a rapid estimate of the density, $n(\mathbf{r})$, which would be desirable in many situations, for example, when discussing charge accumulation at an interface or as an initial guess for the density in the KS self-consistency loop.

9.1 Charge density of Silicon

In order to give a realistic example, we used the charge density of bulk silicon as a target. Here we are not concerned about the quality of the target density itself, but rather by how well the approximations can reproduce it. To obtain the density, we used the GPAW code [111]. We first express the original Kohn-Sham potential in a plane wave basis. Then, using this potential, we have extracted an effective local potential that contains the effect of non-local pseudo-potentials. The Hamiltonian was then constructed using the effective local potential, and the target charge density was computed by diagonalizing this Hamiltonian and summing the squares of the wavefunctions in the four occupied valence bands. We utilized a real space grid with $16 \times 16 \times 16$ grid

points, which corresponds to a 11 Ha plane wave cutoff, and a k-point grid with $8 \times 8 \times 8$ grid points.

9.2 In principle exact connector

The aim is to calculate the density $n(\mathbf{r})$ at a given point in space $\mathbf{r}$ by taking its value from a a to-be-determined HEG. Because the absolute energy scale in an extended system is arbitrary, the density in the HEG is determined by the relative values of the Kohn-Sham and chemical potentials,v_h and μ_h. We therefore set $\mu_h = 0$ in the following, thus the density of the HEG becomes a function $n_h(v_h)$. Similarly, in the real system with the chemical potential set to zero, the density is a potential functional $n(\mathbf{r}, [v_{\mathrm{KS}}])$ The exact connector condition is then

$$n(\mathbf{r}, [v_{\mathrm{KS}}]) = n_h(v_h^c), \tag{9.1}$$

which defines the connector potential v_h^c. Since the relation between the density and the potential in the HEG for $\mu_h = 0$ reads

$$n_h = \frac{[-2v_h]^{3/2}}{3\pi^2}, \tag{9.2}$$

the exact connector potential in a point $\mathbf{r}$ is

$$v_{h\mathbf{r}}^c = -\frac{[3\pi^2 n(\mathbf{r})]^{2/3}}{2}. \tag{9.3}$$

Note that $v(\mathbf{r})$ is *one* $\mathbf{r}$-dependent potential, whereas $v_{h\mathbf{r}}^c$ represents a *different, homogeneous* potential for each point in space, as indicated by the use of a subscript for $\mathbf{r}$. Finally, the density is obtained as follows:

$$n^c(\mathbf{r}) = n_h(v_{h\mathbf{r}}^c) = \frac{[-2v_{h\mathbf{r}}^c]^{3/2}}{3\pi^2}. \tag{9.4}$$

This is naturally equal to the target density. In practice, we do not know the target density, thus we have to approximate the expression (9.3).

9.3 Linear response approximation

In order to get an estimate of the target density, we may expand it in small variations of the potential around some homogeneous potential v_0,

$$n(\boldsymbol{r}, [v_{\mathrm{KS}}]) \approx n_h(v_0) + \int d\mathbf{r}' \left.\frac{\delta n(\boldsymbol{r})}{\delta v_{\mathrm{KS}}(\boldsymbol{r}')}\right|_{v_0} \left[v_{\mathrm{KS}}(\boldsymbol{r}') - v_0\right]. \tag{9.5}$$

In the HEG, this approximation reads

$$n_h(v_h) \approx n_h(v_0) + \left.\frac{dn_h(v_h)}{dv_h}\right|_{v_0} [v_h - v_0]. \tag{9.6}$$

These are straightforward approximations by themselves. However, in the following we will employ them in order to design an approximate connector that yields a more accurate result than this direct approximation.

9.4 Linear response connector

Here we build an approximate functional for the density by following the connector scheme described in Fig. 3.1, with $O \equiv n(\mathbf{r}, [v_{\rm KS}])$, and $\mathcal{O} \equiv n_h(v_h)$. To accomplish this, we use the linear response approximations (9.5) and (9.6) in the exact connector condition (9.1). Then, we solve for v_h to obtain the approximate connector

$$v_{h\mathbf{r}}^{c,\text{approx}} = \left(\left. \frac{dn_h(v_h)}{dv_h} \right|_{v_0} \right)^{-1} \int d\mathbf{r}' \chi_0(|\mathbf{r}-\mathbf{r}'|, v_0)\, v_{\rm KS}(\boldsymbol{r}'), \tag{9.7}$$

where

$$\chi_0(|\mathbf{r}-\mathbf{r}'|, v_0) = \left. \frac{\delta n(\boldsymbol{r})}{\delta v_{\rm KS}(\boldsymbol{r}')} \right|_{v_0} \tag{9.8}$$

is the Lindhard function [112] and

$$\left. \frac{dn_h(v_h)}{dv_h} \right|_{v_0} = -\frac{\sqrt{-2v_0}}{\pi^2} \tag{9.9}$$

is its macroscopic average. Given that the Lindhard function is known analytically as a function of the density, and hence of v_0,[1] expression (9.7) is easily computed and input into (9.2) to obtain the final density

$$n^{c,\text{approx}}(\mathbf{r}) = \frac{[-2v_{h\mathbf{r}}^{c,\text{approx}}]^{3/2}}{3\pi^2}. \tag{9.10}$$

For $v_{h\mathbf{r}}^{c,\text{approx}}$ equal to the local potential,[2] this approximation yields the Thomas-Fermi potential functional. The latter functional and other work on potential functionals can be found in this Ref. [113]. To avoid confusion, note again that here the density, $n^{c,\text{approx}}(\mathbf{r})$ is the observable that we want to calculate, whereas the potentiel $v_{h\mathbf{r}}^{c,\text{approx}}$ is used as connector. The connector approximation (9.10) depends on the homogeneous potential, v_0, around which the system is expanded. If a clear set of criteria can be established, one can exploit this dependency to optimize the approximation without turning the approach into a fitting procedure. In this example, we propose a reasonable

[1] it can be written in the reciprocal space as

$$\chi_0(q, v_0) = -\frac{k_F}{2\pi^2}\left\{1 - \frac{Q}{4}\left(1 - \frac{4}{Q^2}\right)\ln\left|\frac{Q+2}{Q-2}\right|\right\},$$

where $Q = q/k_F$, and $k_F = \sqrt{-2v_0}$.

[2] this can be seen as a local potential approximation analogous to the LDA.

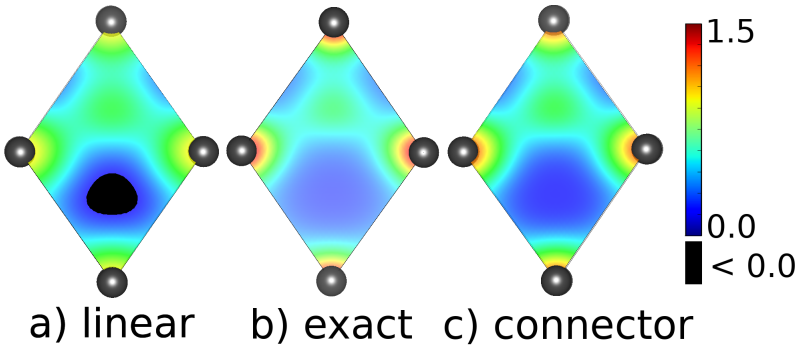

FIGURE 9.1: Charge density of silicon in the (100) plane. Left, linear response approximation. Middle, reference result. Right, linear response connector approximation.

and unambiguous choice, which is an expansion around the local KS potential: this means that in each point $\mathbf{r}$ we choose a different starting homogeneous potential $v_{0\mathbf{r}} = v_{\mathrm{KS}}(\mathbf{r})$. All of the preceding formulas can then be used by simply substituting $v_0 \to v_{0\mathbf{r}}$. Now the connector result is in principle well defined, yielding an approximate average density as well as approximate density variations. In practice one is not interested in computing the average density, which is given by the number of electrons, but only in the density variations. This allows us to impose the correct number of electrons as a condition on the connector, by adjusting the energy scale of the external potential to reach the correct average density.

In Fig. 9.1 we show the results for the density of silicon in the (100) plane. Already the linear response result (9.5) on the left is similar to the target density obtained by diagonalizing the hamiltonian (middle). However, for this approximation the total relative error $\int d\mathbf{r}\, |n(\mathbf{r}) - n^{\mathrm{approx}}(\mathbf{r})| \,/N$, with N the number of electrons, is about 24%. There are even unphysical regions, where the density is negative. Using the connector approximation (9.10), the error is decreased by more than a factor of two , as illustrated in the right panel. Additionally, the connector does not lead to negative densities. This improvement is accomplished at no additional computational expense.

While the precision of the connector approximation, discussed in this chapter, is not yet sufficient, it results in a very simple and direct expression for calculating the density. This can be quite advantageous as a starting point for iterative procedures. For future work, it seems to be encouraging to take into account the lessons learned from the previous chapters, in particular, the idea to build connectors based on a symmetric choice for n_0, which could be easily done also in the present case, and might further improve the results.

Chapter 10

Density matrix as functional of the density

The one-body reduced density matrix (DM) is a very interesting quantity. It provides access to many observables, such as the kinetic energy, the occupation numbers and the exchange energy. As a consequence of the Hohenberg-Kohn theorem, the DM is a functional of the density as shown in Ch. 2. Unfortunately, this functional is not known, except for simple systems. Many efforts have been made to study the DM, but there are still no suitable approximations to express it as a simple functional of the density. In this chapter, I will discuss building connector approximations for the DM as a functional of the density. Previously, in Ch. 6 and in Ch. 9 the density was our target, while here it will be our variable, via which we connect the model and the real system. As in that chapter, here I used the same DFT code to compute the Kohn-Sham density matrix (KS-DM) which will serve as a benchmark in the case of real materials. In the following, I will first present the study of the single electron case where the exact DM is known analytically. I will use it as a target and discuss how to approximate it using expansions and connector theory. Then I will discuss how well these approximations perform. Following that, I will use the single electron DM expression as a direct approximation for the KS many electron DM. Using connector theory, this approximation is then utilized to construct a density functional for the KS-DM. In the connector scheme, I used the HEG as a model to simulate the KS-DM of solid Helium and bulk silicon. Finally, I will compare the connector and the direct approximation results by analyzing their performance in describing the benchmark KS-DM and estimating the corresponding exchange energy. The results of this chapter have been published in the article [114].

10.1 Single electron density matrix

First, let us consider the case of a single electron, which is far more straightforward than the case of a many electron density matrix. In this case, the exact answer can be found analytically, which is quite valuable for gaining some insight into the general case.

For one electron, the occupied orbital is the square root of the density, and the exact density matrix reads

$$n(\mathbf{r}_1, \mathbf{r}_2) = \sqrt{n(\mathbf{r}_1) n(\mathbf{r}_2)}. \tag{10.1}$$

This DM depends only on the densities in $\mathbf{r_1}$ and $\mathbf{r_2}$: this can be seen as a generalized nearsightedness [68, 35] for an object evaluated in points $(\mathbf{r_1}, \mathbf{r_2})$.

In the next sections, we will consider the exact expressions as the benchmark, which we will describe using approximations based on expansions and connector theory.

10.1.1 Expansions

One of the most intuitive approximations that one can consider are Taylor expansions. To get some insight, let us expand the single electron DM around the density of a model system.

10.1.1.1 First order expansion

A first order expansion of (10.1) around a model density, n^{m}, yields

$$n(\mathbf{r_1}, \mathbf{r_2}) \approx n^{\mathrm{m}}(\mathbf{r_1}, \mathbf{r_2}) \Big[1 + \frac{\Delta n(\mathbf{r_2})}{2n^{\mathrm{m}}(\mathbf{r_2})} + \frac{\Delta n(\mathbf{r_1})}{2n^{\mathrm{m}}(\mathbf{r_1})} \Big], \tag{10.2}$$

where $n^m(\mathbf{r_1}, \mathbf{r_2}) \equiv \sqrt{n^m(\mathbf{r}_1) n^m(\mathbf{r}_2)}$ is the DM of the model. Note that here "nearsightedness" only applies to the difference Δn, not to the density itself; this is perfectly suitable for our purpose of finding approximations *given the results of the model system*, but different from the more general topic about the behavior of the system. If the model is the HEG, then "nearsightedness" refers to the nearsightedness with respect to density variations, which is closer to the general concept.

10.1.1.2 Choice of the zero order

The result of (10.2) and higher orders depend on the choice of the model density $n^{\mathrm{m}}(\mathbf{r})$, and consequently, on $\Delta n(\mathbf{r_1})/n^{\mathrm{m}}(\mathbf{r_1})$ and $\Delta n(\mathbf{r_2})/n^{\mathrm{m}}(\mathbf{r_2})$. These ratios must be small for the expansion to converge. This can be used as guideline to choose the zero-order of the expansion.

The simplest choice would be to start the expansion with one and the same HEG to approximate all elements of the DM, $n^{\mathrm{m}}(\mathbf{r_1}) = n^{\mathrm{m}}(\mathbf{r_2}) = n^{\mathrm{m}}$, for example, the average density of the system. However, whereas this might be good if the density is quasi-homogeneous, in strongly inhomogeneous systems one could have $\Delta n(\mathbf{r_1})/n^{\mathrm{m}} \geq 1$, which would lead to divergence of the series. Instead of the average density, one could take the average between the highest and lowest occurring density, $(n_{\max} + n_{\min})/2$. In that case $\Delta n(\mathbf{r_1})/n^{\mathrm{m}} \leq 1$ everywhere. Still, the series will converge less well when the density is close to the maximum or minimum in points $\mathbf{r_1}$ and/or $\mathbf{r_2}$, and

extremely slowly when the minimum density is zero. So, such an expansion would work straightforwardly for systems where the density variation has a small amplitude compared to the average density.

The choice of the HEG as model system can be optimized further by allowing a different HEG for each pair $(\mathbf{r_1}, \mathbf{r_2})$. The most natural choice would be a homogeneous density defined as $n^{\mathrm{m}}_{\mathbf{r_1}\mathbf{r_2}}(\mathbf{r}) = (n(\mathbf{r_1}) + n(\mathbf{r_2}))/2$, independent of $\mathbf{r}$ but different for each pair $(\mathbf{r_1}, \mathbf{r_2})$. In that case, $\Delta n(\mathbf{r_1})/n^{\mathrm{m}}(\mathbf{r_1}) = (n(\mathbf{r_1}) - n(\mathbf{r_2}))/(n(\mathbf{r_1}) + n(\mathbf{r_2})) \leq 1$, as desired, and similarly for $\mathbf{r_2}$. Again, however, one would expect bad convergence when one of the densities approaches zero. Note that taking $n(\frac{\mathbf{r_1}+\mathbf{r_2}}{2})$ would be meaningless.

To go further, let us make the hypothesis that even beyond a single electron the density matrix is generalized nearsighted, in the sense that for a matrix element at given $(\mathbf{r_1}, \mathbf{r_2})$ only the density near $\mathbf{r_1}$ and $\mathbf{r_2}$ is important. Supposing, as in the LDA, that close to those points the density is slowly varying, one could build an *inhomogeneous* model, with the requirement that $(n(\mathbf{r}_i) - n^{\mathrm{m}}_{\mathbf{r_1}\mathbf{r_2}}(\mathbf{r}_i))/n^{\mathrm{m}}_{\mathbf{r_1}\mathbf{r_2}}(\mathbf{r}_i) \ll 1$ for $i = 1, 2$. The density $n^{\mathrm{m}}_{\mathbf{r_1}\mathbf{r_2}}(\mathbf{r})$ of this model would in general be different for every $(\mathbf{r_1}, \mathbf{r_2})$. Although inhomogeneous, such a model should still be simple enough to be solved with advanced methods for the entire sequence of its parameters. An example could be crystals with only one fourier component. Such a venture would have been unthinkable when DFT was founded, but is today possible.

10.1.1.3 Second order expansion

If the model is homogeneous, for any density n^m the first order Eq. 10.2 yields

$$n(\mathbf{r_1}, \mathbf{r_2}) = \frac{n(\mathbf{r_1}) + n(\mathbf{r_2})}{2}. \tag{10.3}$$

Instead, if we expand to the second order, the result depends on n^m, yielding:

$$n(\mathbf{r_1}, \mathbf{r_2}) \approx \frac{n(\mathbf{r_1}) + n(\mathbf{r_2})}{2} - \frac{(n(\mathbf{r_1}) - n(\mathbf{r_2}))^2}{8n^m}.$$

If $n^{\mathrm{m}}_{\mathbf{r_1}\mathbf{r_2}} = (n(\mathbf{r_1}) + n(\mathbf{r_2}))/2$,

$$n(\mathbf{r_1}, \mathbf{r_2}) \approx \frac{n(\mathbf{r_1}) + n(\mathbf{r_2})}{4} + \frac{n(\mathbf{r_1})n(\mathbf{r_2})}{n(\mathbf{r_1}) + n(\mathbf{r_2})}. \tag{10.4}$$

For a general non-homogeneous model the result reads:

$$n(\mathbf{r_1}, \mathbf{r_2}) \approx n^{\mathrm{m}}(\mathbf{r_1}, \mathbf{r_2}) \left(1 + \frac{\Delta n(\mathbf{r_1})}{2n^{\mathrm{m}}(\mathbf{r_1})} + \frac{\Delta n(\mathbf{r_2})}{2n^{\mathrm{m}}(\mathbf{r_2})} + \frac{\Delta n(\mathbf{r_1})\Delta n(\mathbf{r_2})}{4n^{\mathrm{m}}(\mathbf{r_1})n^{\mathrm{m}}(\mathbf{r_2})} - \frac{(\Delta n(\mathbf{r_1}))^2}{8(n^m(\mathbf{r_1}))^2} - \frac{(\Delta n(\mathbf{r_2}))^2}{8(n^m(\mathbf{r_2}))^2}\right). \tag{10.5}$$

The second order correction is of course small when Δn is small, but it is also small when the ratio between the real and the model densities is similar in

$\mathbf{r_1}$ and $\mathbf{r_2}$, which is a less demanding requirement that a non-homogeneous model can satisfy.

10.1.2 Connector approximation

In the connector philosophy, our principal aim is to use the model data to simulate the real system. In order to accomplish this, we need to establish a connector between the two systems and this the reason why we use approximations. When we use expansions around the model parameter, the zero-order term becomes equivalent to the model quantity. Thus, by using the connector approach, we do not want to find the best expansion of the result around some point, but to optimize the zero-order term, which means that we aim to find the model parameter that gives directly the correct result. As explained in Ch. 3, one way to *find* the parameter of this model is to use a first order expansion. So the expansion is not used to produce directly the final result, but only to determine the parameters of the model, from which the result is taken. We will examine the connector approximation *for the single-electron case*, where we do not need it, of course, but where we can hope to learn something about connector approximations based on expansions.

The DM for the single homogeneous electron is peculiar, because its density matrix is linear in the density: it is simply the density itself (see (10.3) with homogeneous density). Therefore, the first-order expansion is exact in the homogeneous model. Following the general notation of Ch. 3, this means for the model $\mathcal{O}^{-1}_{\text{approx}} = \mathcal{O}^{-1}$ and therefore the approximate connector is given by $\mathcal{Q}^{c,\text{approx}} = \mathcal{O}^{-1}(O_{\text{approx}}(Q^R))$, where $\mathcal{O}$ is O on the subspace of model densities. The final result proposed by the connector is then $O^c = \mathcal{O}(\mathcal{Q}^{c,\text{approx}}) = O_{\text{approx}}(Q^R)$, which is equal to the first-order approximation itself. Since the approximation equals the exact solution in the model, there is no error cancelling, and nothing is gained by the connector. In order for the first-order connector to be useful in the single-electron example, the model system must therefore be inhomogeneous. To fulfill this requirement, we choose a model system with a density that has only one Fourier component, $n^{\text{m}}(\mathbf{r}) = A^{\text{m}}\cos(a^{\text{m}}\mathbf{r}) + B^{\text{m}}$, with parameters A^{m}, a^{m} and B^{m} that can be varied to match the connector equality condition. The latter reads

$$\sqrt{n(\mathbf{r_1})n(\mathbf{r_2})} = \sqrt{(A^{\text{m}}\cos(\mathbf{a}^{\text{m}}.\mathbf{r_1}) + B^{\text{m}})(A^{\text{m}}\cos(\mathbf{a}^{\text{m}}.\mathbf{r_2}) + B^{\text{m}})}. \tag{10.6}$$

In principle the exact real DM, which is the left hand side of this equation, is unknown. However, an approximate version of the equality is accessible by performing a first order expansion for the real and the model DM around a homogeneous density (see (10.3)). This yields

$$n(\mathbf{r_1}) + n(\mathbf{r_2}) = A^{\text{m}}\left(\cos(\mathbf{a}^{\text{m}}.\mathbf{r_1}) + \cos(\mathbf{a}^{\text{m}}.\mathbf{r_2})\right) + 2B^{\text{m}}. \tag{10.7}$$

The three model parameters A^{m}, a^{m} and B^{m} cannot be uniquely defined by this equation. This requires one to impose additional constraints and solve for the remaining free model parameter(s), to finally obtain the connector set

A^c, a^c, B^c. Since we have never studied the connector for such a case in the previous chapters, it is interesting to explore what is the most promising way to set the model parameters.

In the following, we will test different approximations, including various connector approximations, for single-electron systems.

10.1.3 Comparative analysis of the approximations

Although the single-electron case can be solved exactly, testing approximations to it will give guidelines for the many-electron case. We therefore start with a numerical illustration for a single electron with density

$$n(\mathbf{r}) = A_1 \cos(a_1 \mathbf{r}) + A_2 \cos(a_2 \mathbf{r}) + A_3 \cos(a_3 \mathbf{r}) + B, \tag{10.8}$$

where $\mathbf{a} = a\hat{\mathbf{x}}$ in a cube of side length 2π.

To study the performance of different approximations, we show in Fig. 10.1 the relative error of the approximate density matrix with respect to the exact one, with $\mathbf{r_1}$ and $\mathbf{r_2}$ in direction $\hat{\mathbf{x}}$. To characterize the results in a single number, the captions also show the mean relative errors (MRE). The three panels in the left column display the result of first- and second-order expansions around different starting homogeneous densities. The same scale has been imposed to all results, which implies that in the bright yellow regions the error exceeds the maximum error set by the scale. The upper panel is the first order result. The error is largest in points $(\mathbf{r_1}, \mathbf{r_2})$ for which the density is very small in one point and and large in the other, which may lead to $\Delta n(\mathbf{r}_i)/n^{\mathrm{m}} \geq 1$. As pointed out above, the result of the first order expansion does not depend on the homogeneous starting point. The next two panels are the results of second order expansion, evaluated at the mean density of the system, or at $n^{\mathrm{m}}_{\mathbf{r_1 r_2}} = 0.5(n(\mathbf{r_1}) + n(\mathbf{r_2}))$, respectively. In the first case, the error is larger than that of the first order result, with maxima where one of the two densities is small, i.e. in regions where already the first order is problematic. In the second case instead, where a different homogeneous system is chosen for each pair $(\mathbf{r_1}, \mathbf{r_2})$, which can be seen as a generalization of the LDA, the result improves significantly.

The three panels in the right column of Fig. 10.1 show the result of the first order connector approximation. This result is obtained using the same approximation as the one that gave the topmost panel in the left column, but now used within the connector scheme. Fig. 10.1 shows that the connector result depends strongly on the way the parameters are set: the best result is obtained when the average density of the model, $B^c_{\mathbf{r_1 r_2}}$, is used as free parameter to optimize each pair of points $(\mathbf{r_1}, \mathbf{r_2})$, while the amplitude and periodicity of the dominant Fourier component equals that of the real system, i.e. $A^{\mathrm{m}} = A_1$ and $a^{\mathrm{m}} = a_1$. As can be seen by comparing the left and right panels of Fig. 10.1a, using the same first-order expansion the connector result is clearly superior with respect to the direct approximation while, when the model results are tabulated, the workload to calculate a real system is the same in both cases. The connector result worsens when the amplitude of the

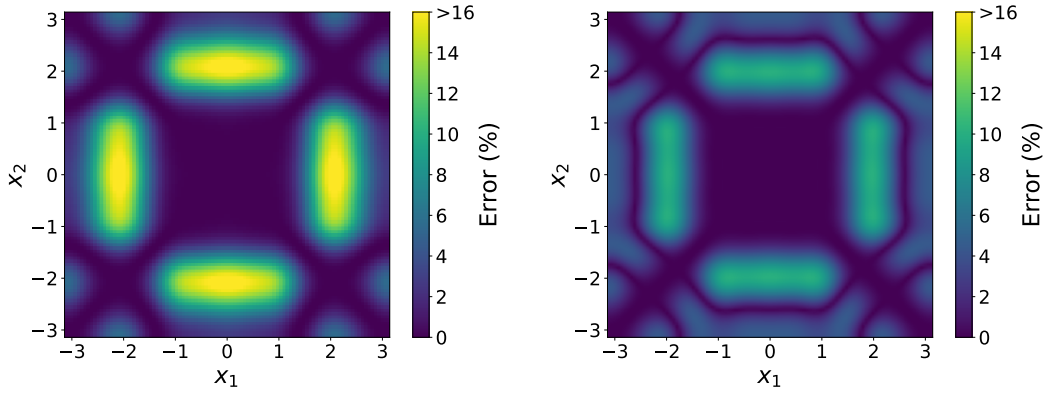

(A) First order approximation.(Left) Direct approximation. Mean relative error (MRE) = 4.33% (Right) CT fixing $A^c = A_1$ and $a^c = a_1$. MRE =2.88% .

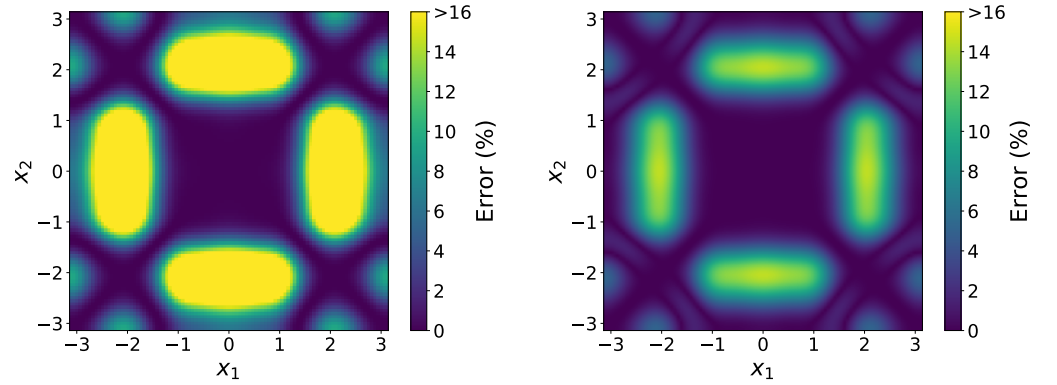

(B) (Left) Second order approximation starting from $n^{\mathrm{m}} = B$. MRE = 8.48% (Right) First-order CT fixing $A^c = (A_1 + A_2 + A_3)/3$ and $a^c = a_1$. MRE = 3.51%

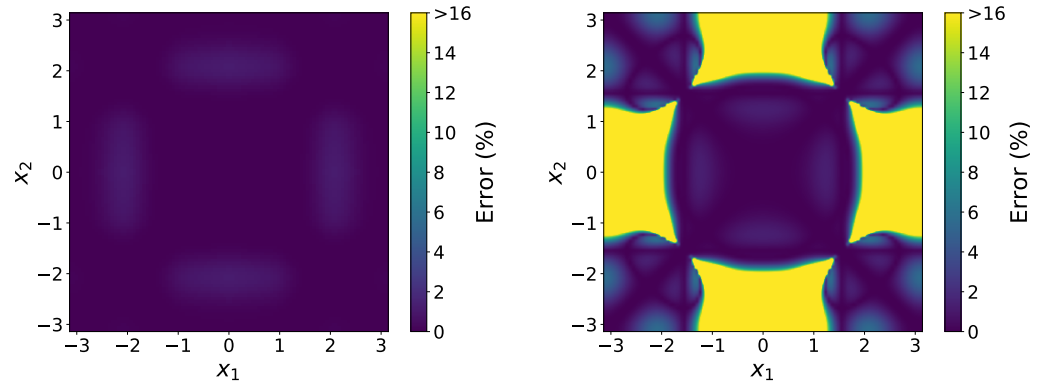

(C) (Left) As (b), with $n^{\mathrm{m}} = 0.5(n(\mathbf{r_1}) + n(\mathbf{r_2}))$. MRE = 0.19%
(Right) First-order CT fixing $B^c = B$ and $a^c = a_1$. MRE = 27.95 %

FIGURE 10.1: Relative error of approximations to the density matrix for a system with $n(\mathbf{r}) = A_1 \cos(\mathbf{a}_1\mathbf{r}) + A_2 \cos(\mathbf{a}_2\mathbf{r}) + A_3 \cos(\mathbf{a}_3\mathbf{r}) + B$, where $\mathbf{a} = a\hat{\mathbf{x}}$, with $A_1 = 2$, $A_2 = 1$, $A_3 = 0.5$, $a_1 = 1$, $a_2 = 2$, $a_3 = 3$ and $B = 3.1$. Left column: first and second order expansions. Right column: connector theory (CT) approximations based on first-order expansion around a homogeneous system, using for the connector a model with density $n^{\mathrm{m}}(\mathbf{r}) = A \cos(a\hat{\mathbf{x}}\mathbf{r}) + B$. In principle A, a and/or B can be varied to connect the real and the model system; the results shown in the different panels are obtained with different choices.

first Fourier component is set to an average value, $A^{\mathrm{m}} = (A_1 + A_2 + A_3)/3$, but it is still better than the direct approximation. The worst results are obtained when the average density is kept fixed, and the connector is set by the amplitude of the oscillation, as shown in the last panel. In all cases, the worst results are obtained when one of the densities, $n(\mathbf{r}_1)$ or $n(\mathbf{r}_2)$, is small. Note that in the last panel the connector equation would even yield regions with negative densities; in those cases, the density matrix has been set to zero.

The best result is the second-order expansion in panel (c) in the left column; however, it would require in practice a higher computational effort. When the average density B is much lower, e.g., $B = 1$, results become worse. Still, for $n^{\mathrm{m}} = (n_{\max} + n_{\min})/2$ the expansion converges, though more slowly. Altogether, the results indicate that one may obtain practicable approximations using expansions, even around a homogeneous system, and that in particular connector combined with a low-order expansion is a promising direction.

10.2 Many-electron density matrix

Real systems cannot be solved analytically in general, but we can try to use insight from the single-electron case to approximate the density matrix of real systems[1]. In the following, we will use the single electron DM to approximate the non-interacting, or Kohn-Sham, DM of extended systems such as bulk silicon and helium in two different ways. The simplest one is to directly substitute the density $n(\mathbf{r})$ in (10.1) by the density of the real system. The smarter one is to use the *exact* single-electron results as *an approximation* to design a connector *for the many-electron case*.

10.2.1 Helium and silicon

As a first guess, one could assume that generalized nearsightedness holds for the many-electron system and derive direct approximation based on it. When the nearsightedness fails, one can go a step further and design connector approximations, which can be helpful because they can interpolate between the nearsightedness and the farsightedness. This will be illustrated in the following, with a focus on the connector theory.

First, we should keep in mind that expansions are only one possible way to design practical connectors. The general strategy requires to do equivalent approximations on the real and the model system, regardless of the type of approximation. Thus, here instead of expanding the many-electron DM, which is a possibility, we will benefit from the analytic single electron case by using its DM as an approximation to build the connector.

We will study two real systems, bulk silicon [116] and solid He [117], at the Kohn-Sham level. Our model system will be the homogeneous electron

[1] Also in the asymptotic region $\mathbf{r_1}, \mathbf{r_2} \to \infty$ of a finite system the density matrix $n(\mathbf{r_1}, \mathbf{r_2})$ behaves like[115] $\sqrt{n(\mathbf{r_1})n(\mathbf{r_2})}$.

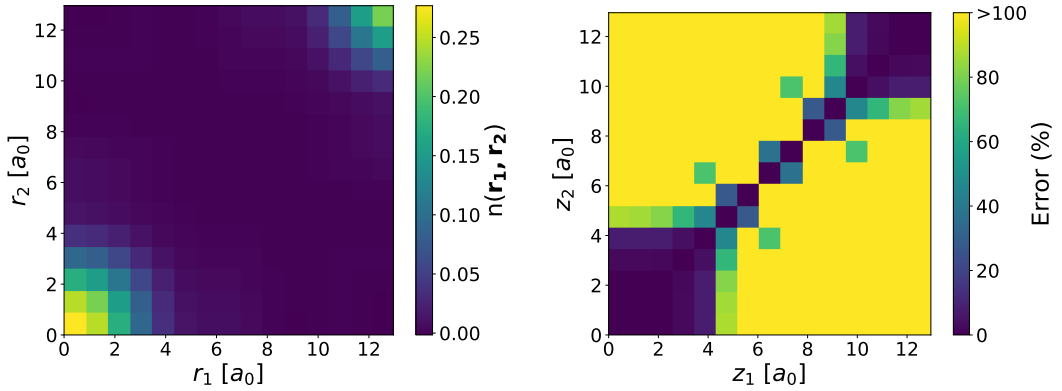

(A) (Left) Kohn-Sham DM. (Right) Direct single-electron approximation.

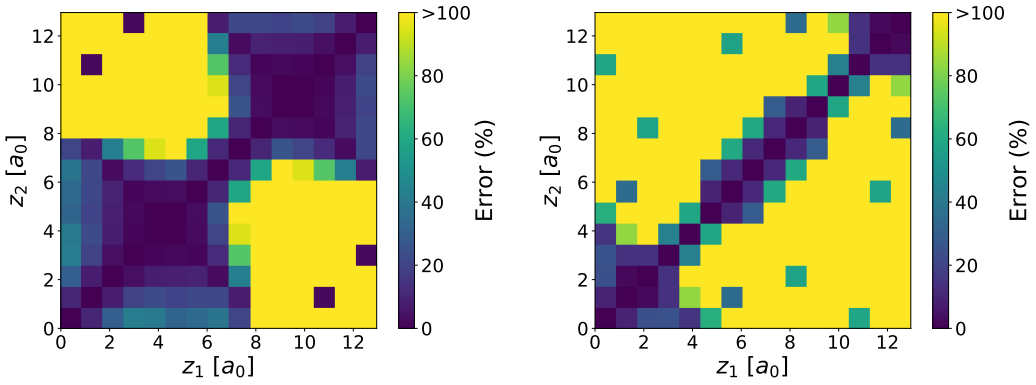

(B) (Left)CT with single-electron approximation
(Right) CT with $n^{\mathrm{m}}_{\mathbf{r}_1\mathbf{r}_2} = 0.5(n(\mathbf{r_1}) + n(\mathbf{r_2}))$

FIGURE 10.2: DM and relative error of approximations to the DM for solid helium along the [1,1,1] direction.

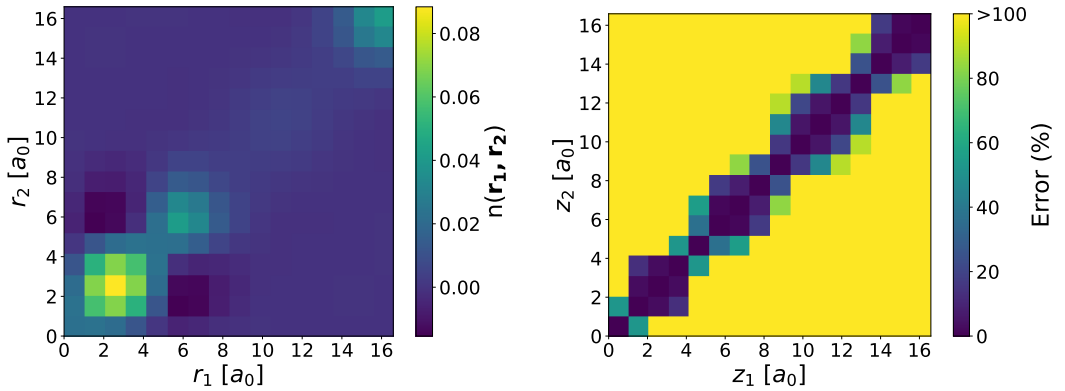

(A) (Left) Kohn-Sham DM. (Right) Direct single-electron approximation

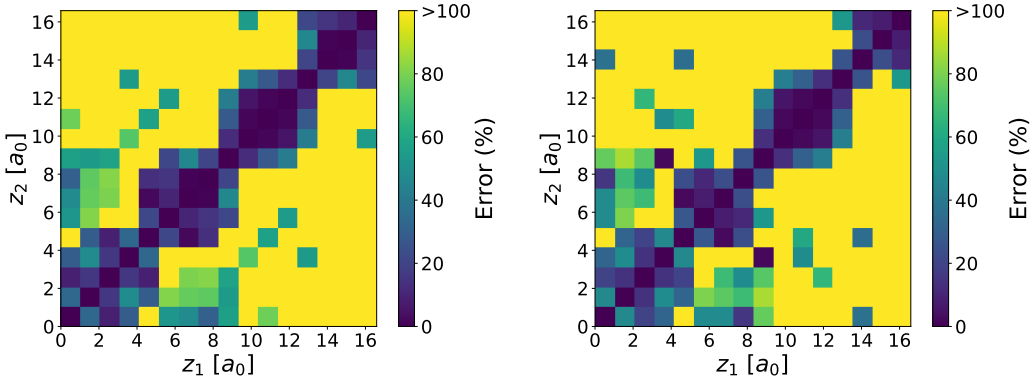

(B) (Left) CT with single-electron approximation
(Right) CT with $n^{\mathrm{m}}_{\mathbf{r_1}\mathbf{r_2}} = 0.5(n(\mathbf{r_1}) + n(\mathbf{r_2}))$

FIGURE 10.3: DM and relative error of approximations to the DM for bulk silicon along the [1,1,1] direction.

gas, its density matrix, γ,is characterized by the density, n^h, and it reads [118]

$$\gamma(x, n^h) = \frac{\sin(k_{\mathrm{F}}x) - k_{\mathrm{F}}x\cos(k_{\mathrm{F}}x)}{\pi^2 x^3}, \tag{10.9}$$

with $x = |\mathbf{r_1} - \mathbf{r_2}|$ and $k_{\mathrm{F}} = (3\pi^2 n^h)^{1/3}$. Employing the single electron approximation for both $\gamma(x, n^c)$ and the real DM $n(\mathbf{r_1}, \mathbf{r_2})$, we obtain the following connector equality

$$n^c_{\mathbf{r_1}\mathbf{r_2}} = \sqrt{n(\mathbf{r_1})n(\mathbf{r_2})}. \tag{10.10}$$

The density matrix $n(\mathbf{r_1}, \mathbf{r_2})$ in a pair of points is then obtained in the connector approximation by evaluating the density matrix of the HEG with homogeneous density $n^c_{\mathbf{r_1}\mathbf{r_2}}$. This result which consists of using the HEG with geometric mean density as an approximation is quiet intuitive, and it has been used, for example, as ingredient for an energy functional describing van der Waals interaction [119].

Figs. 10.2 and 10.3 show, for helium and silicon, respectively, the Kohn-Sham density matrix $n(\mathbf{r_1}, \mathbf{r_2})$, the direct single-electron approximation

$$n(\mathbf{r_1}, \mathbf{r_2}) \approx \sqrt{n(\mathbf{r_1})n(\mathbf{r_2})}, \tag{10.11}$$

and the connector approximation

$$n(\mathbf{r_1}, \mathbf{r_2}) \approx \gamma(|\mathbf{r_1} - \mathbf{r_2}|, n^c_{\mathbf{r_1}\mathbf{r_2}}). \tag{10.12}$$

Figs. 10.2 and 10.3 also show results of the connector approximation with guesses for the connector inspired by the single electron case. The error on diagonal terms is zero for all approximations since by construction they give the exact density. For the off diagonal terms the connector approximation looks better than the direct ones along the direction [1,1,1]. To get an idea about the quality of the approximated DM in the entire unit cell, one could look at the total error on the DM and the resulting exchange energy, which can be calculated using (2.75). The relative error on DM and the exchange energy calculated over one unit cell is given in in Table 10.1.

TABLE 10.1: Total error on density matrix (DM) and the exchange energy, E_x, (in %) for solid helium and bulk silicon.

	He		Si	
	DM	E_x	DM	E_x
Direct single-electron	6056	167	64660	575
Direct $0.5(n(\mathbf{r_1}) + n(\mathbf{r_2}))$	18008	1117	7098	663
Direct average density	126190	1455	72524	663
Connector single-electron	3741	51	1510	6
Connector $0.5(n(\mathbf{r_1}) + n(\mathbf{r_2}))$	5883	134	1548	6
Connector average density	65143	833	1854	10

Errors are now significantly larger than in the previous section, this was expected since a single-electron system is far from an infinite many-electron material. However, the results show the same trend as before: the connector significantly improves the results compared to using direct approximations. The exchange energy errors are far smaller than the error in the density matrix itself. This is due to the small terms of the DM that contribute very little to the exchange energy but lead to a large relative error on the DM. When we use the connector to estimate the exchange energy of silicon, which is closer to the HEG, i.e., closer to the model, we get an interesting result with an error that might even be acceptable for some applications. Also for helium the connector improves the results, but compared to silicon the direct approximation is better and the connector result is worse. This can be the consequence of using the HEG as model for this very in-homogeneous system.

10.3 Conclusion

In this chapter we have concentrated on the density matrix as object to be approximated. This was done as a part of the study to investigate if the connector theory is an appealing direction to build simple and explicit density functionals. Our analysis and numerical results indicate a positive answer. In the study of the single electron density matrix, we have shown that expansions can be a suitable starting point for approximations, they may converge quickly for systems where the variations in the density are significantly smaller than the average density. The starting point of expansions turns out to be crucial. In the simplest case one expands around the HEG, and the best results are obtained when a different HEG is taken for each pair of points $(\mathbf{r_1}, \mathbf{r_2})$ in $n(\mathbf{r}_1, \mathbf{r}_2)$, namely a homogeneous density with $n^{\mathrm{m}}_{\mathbf{r}_1,\mathbf{r}_2} = (n(\mathbf{r}_1) + n(\mathbf{r}_2))/2$. This approach follows a generalized local density approximation. Using the connector theory on top of the expansions improves the result while incurring the same computational cost. This is thanks to two factors : the availability of the model data and the optimize use of the latter by the connector approach.

In this study we have also explored the use of inhomogeneous model, described by one Fourier component. This kind of model can be generalized for periodic system since it is described by a limited number of parameters, and could still be tabulated if it proves to be useful. For the case of many electron density we have shown that the connector is not limited to expansions, and that other approximations, such as the single electron case, can be used. Even though we used very rough approximations, the connector result on exchange energy was very interesting for silicon. For helium, the exchange energy could be brought into an acceptable level by using non-homogeneous model or by substituting the single electron approximation with that of a periodic array of single electrons. Finally we note that finding simple density functionals for the non-interacting density matrix is an important topic because it could for example allow one to speed up calculations based on hybrid functionals. The practical part of the second section was devoted to the exchange energy. The results indicate that it may be worthwhile to investigate the connector strategy for the interacting scenario in the future.

Chapter 11

Conclusion and outlook

In this thesis, I presented an exact and very broad approach inspired by the Kohn-Sham strategy for approximating density functionals using the homogeneous electron gas. The aim of this approach is to calculate and store, once and for all, an observable or another object in a model system with the highest possible precision. These results are then used smartly to approximate the same object in real systems using a prescription called connector theory (COT). Each target object requires a distinct connector, which must be approximated. The quality of the connector results depends mainly on two critical factors: the model and the chosen approximation, which require care and physical insight. However, through the applications discussed in this thesis, I have demonstrated, and explained why, a given approximation is often far more powerful when applied within connection theory than when applied directly to the object of interest.

The connector theory can be used to improve density functionals by designing non-local approximations. This was demonstrated by using the connector to reproduce the weighted density approximation functional. In this example, I gave two practical ways to approximate the exact connector: one is based on expansions and the other one is a modification of the Coulomb interaction. The results show a significant improvement by COT compared to directly applying the approximation to the observable of interest.

Along the same lines, I have used the homogeneous electron gas as a model to develop a connector non-local density functional approximation to the exchange correlation potential. From this functional we can derive the local density approximation as a limit case in the regime of slowly varying density. It is worth to note that the free parameters in this connector, which stem from the expansion, can be turned into strength for the connector functional by adjusting them to satisfy exact constraints. Used within the Kohn-Sham scheme, the connector approximation turns out to yield a very accurate density for silicon and quite good result for sodium chloride, without increasing the computational cost. This result can be always improved since the connector is based on a systematic approach. By improving the approximation used in the connector scheme or choosing a model closer to the system, the approximate connector tends to the exact answer.

The connector approach also allows us to profit from the model data that are already available in the literature, and any improvement of these quantities increases the accuracy of the connector approximation as well.

Independently of COT, I have constructed accurate xc potentials for silicon and sodium chloride by inverting densities calculated with QMC methods [14]. These potentials can serve as a benchmark to guide the development of new approximations for the xc functional. They were used in Ch. 7 in order to extract the near-exact xc energy from the QMC total energy. Then, by using this xc energy as a reference, I have evaluated the performance of the COT approximation and the other xc energy functionals. After optimizing the first order expansion, the connector functional yields the closest estimation of the QMC energy. This is a promising result, but of course to get a conclusive evaluation on its quality, this connector energy functional and its corresponding xc potential should be tested on more systems.

The connector theory is not limited to DFT, indeed, I have shown, through the example discussed in Ch. 9, that COT can be used to approximate observables as functionals of the external potential. This application paves the way for fast computational methods, which I have illustrated with a quick estimation the density. In addition to that, I discussed, in Ch. 10, the use of COT to approximate a non-local object, namely the density matrix. I have demonstrated again the improvement of the connector over the direct approximation, this time for the density matrix and the exchange energy as the observables. In the single electron case, I have highlighted that non-homogeneous models can be used, instead of the HEG.

As an outlook, one can use models beyond the HEG that are closer to the real system of interest. For example one can choose germanium as model for wide range of semiconductors. Indeed, more complex models may necessitate high-throughput calculations, but with today's computer power it is worth going in this way and exploring whether the use of new interacting model systems beyond the HEG could be a promising direction to take, as this would theoretically allow for the calculation of the majority of the interaction effects once and for all. The results of these calculations can be then interpolated using modern machine learning methods or stored using today's storage capacities. Thus, from a COT point of view, the calculations for a variety of real materials would essentially consist of assembling the Lego pieces obtained from the model.

One can also explore the generalization of the connector xc potential developed in Ch. 4 to the time-dependent case, this should be in principle possible since a non-local and non adiabatic xc kernel is available in the literature [120]. Besides that, since the connector can build non-local density functionals, one can investigate whether it is possible to describe Van der Waals quantum interactions using connector theory. Finally, we can reformulate the connector theory by using Green's functions instead of density, which would make it easier to work with approximations of the Coulomb interaction, since the interaction appears explicitly in many-body perturbation theory. This offers even more freedom to build new functionals for electronic properties in general.

In conclusion, in this thesis I have contributed to bring the connector approach from an abstract idea to the level of a clear scheme that can be used in practice in various contexts. I used this approach to construct new non-local

approximations to the Kohn-Sham xc potential and the xc energy. I tested these approximations for real materials. The findings show that the connector theory is a promising strategy to develop powerful approximations, and they motivate us to calculate more complex models beyond the HEG.

Appendix A

Correction to first-order connector approximation from second-order density response theory

Here I will show how to obtain the explicit gradient correction (4.15) to the connector xc potential defined in (4.6).

The exact functional $v_{\rm xc}([n],\mathbf{r})$, being a differentiable functional of the density n, can be expanded to the second order around a fixed density n_0:

$$v_{\rm xc}([n],\mathbf{r}) = v_{\rm xc}(n_0) + \int d\mathbf{r}_1 f_{\rm xc}(|\mathbf{r}-\mathbf{r}_1|,n_0)\delta n(\mathbf{r}_1) + \frac{1}{2}\int d\mathbf{r}_1 d\mathbf{r}_2 g_{\rm xc}(\mathbf{r},\mathbf{r}_1,\mathbf{r}_3,n_0)\delta n(\mathbf{r}_1)\delta n(\mathbf{r}_2) \quad \text{(A.1)}$$

The expression of the approximate functional that comes from first-order connector is:

$$v^c_{\rm xc}([n],\mathbf{r}) = v_{\rm xc}(n^c_{\rm xc}),$$

with $n^c_{\rm xc} = \frac{1}{f_{\rm xc}(n_0)}\int d\mathbf{r}' f_{\rm xc}(|\mathbf{r}-\mathbf{r}'|,n_0)n(\mathbf{r}')$. Also the potential $v^c_{\rm xc}$ can be expanded to second order in the density deviations from a constant density of the electron gas n_0:

$$v^c_{\rm xc}([n],\mathbf{r}) = v_{\rm xc}(n_0) + \int d\mathbf{r}_1 f_{\rm xc}(|\mathbf{r}-\mathbf{r}_1|,n_0)\delta n(\mathbf{r}_1) + \frac{1}{2(f_{\rm xc}(n_0))^2}\int d\mathbf{r}_1 d\mathbf{r}_2 f_{\rm xc}(|\mathbf{r}-\mathbf{r}_1|,n_0) f_{\rm xc}(|\mathbf{r}-\mathbf{r}_2|,n_0) g_{\rm xc}(n_0) \times \delta n(\mathbf{r}_1)\delta n(\mathbf{r}_2) \quad \text{(A.2)}$$

Since the connector is exact for a linear functional, the first two terms of this expression are the same as the first two terms on rhs of (A.1). Subtracting

(A.2) from (A.1) yields:

$$v_{xc}([n],\mathbf{r}) = v^{c}_{xc}([n],\mathbf{r}) + \frac{1}{2}\int d\mathbf{r}_1 d\mathbf{r}_2 \delta n(\mathbf{r}_1)\delta n(\mathbf{r}_2)\times \left[g_{xc}(\mathbf{r},\mathbf{r}_1,\mathbf{r}_3,n_0) - \frac{f_{xc}(|\mathbf{r}-\mathbf{r}_1|,n_0)f_{xc}(|\mathbf{r}-\mathbf{r}_2|,n_0)}{(f_{xc}(n_0))^2} g_{xc}(n_0)\right] \quad (A.3)$$

In the reciprocal space and because of the translation invariance of gas, we can write:

$$f_{xc}(\mathbf{r},\mathbf{r}_1,n_0) = \sum_{\mathbf{q}} f_{xc}(\mathbf{q},n_0)e^{i\mathbf{q}.(\mathbf{r}-\mathbf{r}_1)} \quad (A.4)$$

and

$$g_{xc}(\mathbf{r},\mathbf{r}_1,\mathbf{r}_2,n_0) = \sum_{\mathbf{q},\mathbf{q}'} g_{xc}(\mathbf{q},\mathbf{q}',n_0)e^{i\mathbf{q}.(\mathbf{r}-\mathbf{r}_2)}e^{-i\mathbf{q}'.(\mathbf{r}_1-\mathbf{r}_2)} \quad (A.5)$$

where $\sum_{\mathbf{q}}$ is short for $\int d^3\mathbf{q}(2\pi)^{-3}$. Using these definitions in (A.3) we obtain:

$$v_{xc}([n],\mathbf{r}) = v^{c}_{xc}([n],\mathbf{r}) + \frac{1}{2}\sum_{\mathbf{q},\mathbf{q}'} \delta n_{\mathbf{q}'}\delta n_{\mathbf{q}-\mathbf{q}'}e^{i\mathbf{q}.\mathbf{r}}\times \left[g_{xc}(\mathbf{q},\mathbf{q}',n_0) - \frac{f_{xc}(\mathbf{q}',n_0)f_{xc}(\mathbf{q}-\mathbf{q}',n_0)}{(f_{xc}(n_0))^2} g_{xc}(\mathbf{0},n_0)\right] \quad (A.6)$$

Assuming that both response functions f_{xc} and g_{xc} are analytic, we can write in the small-q limit :

$$f_{xc}(\mathbf{q},n) = f^{(0)}_{xc}(n) + f^{(2)}_{xc}(n)q^2 + ... \quad (A.7)$$

Based on symmetry arguments [38], g_{xc} can be expanded as :

$$g_{xc}(\mathbf{q},\mathbf{q}',n) = g^{(0)}_{xc}(n) + g^{(2)}_{xc}(n)(q^2 + q'^2 - \mathbf{q}.\mathbf{q}') + ... \quad (A.8)$$

Using this expansion in (A.6), we obtain:

$$v_{xc}([n],\mathbf{r}) = v^{c}_{xc}([n],\mathbf{r}) + \frac{1}{2}\sum_{\mathbf{q},\mathbf{q}'} \delta n_{\mathbf{q}'}\delta n_{\mathbf{q}-\mathbf{q}'}e^{i\mathbf{q}.\mathbf{r}} \times \left(\alpha_1 q^2 + \alpha_2 q'^2 - \alpha_2 \mathbf{q}.\mathbf{q}'\right) \quad (A.9)$$

where :

$$\alpha_1 = \left(g^{(2)}_{xc}(n_0) - \frac{f^{(2)}_{xc}(n_0)g^{(0)}_{xc}(n_0)}{f_{xc}(n_0)}\right)$$

$$\alpha_2 = \left(g^{(2)}_{xc}(n_0) - 2\frac{f^{(2)}_{xc}(n_0)g^{(0)}_{xc}(n_0)}{f_{xc}(n_0)}\right)$$

Now we show how the dependencies on q in (A.9) become a gradient corrections in real space. First we need to show the following:

$$\begin{aligned}\sum_{\mathbf{q},\mathbf{q}'}(q'^2+q^2-2\mathbf{q}.\mathbf{q}')\delta n_{\mathbf{q}'}\delta n_{\mathbf{q}-\mathbf{q}'}e^{i\mathbf{q}.\mathbf{r}} &= -\sum_{\mathbf{q},\mathbf{q}'}e^{i\mathbf{q}.\mathbf{r}}\int d\mathbf{r}_1\delta n(\mathbf{r}_1)e^{-i\mathbf{r}_1.\mathbf{q}'}\int d\mathbf{r}_2\delta n(\mathbf{r}_2)\nabla^2_{\mathbf{r}_2}e^{-i\mathbf{r}_2.(\mathbf{q}-\mathbf{q}')}\\ &= -\sum_{\mathbf{q},\mathbf{q}'}e^{i\mathbf{q}.\mathbf{r}}\int d\mathbf{r}_1\delta n(\mathbf{r}_1)e^{-i\mathbf{r}_1.\mathbf{q}'}\int d\mathbf{r}_2 e^{-i\mathbf{r}_2.(\mathbf{q}-\mathbf{q}')}\nabla^2_{\mathbf{r}_2}\delta n(\mathbf{r}_2)\\ &= -\int d\mathbf{r}_1 d\mathbf{r}_2\delta n(\mathbf{r}_1)\delta(\mathbf{r}_1-\mathbf{r}_2)\delta(\mathbf{r}-\mathbf{r}_2)\nabla^2_{\mathbf{r}_2}\delta n(\mathbf{r}_2)\end{aligned}$$

Then:

$$\sum_{\mathbf{q},\mathbf{q}'}(q'^2+q^2-2\mathbf{q}.\mathbf{q}')\delta n_{\mathbf{q}'}\delta n_{\mathbf{q}-\mathbf{q}'}e^{i\mathbf{q}.\mathbf{r}} = -\delta n(\mathbf{r})\nabla^2_{\mathbf{r}}n(\mathbf{r}) \tag{A.10}$$

We have also:

$$\begin{aligned}\sum_{\mathbf{q},\mathbf{q}'}q'^2\delta n_{\mathbf{q}'}\delta n_{\mathbf{q}-\mathbf{q}'}e^{i\mathbf{q}.\mathbf{r}} &= -\sum_{\mathbf{q},\mathbf{q}'}e^{i\mathbf{q}.\mathbf{r}}\int d\mathbf{r}_1\delta n(\mathbf{r}_1)\nabla^2_{\mathbf{r}_1}e^{-i\mathbf{r}_1.\mathbf{q}'}\int d\mathbf{r}_2\delta n(\mathbf{r}_2)e^{-i\mathbf{r}_2.(\mathbf{q}-\mathbf{q}')}\\ &= -\sum_{\mathbf{q},\mathbf{q}'}e^{i\mathbf{q}.\mathbf{r}}\int d\mathbf{r}_1 e^{-i\mathbf{r}_1.\mathbf{q}'}\nabla^2_{\mathbf{r}_1}\delta n(\mathbf{r}_1)\int d\mathbf{r}_2\delta n(\mathbf{r}_2)e^{-i\mathbf{r}_2.(\mathbf{q}-\mathbf{q}')}\\ &= -\int d\mathbf{r}_1 d\mathbf{r}_2\delta n(\mathbf{r}_2)\delta(\mathbf{r}_1-\mathbf{r}_2)\delta(\mathbf{r}-\mathbf{r}_2)\nabla^2_{\mathbf{r}_1}\delta n(\mathbf{r}_1)\end{aligned}$$

Then:

$$\sum_{\mathbf{q},\mathbf{q}'}q'^2\delta n_{\mathbf{q}'}\delta n_{\mathbf{q}-\mathbf{q}'}e^{i\mathbf{q}.\mathbf{r}} = -\delta n(\mathbf{r})\nabla^2_{\mathbf{r}}n(\mathbf{r}) \tag{A.11}$$

We have also:

$$\begin{aligned}\sum_{\mathbf{q},\mathbf{q}'}(q'^2-\mathbf{q}.\mathbf{q}')\delta n_{\mathbf{q}'}\delta n_{\mathbf{q}-\mathbf{q}'}e^{i\mathbf{q}.\mathbf{r}} &= \sum_{\mathbf{q},\mathbf{q}'}e^{i\mathbf{q}.\mathbf{r}}\int d\mathbf{r}_1\delta n(\mathbf{r}_1)\nabla_{\mathbf{r}_1}e^{-i\mathbf{r}_1.\mathbf{q}'}\int d\mathbf{r}_2\delta n(\mathbf{r}_2)\nabla_{\mathbf{r}_2}e^{-i\mathbf{r}_2.(\mathbf{q}-\mathbf{q}')}\\ &= \sum_{\mathbf{q},\mathbf{q}'}e^{i\mathbf{q}.\mathbf{r}}\int d\mathbf{r}_1 e^{-i\mathbf{r}_1.\mathbf{q}'}\nabla_{\mathbf{r}_1}\delta n(\mathbf{r}_1)\int d\mathbf{r}_2 e^{-i\mathbf{r}_2.(\mathbf{q}-\mathbf{q}')}\nabla_{\mathbf{r}_2}\delta n(\mathbf{r}_2)\\ &= \int d\mathbf{r}_1 d\mathbf{r}_2\delta(\mathbf{r}_1-\mathbf{r}_2)\delta(\mathbf{r}-\mathbf{r}_2)\nabla_{\mathbf{r}_1}\delta n(\mathbf{r}_1)\nabla_{\mathbf{r}_2}\delta n(\mathbf{r}_2)\end{aligned}$$

Then:

$$\sum_{\mathbf{q},\mathbf{q}'}(q'^2-\mathbf{q}.\mathbf{q}')\delta n_{\mathbf{q}'}\delta n_{\mathbf{q}-\mathbf{q}'}e^{i\mathbf{q}.\mathbf{r}} = -|\nabla_{\mathbf{r}}n(\mathbf{r})|^2 \tag{A.12}$$

From (A.10) and (A.11) we deduce :

$$\sum_{\mathbf{q},\mathbf{q}'}q^2\delta n_{\mathbf{q}'}\delta n_{\mathbf{q}-\mathbf{q}'}e^{i\mathbf{q}.\mathbf{r}} = \sum_{\mathbf{q},\mathbf{q}'}2\mathbf{q}.\mathbf{q}'\delta n_{\mathbf{q}'}\delta n_{\mathbf{q}-\mathbf{q}'}e^{i\mathbf{q}.\mathbf{r}}$$

By subtracting (A.12) from (A.11) we get:

$$\sum_{\mathbf{q},\mathbf{q}'} \mathbf{q}.\mathbf{q}'\delta n_{\mathbf{q}'}\delta n_{\mathbf{q}-\mathbf{q}'}e^{i\mathbf{q}.\mathbf{r}} = |\nabla_{\mathbf{r}} n(\mathbf{r})|^2 - \delta n(\mathbf{r})\nabla^2_{\mathbf{r}} n(\mathbf{r})$$

Now we have all the ingredients to write (A.9) in real space:

$$v_{\mathrm{xc}}([n],\mathbf{r}) \quad = \quad v^c_{\mathrm{xc}}([n],\mathbf{r}) - \alpha_1\delta n(\mathbf{r})\nabla^2_{\mathbf{r}} n(\mathbf{r}) + (\alpha_1 - \frac{\alpha_2}{2})|\nabla_{\mathbf{r}} n(\mathbf{r})|^2 \quad \text{(A.13)}$$

This equation gives a gradient correction to first order connector. The coefficient α_1 and α_2 can be determined by noticing:

$$\frac{\partial f_{\mathrm{xc}}(\mathbf{q}, n_0)}{\partial n_0} = g_{\mathrm{xc}}(\mathbf{q}, \mathbf{q}, n_0)$$

This equation together with (A.7) and (A.8) yield :

$$\frac{\partial f_{\mathrm{xc}}(n_0)}{\partial n_0} = g^{(0)}_{\mathrm{xc}}(n_0)$$
$$\frac{\partial f^{(2)}_{\mathrm{xc}}(n_0)}{\partial n_0} = g^{(2)}_{\mathrm{xc}}(n_0)$$

So all we need to determine α_1 and α_2 is the coefficient $f^{(2)}_{\mathrm{xc}}(n_0)$. These coefficients can be derived from an available result for the static nonlocal xc kernel of the HEG [75, 76].

Appendix B

Weighted Density Approximation

In the following, I will give more details concerning the target functional used in Ch. 5. It is based on the weighted density approximation (WDA) of the xc hole $n_{\rm xc}$ introduced in [57, 58, 59, 60], with the weight function proposed in [61]. The xc energy is given in (5.1). The two functions λ and C are

$$\lambda(n) = \left(\frac{-3\Gamma\left(\frac{3}{5}\right)}{4\Gamma\left(\frac{2}{5}\right)\varepsilon_{\rm xc}(n)} \right)^5 \text{ and } C(n) = \frac{-3/4\pi}{\Gamma\left(\frac{2}{5}\right)\left(\lambda(n)\right)^{\frac{3}{5}} n}, \tag{B.1}$$

where $\varepsilon_{\rm xc}(n)$ is the exact xc energy per particle of the HEG, whose correlation part we take from the Perdew-Zunger parameterization [32].

To get the target xc potential we perform the functional derivative of the xc energy, $\frac{\delta E_{\rm xc}[n]}{\delta n(\mathbf{r})}$. It yields :

$$\begin{aligned} v_{\rm xc}^{\rm WDA}(\mathbf{r},[n]) = \frac{1}{2}\Bigg[& \int d\mathbf{r}' \frac{2n(\mathbf{r}')}{|\mathbf{r}'-\mathbf{r}|} C(\tilde{n}(\mathbf{r}',\mathbf{r})) \left(1 - e^{\frac{-\lambda(\tilde{n}(\mathbf{r}',\mathbf{r}))}{|\mathbf{r}'-\mathbf{r}|^5}}\right) \\ & + n(\mathbf{r}) \int d\mathbf{r}' \frac{n(\mathbf{r}')}{|\mathbf{r}'-\mathbf{r}|} C'(\tilde{n}(\mathbf{r}',\mathbf{r})) \left(1 - e^{\frac{-\lambda(\tilde{n}(\mathbf{r}',\mathbf{r}))}{|\mathbf{r}'-\mathbf{r}|^5}}\right) \\ & + n(\mathbf{r}) \int d\mathbf{r}' \frac{n(\mathbf{r}')}{|\mathbf{r}'-\mathbf{r}|^6} C(\tilde{n}(\mathbf{r}',\mathbf{r}))\lambda'(\tilde{n}(\mathbf{r}',\mathbf{r})) e^{\frac{-\lambda(\tilde{n}(\mathbf{r}',\mathbf{r}))}{|\mathbf{r}'-\mathbf{r}|^5}} \Bigg], \end{aligned} \tag{B.2}$$

with $\tilde{n}(\mathbf{r},\mathbf{r}') = [n(\mathbf{r}) + n(\mathbf{r}')]/2$ [82]. Further functional derivative yields the exchange-correlation kernel, which can be expressed as the sum of six terms, $f_{\rm xc}^{\rm WDA}(|\mathbf{r}-\mathbf{r}'|;n_0) = \sum_{i=1}^{6} f_i$. Evaluated in the HEG with density n_0 these

terms read:

$$
\begin{aligned}
f_1 = &\quad \left[C(n_0) + n_0 C'(n_0) + \tfrac{1}{4} n_0^2 C''(n_0)\right] \frac{1 - e^{\frac{-\lambda(n_0)}{|\mathbf{r}-\mathbf{r}'|^5}}}{|\mathbf{r}-\mathbf{r}'|} \\
f_2 = &\quad 2\pi\Gamma\left(\tfrac{3}{5}\right) \left(\lambda(n_0)\right)^{\frac{2}{5}} \left[n_0 C'(n_0) + \tfrac{1}{4} n_0^2 C''(n_0)\right] \delta(\mathbf{r}-\mathbf{r}') \\
f_3 = &\quad \left[n_0 C(n_0)\lambda'(n_0) + \tfrac{1}{2} n_0^2 C'(n_0)\lambda'(n_0) + \tfrac{1}{4} n_0^2 C(n_0)\lambda''(n_0)\right] \\
&\qquad \times \frac{e^{\frac{-\lambda(n_0)}{|\mathbf{r}-\mathbf{r}'|^5}}}{|\mathbf{r}-\mathbf{r}'|^6} \\
f_4 = &\quad \frac{4\pi\Gamma\left(\frac{3}{5}\right)}{5\left(\lambda(n_0)\right)^{\frac{3}{5}}} \left[n_0 C(n_0)\lambda'(n_0) + \tfrac{1}{2} n_0^2 C'(n_0)\lambda'(n_0)\right. \\
&\qquad \left. + \tfrac{1}{4} n_0^2 C(n_0)\lambda''(n_0)\right] \delta(\mathbf{r}-\mathbf{r}') \\
f_5 = &\quad -\tfrac{1}{4} n_0^2 C(n_0) \left(\lambda'(n_0)\right)^2 \frac{e^{\frac{-\lambda(n_0)}{|\mathbf{r}-\mathbf{r}|^5}}}{|\mathbf{r}-\mathbf{r}|^{11}} \\
f_6 = &\quad -\frac{\pi\Gamma\left(\frac{8}{5}\right)}{5\left(\lambda(n_0)\right)^{\frac{8}{5}}} n_0^2 C(n_0) \left(\lambda'(n_0)\right)^2 \delta(\mathbf{r}-\mathbf{r}'|)\,.
\end{aligned}
\tag{B.3}
$$

Appendix C

DFT code

Here I present the code that I used to calculate the charge density in Ch. 6 and the Kohn-Sham (KS) density matrix in Ch. 10. With small adjustments, the same code was used to invert the exchange correlation potential from the density in Ch. 7. Indeed, many DFT codes already exist, but since I need to use some connector approximations and to control specific parameters, I opted to implement my own code. This also gives me more flexibility to use any external potential and easily modify any part of the code.

The code uses the plane wave method [23] to solve the Kohn-Sham equations presented in Ch. 2. This method is particularly well-suited for studying periodic crystals, where it offers an intuitive understanding and simple algorithms for practical calculations, thanks to the Bloch theorem.

C.1 Input file

The code is written in Python. To use it, we first need to generate the pseudo potential in the plane wave basis, using *abinit* [121] for example, then prepare the input file and execute the following command

```
$ python run_DFT_KS.py -i <input file> <output file>
```

In the input file one should define the specific material parameters and choose an approximation for the xc potential. Here below I show an example of an input file for silicon.

```
#Definition of the unit cell

acell= [10.263087]*3 # [bohr]; same as [10.263087,10.263087,10.263087]
Mt= [[1, 0, 0],      # FCC primitive vectors (to be scaled by acell)
     [0, 1, 0],
     [0, 0, 1]]

n_occup=8     # number of electrons in the valence band

# Definition of the plane wave basis set

nkpt = [4,4,4] # Density of k points in Brillouin Zone
ecut= 12.5     # Maximal kinetic energy cut-off, in Hartree

```

```
#Path to read the local and the non-local part of the pseudo
   potential

local_pseudo=  "VPSP_loc.dat"
non_local_pseudo= "VPSP_nl.dat"

#By Default the code use the Perdew-Zunger parameterization for
   the correlation energy of the HEG.
#To use the Chachiyo parameterization turn on the following
   variable

Chachiyo=0

# specify the choice of the xc potential functional.

choose_vxc="connector_n0mean" # or "LDA" or other functional.

tol_e= 1e-8 # Tolerance on the total energy, which defines the
   convergence condition.


density_matrix=0 #Change to True to calculate and write the
   density matrix

#initial_density="dens.dat"   # Uncomment this line to specify
   the initial density
```

LISTING C.1: Input file for silicon

C.2 Calculation of the density and the density matrix

The most important operation in any DFT code is the self-consistent solution of the KS equation to calculate the electronic density. It is calculated as a modulus squared sum of the KS orbitals. Using these orbitals one can easily calculate the KS density matrix. Here we give a brief presentation of the method that I have adopted for calculating the density.

For a periodic system, or a crystal, treated using KS DFT theory, the density can be written as

$$n(\mathbf{r}) = \sum_{\mathbf{k},i} f(\epsilon_{i,\mathbf{k}}) n_{i,\mathbf{k}}(\mathbf{r}), \quad \text{with } n_{i,\mathbf{k}}(\mathbf{r}) = |\psi_{i,\mathbf{k}}(\mathbf{r})|^2, \tag{C.1}$$

where $\mathbf{k}$ lies in the first Brillouin Zone, i denotes a band and f is the Fermi function. The function $\psi_{i,\mathbf{k}}(\mathbf{r})$ denotes the KS orbital for each point $\mathbf{k}$ and band i. It can be written as

$$\psi_{i,\mathbf{k}}(\mathbf{r}) = \sum_{\mathbf{G}} c_{i,\mathbf{k}}(\mathbf{G}) \times \frac{1}{\sqrt{\Omega}} e^{\mathrm{i}(\mathbf{k}+\mathbf{G})\cdot\mathbf{r}} = e^{\mathrm{i}\mathbf{k}\cdot\mathbf{r}} \frac{1}{\sqrt{N_k}} u_{i,\mathbf{k}}(\mathbf{r}), \tag{C.2}$$

where $c_{i,\mathbf{k}}(\mathbf{G})$ are the eigenvectors of the KS Hamiltonian in the basis of orthonormal plane waves $|\mathbf{k}+\mathbf{G}\rangle$, Ω is the volume of the crystal and so

$\Omega = N_k \Omega_{\text{cell}}$, and

$$u_{i,\mathbf{k}}(\mathbf{r}) = \frac{1}{\sqrt{\Omega_{\text{cell}}}} \sum_{\mathbf{G}} c_{i,\mathbf{G}}(\mathbf{k})\, e^{\mathrm{i}\mathbf{G}\cdot\mathbf{r}}, \tag{C.3}$$

which has the periodicity of the crystal according to Bloch theorem. The density can be then calculated from one primitive cell as

$$n(\mathbf{r}) = \frac{1}{N_k} \sum_{\mathbf{k},i} f(\epsilon_{i,\mathbf{k}}) |u_{i,\mathbf{k}}(\mathbf{r})|^2 \tag{C.4}$$

and in the reciprocal space as

$$n(\mathbf{G}) = \frac{1}{N_k} \sum_{\mathbf{k},i} \sum_{\mathbf{G},\mathbf{G}'} f(\epsilon_{i,\mathbf{k}}) u^*_{i,\mathbf{k}}(\mathbf{G}) u_{i,\mathbf{k}}(\mathbf{G}')\, e^{\mathrm{i}(\mathbf{G}-\mathbf{G}')\cdot\mathbf{r}}. \tag{C.5}$$

Similarly, the density matrix reads

$$n(\mathbf{r},\mathbf{r}') = \frac{1}{N_k} \sum_{\mathbf{k},i} f(\epsilon_{i,\mathbf{k}}) u^*_{i,\mathbf{k}}(\mathbf{r}) u_{i,\mathbf{k}}(\mathbf{r}') e^{\mathrm{i}\mathbf{k}\cdot(\mathbf{r}-\mathbf{r}')}. \tag{C.6}$$

Fig. C.1 illustrates the algorithm implemented in the code to obtain the density using (C.3) and (C.4).

In practice, to calculate the density, we first define the material parameters in the input file, then we execute the file `run_DFT_KS.py`. The code begins by importing the necessary functions, then on the basis of the energy cut-off, E_{cutoff}, it generates a list of the reciprocal lattice vector, $\mathbf{G}$, corresponding to each point $\mathbf{k}$ in the first Brillouin zone, so that

$$\frac{1}{2}|\mathbf{k}+\mathbf{G}|^2 < E_{\text{cutoff}}. \tag{C.7}$$

It also generates a larger list of $\mathbf{G}$ vectors to perform the double sum needed for the Fourier transform of the density defined in (C.5). The next step is to construct the Hamiltonian matrix, $H_{\mathbf{k}}(\mathbf{G},\mathbf{G}')$, in the plane wave basis $|\mathbf{k}+\mathbf{G}\rangle$. To achieve this, we sum the matrix of the kinetic energy operator, the Hartree potential, the xc potential and the pseudo potential

$$H_{\mathbf{k}}(\mathbf{G},\mathbf{G}') = \frac{1}{2}|\mathbf{k}+\mathbf{G}|^2 + 4\pi \frac{n\left(\mathbf{G}-\mathbf{G}'\right)}{|\mathbf{G}-\mathbf{G}'|^2} + v_{\text{xc}}\left(\mathbf{G}-\mathbf{G}'\right) + V^{\text{PSP}}_{\mathbf{k}}\left(\mathbf{G}-\mathbf{G}'\right), \tag{C.8}$$

where V^{PSP} is the pseudo potential. Once the Hamiltonian matrix is built, it will be diagonalized for each point $\mathbf{k}$ to obtain the eigenvalues and the eigenvectors, $c_{i,\mathbf{k}}(\mathbf{G})$, which represent the KS orbitals in the reciprocal space. Next, the code determines the Fermi level and calculate the sum (C.4) using the scheme shown in Fig. C.1 to obtain the density $n(\mathbf{r})$ for the first iteration. The resulting density will be used to construct the Hamiltonian for the next iteration. The code keep iterating using a *while* loop until the total energy is converged. At the end, if the KS density matrix was requested in the input file, the converged KS orbitals will be used to calculate it, see Fig. C.1.

The code generates an output file that contains, by default, the density, the

xc potential, the Hartree potential, the total energy and its component, and the density matrix if it was requested. Other quantities can also be retrieved by making slight modification to the script `run_DFT_KS.py`.

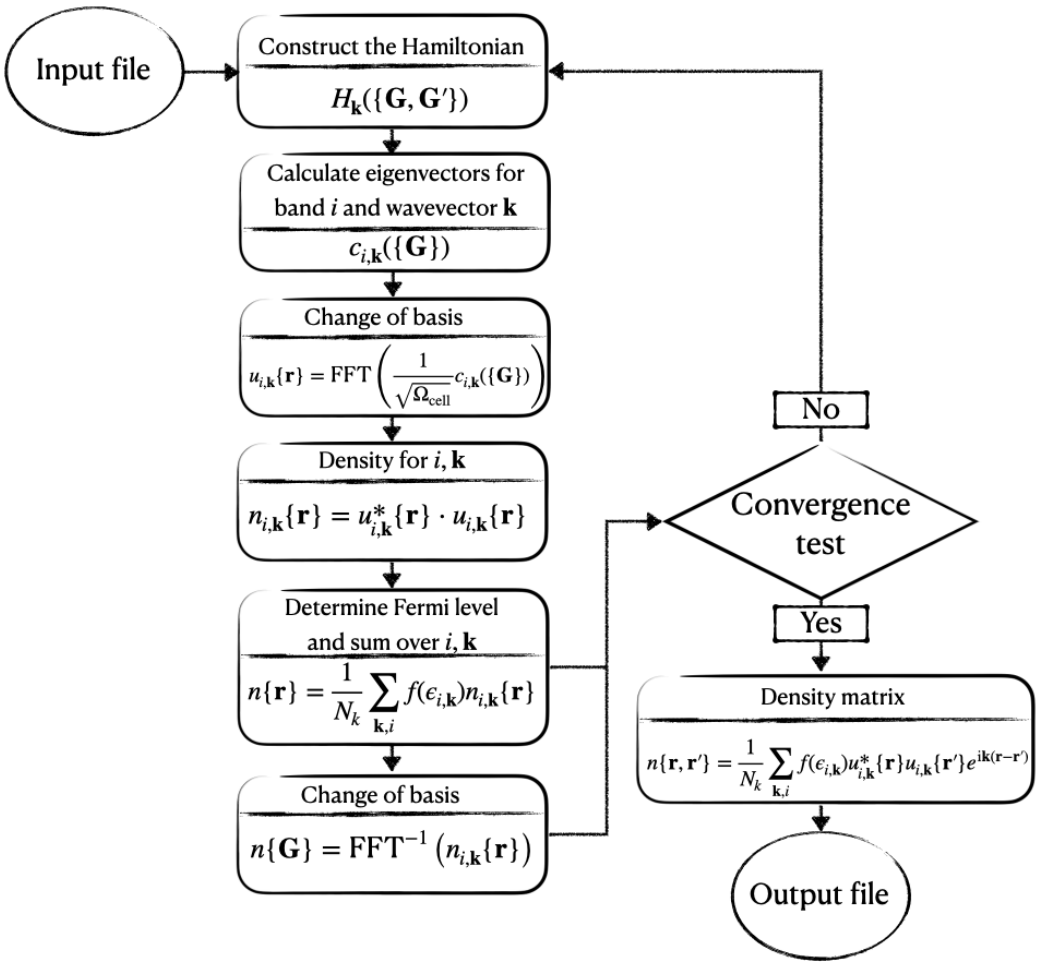

FIGURE C.1: Self consistent scheme to calculate the density and density matrix: The input file contains the choice of the approximation for the xc potential, and the initial density, if specified, otherwise the algorithm start with a constant density. The notation $\{\mathbf{G}\}$ and $\{\mathbf{r}\}$ denotes the sets of the reciprocal space vectors $\mathbf{G}$ selected according to the cut-off energy, and the grid points $\mathbf{r}$ in real space. The fast Fourier transform (FFT) is used here to calculate $n\{\mathbf{G}\}$ in N log N operations instead of the double sum (C.5) that scales as N^2, where N is the size of the set $\{\mathbf{r}\}$.

Appendix D

List of publications

- A. Aouina, M. Gatti and L. Reining, *Strategies to build functionals of the density, or functionals of Green's functions: what can we learn?*, Faraday Discussions 224, 27 (2020) [114].
- M. Vanzini [1], A. Aouina [1] , M. Panholzer, M. Gatti and L. Reining, *Reusing model results to determine materials properties: connector theory approach*, accepted, npj Computational Materials (2022), arXiv:1903.07930.
- A. Aouina, M. Gatti, S. Chen, S. Zhang, and L. Reining, *Kohn-Sham exchange-correlation potential of solids: answers from the ground state density*, in preparation

[1] contributed equally to the work.

Acknowledgements

والحمد لله في بدء وفي ختم [1]

مقتطف من قصيدة البردة

Through these lines, I would like to thank all the people who contributed directly or indirectly to this thesis. I will mention some of them and ask forgiveness to the others, because naming them all would require another chapter and, probably, a book to express my gratitude.

I am deeply thankful to my supervisors, Lucia and Matteo. Without your assistance, this thesis would not have been possible. I was lucky enough to meet, at the same time, two wonderful, excellent, smart, and kind supervisors like you. I want to thank you for believing in me to conduct this work, for giving me the freedom to explore various directions, for motivating me, and for always being available to help and discuss. I have learned a lot from you, both scientifically and personally. I am very impressed by your excellent performance in scientific research while also being an extremely nice, understanding, and generous person. I will never forget your continued help and support since our first meeting.

I would also like to thank Marco, who explained to me the *connector* idea and helped me to get a good start. A big thanks to Martin for always being available when I needed him. I have to thank my collaborators, Siyuan Chen and Shiwei Zhang, for the fruitful discussions about the QMC density and the Kohn-Sham inversion. I would like to thank my colleagues from the theoretical spectroscopy group: Shalu, Francesco, Andrea, Christine, Jaako, Valérie, Stefano, Arnaud, Jack, Paola, Georg, Raj, Vitaly, Abdallah, Alam, Lionel, Marc, and Laura. Thank you for the stimulating discussions, as well as your comments and remarks on my work and presentations. I would like to thank Francesco in particular for always being enthusiastic and available to answer my questions. A special thanks to Andrea for solving all my problems with nero.

I would also like to thank my colleagues at LSI. I am grateful to Michèle, Marylène, and Elodie for making all of the administrative procedures so simple for me.

Many thanks to Emmanuel Fromager, Nikitas Gidopoulos, and Carsten Ullrich for accepting to be part of my jury, and to Silvana Botti and Neepa Maitra for accepting to review my manuscript. Thank you for your questions, comments, corrections, and compliments.

A big thank you to Antar, Ilyes, Aissa, Farid and Samir for welcoming and assisting me in France. Thanks to all my friends, including Haithem, Hacene, Yahia, Bassem, Khaled, Okba, Nawro, the twins S&Y, Saad Elbassiti, Ismail, Muhammad Shahnawaz, Abdelhamid, just to name a few. Thank you for the wonderful atmosphere that has always been family-like.

[1] "And all praise is due to God in its beginning and its end", from *Qasida Al Burda.*

Last but not least, I am eternally grateful to my beloved parents, who were my very first teachers and educators. Thanks to my brother Ishak and my cousin Reda, who encouraged me to pursue my studies in France when I was not considering the idea at all. I would like to thank my aunt Nadira for her financial and moral support. Thank you for all the food recipes I have yet to try :) Many thanks to Mohamed, Meriam, Sara, and all my family for your support and unconditional love.

Bibliography

[1] R.M. Martin, L. Reining, and D.M. Ceperley. *Interacting Electrons: Theory and Computational Approaches*. Cambridge University Press, 2016. ISBN: 9781316558560.

[2] W. M. C. Foulkes et al. "Quantum Monte Carlo simulations of solids". In: *Rev. Mod. Phys.* 73 (1 2001), pp. 33–83. DOI: 10.1103/RevModPhys.73.33. URL: https://link.aps.org/doi/10.1103/RevModPhys.73.33.

[3] Giovanni Onida, Lucia Reining, and Angel Rubio. "Electronic excitations: density-functional versus many-body Green's-function approaches". In: *Reviews of Modern Physics* 74.April (2002).

[4] Alexander L Fetter and John Dirk Walecka. *Quantum theory of many-particle systems*. McGraw-Hill, 1971.

[5] P. Hohenberg and W. Kohn. "Inhomogeneous Electron Gas". In: *Phys. Rev.* 136 (3B 1964), B864–B871.

[6] Walter Kohn. "Theory of the Insulating State". In: *Phys. Rev.* 133.1A (1964), A171–A181. DOI: 10.1103/PhysRev.133.A171.

[7] Gerbrand Ceder. "Predicting Properties from Scratch". In: *Science* 280.5366 (1998), pp. 1099–1100. ISSN: 0036-8075. DOI: 10.1126/science.280.5366.1099. URL: http://science.sciencemag.org/content/280/5366/1099.

[8] Nicola Marzari. "The frontiers and the challenges". In: *Nature Materials* 15 (Mar. 2016), pp. 381–. URL: https://doi.org/10.1038/nmat4613.

[9] Stefano Curtarolo et al. "Predicting Crystal Structures with Data Mining of Quantum Calculations". In: *Phys. Rev. Lett.* 91 (13 2003), p. 135503. DOI: 10.1103/PhysRevLett.91.135503. URL: https://link.aps.org/doi/10.1103/PhysRevLett.91.135503.

[10] P. Jain et al. "MgH2 as dopant for improved activation of commercial Mg ingot". In: *J. Alloys Compd.* 575 (2013), pp. 364–369. ISSN: 09258388. DOI: 10.1016/j.jallcom.2013.05.099. URL: http://linkinghub.elsevier.com/retrieve/pii/S0925838813012590.

[11] Anubhav Jain, Yongwoo Shin, and Kristin A. Persson. "Computational predictions of energy materials using density functional theory". In: *Nature Reviews Materials* 1 (Jan. 2016), pp. 15004–. URL: https://doi.org/10.1038/natrevmats.2015.4.

[12] T. L. Gilbert. "Hohenberg-Kohn theorem for nonlocal external potentials". In: *Phys. Rev. B* 12.6 (1975), pp. 2111–2120. DOI: 10.1103/PhysRevB.12.2111.

[13] Per-Olov Löwdin. "Quantum Theory of Many-Particle Systems. I. Physical Interpretations by Means of Density Matrices, Natural Spin-Orbitals, and Convergence Problems in the Method of Configurational Interaction". In: *Phys. Rev.* 97 (6 1955), pp. 1474–1489. DOI: 10.1103/PhysRev.97.1474. URL: https://link.aps.org/doi/10.1103/PhysRev.97.1474.

[14] Siyuan Chen et al. "Ab initio electronic density in solids by many-body plane-wave auxiliary-field quantum Monte Carlo calculations". In: *Phys. Rev. B* 103 (7 2021), p. 075138. DOI: 10.1103/PhysRevB.103.075138. URL: https://link.aps.org/doi/10.1103/PhysRevB.103.075138.

[15] W. Kohn. "Nobel Lecture: Electronic structure of matter—wave functions and density functionals". In: *Rev. Mod. Phys.* 71 (5 1999), pp. 1253–1266. DOI: 10.1103/RevModPhys.71.1253. URL: http://link.aps.org/doi/10.1103/RevModPhys.71.1253.

[16] M. Born and R. Oppenheimer. "Zur Quantentheorie der Molekeln". In: *Annalen der Physik* 389.20 (1927), pp. 457–484. ISSN: 1521-3889. DOI: 10.1002/andp.19273892002. URL: http://dx.doi.org/10.1002/andp.19273892002.

[17] F Sottile. "Response functions of semiconductors and insulators". PhD thesis. L'Ecole Polytechnique, 2003.

[18] Max Born and Kun Huang. "Dynamical Theory of Crystal Lattices". In: *American Journal of Physics* 23.7 (1955), pp. 474–474. DOI: 10.1119/1.1934059. eprint: https://doi.org/10.1119/1.1934059. URL: https://doi.org/10.1119/1.1934059.

[19] D.R. Hartree. In: *Proc. Cambridge Philos. Soc.* 24 (1928), p. 89.

[20] Stefan Kurth and John P. Perdew. "Role of the exchange–correlation energy: Nature's glue". In: *International Journal of Quantum Chemistry* 77.5 (2000), pp. 814–818.

[21] J. C. Slater. "The Theory of Complex Spectra". In: *Phys. Rev.* 34 (10 1929), pp. 1293–1322. DOI: 10.1103/PhysRev.34.1293. URL: https://link.aps.org/doi/10.1103/PhysRev.34.1293.

[22] T.A. Koopmans. In: *Physica* 1 (1933), p. 104.

[23] Richard M. Martin. *Electronic Structure: Basic Theory and Practical Methods*. Cambridge University Press, 2004. DOI: 10.1017/CBO9780511805769.

[24] L.H. Thomas. "Calculation of atomic fields". In: *Proc. Cambridge Phil. Soc.* 23 (1927), p. 542.

[25] E. Fermi. "Application of statistical gas methods to electronic systems". In: *Rend. Accad. Naz. Lincei* 6 (1927), p. 602.

[26] Edward Teller. "On the Stability of Molecules in the Thomas-Fermi Theory". In: *Rev. Mod. Phys.* 34 (4 1962), pp. 627–631. DOI: 10.1103/RevModPhys.34.627. URL: https://link.aps.org/doi/10.1103/RevModPhys.34.627.

[27] Nandor L. Balàzs. "Formation of Stable Molecules within the Statistical Theory of Atoms". In: *Phys. Rev.* 156 (1 1967), pp. 42–47. DOI: 10.1103/PhysRev.156.42. URL: https://link.aps.org/doi/10.1103/PhysRev.156.42.

[28] Elliott H. Lieb and Barry Simon. "Thomas-Fermi Theory Revisited". In: *Phys. Rev. Lett.* 31 (11 1973), pp. 681–683. DOI: 10.1103/PhysRevLett.31.681. URL: https://link.aps.org/doi/10.1103/PhysRevLett.31.681.

[29] W. Kohn and L. J. Sham. "Self-Consistent Equations Including Exchange and Correlation Effects". In: *Phys. Rev.* 140 (4A 1965), A1133–A1138. DOI: 10.1103/PhysRev.140.A1133. URL: http://link.aps.org/doi/10.1103/PhysRev.140.A1133.

[30] J. C. Slater. "Magnetic Effects and the Hartree-Fock Equation". In: *Phys. Rev.* 82.4 (1951), pp. 538–541. DOI: 10.1103/PhysRev.82.538.

[31] D. M. Ceperley and B. J. Alder. "Ground State of the Electron Gas by a Stochastic Method". In: *Phys. Rev. Lett.* 45 (7 1980), pp. 566–569.

[32] J. P. Perdew and Alex Zunger. "Self-interaction correction to density-functional approximations for many-electron systems". In: *Phys. Rev. B* 23.10 (1981), pp. 5048–5079. ISSN: 0163-1829. DOI: 10.1103/PhysRevB.23.5048. URL: http://link.aps.org/doi/10.1103/PhysRevB.23.5048.

[33] Carlos Fiolhais and John P. Perdew. "Energies of curved metallic surfaces from the stabilized-jellium model". In: *Phys. Rev. B* 45 (11 1992), pp. 6207–6215. DOI: 10.1103/PhysRevB.45.6207. URL: https://link.aps.org/doi/10.1103/PhysRevB.45.6207.

[34] O. Gunnarsson and B. I. Lundqvist. "Exchange and correlation in atoms, molecules, and solids by the spin-density-functional formalism". In: *Phys. Rev. B* 13.10 (1976), pp. 4274–4298. DOI: 10.1103/PhysRevB.13.4274.

[35] E. Prodan and W. Kohn. "Nearsightedness of electronic matter". In: *Proceedings of the National Academy of Sciences* 102.33 (2005), pp. 11635–11638. ISSN: 0027-8424. DOI: 10.1073/pnas.0505436102. URL: http://www.pnas.org/content/102/33/11635.

[36] Frank Herman, John P. Van Dyke, and Irene B. Ortenburger. "Improved Statistical Exchange Approximation for Inhomogeneous Many-Electron Systems". In: *Phys. Rev. Lett.* 22 (16 1969), pp. 807–811. DOI: 10.1103/PhysRevLett.22.807. URL: https://link.aps.org/doi/10.1103/PhysRevLett.22.807.

[37] SHANG-KENG Ma and KEITH A. Brueckner. "Correlation Energy of an Electron Gas with a Slowly Varying High Density". In: *Phys. Rev.* 165 (1 1968), pp. 18–31. DOI: 10.1103/PhysRev.165.18. URL: https://link.aps.org/doi/10.1103/PhysRev.165.18.

[38] P. S. Svendsen and U. von Barth. "Gradient expansion of the exchange energy from second-order density response theory". In: *Phys. Rev. B* 54 (24 1996), pp. 17402–17413. DOI: 10.1103/PhysRevB.54.17402. URL: https://link.aps.org/doi/10.1103/PhysRevB.54.17402.

[39] David C. Langreth and John P. Perdew. "Theory of nonuniform electronic systems. I. Analysis of the gradient approximation and a generalization that works". In: *Phys. Rev. B* 21 (12 1980), pp. 5469–5493. DOI: 10.1103/PhysRevB.21.5469. URL: https://link.aps.org/doi/10.1103/PhysRevB.21.5469.

[40] A. D. Becke. "Density-functional exchange-energy approximation with correct asymptotic behavior". In: *Phys. Rev. A* 38 (6 1988), pp. 3098–3100. DOI: 10.1103/PhysRevA.38.3098. URL: https://link.aps.org/doi/10.1103/PhysRevA.38.3098.

[41] David C. Langreth and M. J. Mehl. "Beyond the local-density approximation in calculations of ground-state electronic properties". In: *Phys. Rev. B* 28 (4 1983), pp. 1809–1834. DOI: 10.1103/PhysRevB.28.1809. URL: https://link.aps.org/doi/10.1103/PhysRevB.28.1809.

[42] John P. Perdew. "Density-functional approximation for the correlation energy of the inhomogeneous electron gas". In: *Phys. Rev. B* 33 (12 1986), pp. 8822–8824. DOI: 10.1103/PhysRevB.33.8822. URL: https://link.aps.org/doi/10.1103/PhysRevB.33.8822.

[43] John P. Perdew and Yue Wang. "Accurate and simple analytic representation of the electron-gas correlation energy". In: *Phys. Rev. B* 45 (23 1992), pp. 13244–13249. DOI: 10.1103/PhysRevB.45.13244. URL: https://link.aps.org/doi/10.1103/PhysRevB.45.13244.

[44] John P. Perdew, Kieron Burke, and Matthias Ernzerhof. "Generalized Gradient Approximation Made Simple". In: *Phys. Rev. Lett.* 77 (18 1996), pp. 3865–3868. DOI: 10.1103/PhysRevLett.77.3865. URL: https://link.aps.org/doi/10.1103/PhysRevLett.77.3865.

[45] Axel D. Becke. "Density-functional thermochemistry. III. The role of exact exchange". In: *The Journal of Chemical Physics* 98.7 (1993), pp. 5648–5652. DOI: 10.1063/1.464913. URL: https://doi.org/10.1063/1.464913.

[46] A. Savin. In: *Recent Developments of Modern Density Functional Theory*. Ed. by J. M. Seminario. Amsterdam: Elsevier, 1996, pp. 327–357.

[47] Oleg A. Vydrov and Gustavo E. Scuseria. "Assessment of a long-range corrected hybrid functional". In: *The Journal of Chemical Physics* 125.23 (2006), p. 234109. DOI: 10.1063/1.2409292. eprint: https://doi.org/10.1063/1.2409292. URL: https://doi.org/10.1063/1.2409292.

[48] A. Seidl et al. "Generalized Kohn-Sham schemes and the band-gap problem". In: *Phys. Rev. B* 53 (7 1996), pp. 3764–3774. DOI: 10.1103/PhysRevB.53.3764. URL: https://link.aps.org/doi/10.1103/PhysRevB.53.3764.

[49] Rachel Garrick et al. "Exact Generalized Kohn-Sham Theory for Hybrid Functionals". In: *Phys. Rev. X* 10 (2 2020), p. 021040. DOI: 10.1103/PhysRevX.10.021040. URL: https://link.aps.org/doi/10.1103/PhysRevX.10.021040.

[50] A.M.K. Müller. "Explicit approximate relation between reduced two- and one-particle density matrices". In: *Physics Letters A* 105.9 (1984), pp. 446–452. ISSN: 0375-9601. DOI: https://doi.org/10.1016/0375-9601(84)91034-X. URL: https://www.sciencedirect.com/science/article/pii/037596018491034X.

[51] A. J. Coleman. "Structure of Fermion Density Matrices". In: *Rev. Mod. Phys.* 35 (3 1963), pp. 668–686. DOI: 10.1103/RevModPhys.35.668. URL: https://link.aps.org/doi/10.1103/RevModPhys.35.668.

[52] Valerio Olevano and Lucia Reining. "Excitonic Effects on the Silicon Plasmon Resonance". In: *Phys. Rev. Lett.* 86 (26 2001), pp. 5962–5965. DOI: 10.1103/PhysRevLett.86.5962. URL: http://link.aps.org/doi/10.1103/PhysRevLett.86.5962.

[53] Pierre-François Loos. "Exchange functionals based on finite uniform electron gases". In: *The Journal of Chemical Physics* 146.11 (2017), p. 114108. DOI: 10.1063/1.4978409. eprint: https://doi.org/10.1063/1.4978409. URL: https://doi.org/10.1063/1.4978409.

[54] Adolfo G. Eguiluz et al. "First-principles evaluation of the surface barrier for a Kohn-Sham electron at a metal surface". In: *Phys. Rev. Lett.* 68.9 (1992), pp. 1359–1362. DOI: 10.1103/PhysRevLett.68.1359.

[55] N. Helbig, I. V. Tokatly, and A. Rubio. "Exact Kohn–Sham potential of strongly correlated finite systems". In: *The Journal of Chemical Physics* 131.22 (2009), p. 224105. DOI: 10.1063/1.3271392. eprint: https://doi.org/10.1063/1.3271392. URL: https://doi.org/10.1063/1.3271392.

[56] M. T. Entwistle et al. "Local density approximations from finite systems". In: *Phys. Rev. B* 94 (20 2016), p. 205134. DOI: 10.1103/PhysRevB.94.205134. URL: https://link.aps.org/doi/10.1103/PhysRevB.94.205134.

[57] O. Gunnarsson, M. Jonson, and B.I. Lundqvist. "Exchange and correlation in inhomogeneous electron systems". In: *Solid State Commun.* 24.11 (1977), pp. 765 –768. ISSN: 0038-1098. DOI: https://doi.org/10.1016/0038-1098(77)91185-1. URL: http://www.sciencedirect.com/science/article/pii/0038109877911851.

[58] J.A. Alonso and L.A. Girifalco. "A non-local approximation to the exchange energy of the non-homogeneous electron gas". In: *Solid State Commun.* 24 (0 1977), p. 135. DOI: 10.1016/0038-1098(77)90591-9.

[59] J. A. Alonso and L. A. Girifalco. "Nonlocal approximation to the exchange potential and kinetic energy of an inhomogeneous electron gas". In: *Phys. Rev. B* 17 (10 1978), pp. 3735–3743. DOI: 10.1103/PhysRevB.17.3735. URL: https://link.aps.org/doi/10.1103/PhysRevB.17.3735.

[60] O. Gunnarsson, M. Jonson, and B. I. Lundqvist. "Descriptions of exchange and correlation effects in inhomogeneous electron systems". In: *Phys. Rev. B* 20 (8 1979), pp. 3136–3164. DOI: 10.1103/PhysRevB.20.3136. URL: https://link.aps.org/doi/10.1103/PhysRevB.20.3136.

[61] O. Gunnarsson and R.O. Jones. "Density Functional Calculations for Atoms, Molecules and Clusters". In: *Phys. Scr.* 21 (0 1980), p. 394. DOI: 10.1088/0031-8949/21/3-4/027.

[62] Rogelio Cuevas-Saavedra et al. "Symmetric Nonlocal Weighted Density Approximations from the Exchange-Correlation Hole of the Uniform Electron Gas". In: *J. Chem. Theory Comput.* 8.11 (2012), pp. 4081–4093. DOI: 10.1021/ct300325t. URL: https://doi.org/10.1021/ct300325t.

[63] John P. Perdew and Wang Yue. "Accurate and simple density functional for the electronic exchange energy: Generalized gradient approximation". In: *Phys. Rev. B* 33 (12 1986), pp. 8800–8802. DOI: 10.1103/PhysRevB.33.8800. URL: https://link.aps.org/doi/10.1103/PhysRevB.33.8800.

[64] John P. Perdew et al. "Accurate Density Functional with Correct Formal Properties: A Step Beyond the Generalized Gradient Approximation". In: *Phys. Rev. Lett.* 82 (12 1999), pp. 2544–2547. DOI: 10.1103/PhysRevLett.82.2544. URL: https://link.aps.org/doi/10.1103/PhysRevLett.82.2544.

[65] John P. Perdew et al. "Restoring the Density-Gradient Expansion for Exchange in Solids and Surfaces". In: *Phys. Rev. Lett.* 100 (13 2008), p. 136406. DOI: 10.1103/PhysRevLett.100.136406. URL: https://link.aps.org/doi/10.1103/PhysRevLett.100.136406.

[66] Jianwei Sun, Adrienn Ruzsinszky, and John P. Perdew. "Strongly Constrained and Appropriately Normed Semilocal Density Functional". In: *Phys. Rev. Lett.* 115 (3 2015), p. 036402. DOI: 10.1103/PhysRevLett.115.036402. URL: https://link.aps.org/doi/10.1103/PhysRevLett.115.036402.

[67] Kieron Burke. "Perspective on density functional theory". In: *The Journal of Chemical Physics* 136.15 (2012), p. 150901. DOI: 10.1063/1.4704546. URL: https://doi.org/10.1063/1.4704546.

[68] W. Kohn. "Density Functional and Density Matrix Method Scaling Linearly with the Number of Atoms". In: *Phys. Rev. Lett.* 76 (17 1996), pp. 3168–3171. DOI: 10.1103/PhysRevLett.76.3168. URL: https://link.aps.org/doi/10.1103/PhysRevLett.76.3168.

[69] J. P. Perdew. "What do the Kohn-Sham Orbital Energies Mean? How do Atoms Dissociate?" In: *Density Functional Methods In Physics*. Ed. by Reiner M. Dreizler and João da Providência. Plenum, New York, 1985, pp. 265–308.

[70] Marten A. Buijse, Evert Jan Baerends, and Jaap G. Snijders. "Analysis of correlation in terms of exact local potentials: Applications to two-electron systems". In: *Phys. Rev. A* 40 (8 1989), pp. 4190–4202. DOI: 10.1103/PhysRevA.40.4190. URL: https://link.aps.org/doi/10.1103/PhysRevA.40.4190.

[71] E. J. Baerends and O. V. Gritsenko. "A Quantum Chemical View of Density Functional Theory". In: *The Journal of Physical Chemistry A* 101.30 (1997), pp. 5383–5403. DOI: 10.1021/jp9703768. eprint: https://doi.org/10.1021/jp9703768. URL: https://doi.org/10.1021/jp9703768.

[72] David G. Tempel, Todd J. Martínez, and Neepa T. Maitra. "Revisiting Molecular Dissociation in Density Functional Theory: A Simple Model". In: *Journal of Chemical Theory and Computation* 5.4 (2009), pp. 770–780. DOI: 10.1021/ct800535c. URL: https://doi.org/10.1021/ct800535c.

[73] J. Wetherell et al. "Advantageous nearsightedness of many-body perturbation theory contrasted with Kohn-Sham density functional theory". In: *Phys. Rev. B* 99 (4 2019), p. 045129. DOI: 10.1103/PhysRevB.99.045129. URL: https://link.aps.org/doi/10.1103/PhysRevB.99.045129.

[74] Maurizia Palummo et al. "Nonlocal density scheme for electronic-structure calculations". In: *Phys. Rev. B* 60 (16 1999), pp. 11329–11335. DOI: 10.1103/PhysRevB.60.11329. URL: https://link.aps.org/doi/10.1103/PhysRevB.60.11329.

[75] Saverio Moroni, David M. Ceperley, and Gaetano Senatore. "Static Response and Local Field Factor of the Electron Gas". In: *Phys. Rev. Lett.* 75.4 (1995), pp. 6–9. ISSN: 0031-9007. DOI: 10.1103/PhysRevLett.75.689. URL: http://link.aps.org/doi/10.1103/PhysRevLett.75.689.

[76] Massimiliano Corradini et al. "Analytical expressions for the local-field factor G (q) and the exchange-correlation kernel K xc (r) of the homogeneous electron gas". In: *Physical Review B* 57.23 (1998), pp. 14569–14571. ISSN: 0163-1829. DOI: 10.1103/PhysRevB.57.14569. URL: http://link.aps.org/doi/10.1103/PhysRevB.57.14569.

[77] Valerio Olevano et al. "Exchange and correlation effects beyond the LDA on the dielectric function of silicon". In: *Phys. Rev. B* 60 (20 1999), pp. 14224–14233. DOI: 10.1103/PhysRevB.60.14224. URL: https://link.aps.org/doi/10.1103/PhysRevB.60.14224.

[78] G. Giuliani and G. Vignale. *Quantum Theory of the Electron Liquid*. Cambridge University Press, 2005. ISBN: 9780521821124.

[79] Mel Levy and John P. Perdew. "Hellmann-Feynman, virial, and scaling requisites for the exact universal density functionals. Shape of the correlation potential and diamagnetic susceptibility for atoms". In: *Phys. Rev. A* 32 (4 1985), pp. 2010–2021. DOI: 10.1103/PhysRevA.32.2010. URL: https://link.aps.org/doi/10.1103/PhysRevA.32.2010.

[80] Adrienn Ruzsinszky et al. "Constraint-based wave vector and frequency dependent exchange-correlation kernel of the uniform electron gas". In: *Phys. Rev. B* 101 (24 2020), p. 245135. DOI: 10.1103/PhysRevB.101.245135. URL: https://link.aps.org/doi/10.1103/PhysRevB.101.245135.

[81] Marco Vanzini et al. *Recycling knowledge to explore materials: a connector theory approach*. arXiv1903.07930. 2019. arXiv: 1903.07930 [cond-mat.other].

[82] P. García-González et al. "Image potential and the exchange-correlation weighted density approximation functional". In: *Phys. Rev. B* 62 (23 2000), pp. 16063–16068. DOI: 10.1103/PhysRevB.62.16063. URL: https://link.aps.org/doi/10.1103/PhysRevB.62.16063.

[83] J. P. Perdew, D. C. Langreth, and V. Sahni. "Corrections to the Local Density Approximation: Gradient Expansion versus Wave-Vector Analysis for the Metallic Surface Problem". In: *Phys. Rev. Lett.* 38 (18 1977), pp. 1030–1033. DOI: 10.1103/PhysRevLett.38.1030. URL: https://link.aps.org/doi/10.1103/PhysRevLett.38.1030.

[84] D.C. Langreth and J.P. Perdew. "The exchange-correlation energy of a metallic surface". In: *Solid State Communications* 17.11 (1975), pp. 1425–1429. ISSN: 0038-1098. DOI: https://doi.org/10.1016/0038-1098(75)90618-3. URL: https://www.sciencedirect.com/science/article/pii/0038109875906183.

[85] John P. Perdew, Matthias Ernzerhof, and Kieron Burke. "Rationale for mixing exact exchange with density functional approximations". In: *The Journal of Chemical Physics* 105.22 (1996), pp. 9982–9985. DOI: 10.1063/1.472933. URL: https://doi.org/10.1063/1.472933.

[86] P. J. Stephens et al. "Ab Initio Calculation of Vibrational Absorption and Circular Dichroism Spectra Using Density Functional Force Fields". In: *The Journal of Physical Chemistry* 98.45 (1994), pp. 11623–11627. DOI: 10.1021/j100096a001. eprint: https://doi.org/10.1021/j100096a001. URL: https://doi.org/10.1021/j100096a001.

[87] Michael E. Mura, Peter J. Knowles, and Christopher A. Reynolds. "Accurate numerical determination of Kohn-Sham potentials from electronic densities: I. Two-electron systems". In: *The Journal of Chemical Physics* 106.23 (1997), pp. 9659–9667. DOI: 10.1063/1.473838. URL: https://doi.org/10.1063/1.473838.

[88] K. Peirs, D. Van Neck, and M. Waroquier. "Algorithm to derive exact exchange-correlation potentials from correlated densities in atoms". In: *Phys. Rev. A* 67 (1 2003), p. 012505. DOI: 10.1103/PhysRevA.67.012505. URL: https://link.aps.org/doi/10.1103/PhysRevA.67.012505.

[89] A. Savin, F. Colonna, and R. Pollet. "Adiabatic connection approach to density functional theory of electronic systems". In: *International Journal of Quantum Chemistry* 93.3 (2003), pp. 166–190. DOI: https://doi.org/10.1002/qua.10551. URL: https://onlinelibrary.wiley.com/doi/abs/10.1002/qua.10551.

[90] John P. Perdew, Kieron Burke, and Matthias Ernzerhof. "Generalized Gradient Approximation Made Simple". In: *Phys. Rev. Lett.* 77 (18 1996), pp. 3865–3868. DOI: 10.1103/PhysRevLett.77.3865. URL: https://link.aps.org/doi/10.1103/PhysRevLett.77.3865.

[91] R. van Leeuwen and E. J. Baerends. "Exchange-correlation potential with correct asymptotic behavior". In: *Phys. Rev. A* 49 (4 1994), pp. 2421–2431. DOI: 10.1103/PhysRevA.49.2421. URL: http://link.aps.org/doi/10.1103/PhysRevA.49.2421.

[92] P. R. T. Schipper, O. V. Gritsenko, and E. J. Baerends. "Kohn-Sham potentials corresponding to Slater and Gaussian basis set densities". In: *Theoretical Chemistry Accounts* 98.1 (Oct. 1997), pp. 16–24. ISSN: 1432-2234. URL: https://doi.org/10.1007/s002140050273.

[93] Tim Heaton-Burgess, Felipe A. Bulat, and Weitao Yang. "Optimized Effective Potentials in Finite Basis Sets". In: *Phys. Rev. Lett.* 98 (25 2007), p. 256401. DOI: 10.1103/PhysRevLett.98.256401. URL: https://link.aps.org/doi/10.1103/PhysRevLett.98.256401.

[94] Christoph R. Jacob. "Unambiguous optimization of effective potentials in finite basis sets". In: *The Journal of Chemical Physics* 135.24 (2011), p. 244102. DOI: 10.1063/1.3670414. URL: https://doi.org/10.1063/1.3670414.

[95] Alex P. Gaiduk, Ilya G. Ryabinkin, and Viktor N. Staroverov. "Removal of Basis-Set Artifacts in Kohn–Sham Potentials Recovered from Electron Densities". In: *Journal of Chemical Theory and Computation* 9.9 (2013), pp. 3959–3964. DOI: 10.1021/ct4004146. URL: https://doi.org/10.1021/ct4004146.

[96] D. P. Chong, O. V. Gritsenko, and E. J. Baerends. "Interpretation of the Kohn–Sham orbital energies as approximate vertical ionization potentials". In: *The Journal of Chemical Physics* 116.5 (2002), pp. 1760–1772. DOI: 10.1063/1.1430255. URL: https://doi.org/10.1063/1.1430255.

[97] Stephan Kümmel and Leeor Kronik. "Orbital-dependent density functionals: Theory and applications". In: *Rev. Mod. Phys.* 80 (1 2008), pp. 3–60. DOI: 10.1103/RevModPhys.80.3. URL: http://link.aps.org/doi/10.1103/RevModPhys.80.3.

[98] Seungsoo Nam et al. "Measuring Density-Driven Errors Using Kohn–Sham Inversion". In: *Journal of Chemical Theory and Computation* 16.8 (2020), pp. 5014–5023. DOI: 10.1021/acs.jctc.0c00391. URL: https://doi.org/10.1021/acs.jctc.0c00391.

[99] W. Knorr and R. W. Godby. "Investigating exact density-functional theory of a model semiconductor". In: *Phys. Rev. Lett.* 68 (5 1992), pp. 639–641. DOI: 10.1103/PhysRevLett.68.639. URL: https://link.aps.org/doi/10.1103/PhysRevLett.68.639.

[100] John P. Perdew et al. "Density-Functional Theory for Fractional Particle Number: Derivative Discontinuities of the Energy". In: *Phys. Rev. Lett.* 49 (23 1982), pp. 1691–1694.

[101] L. J. Sham and M. Schlüter. "Density-Functional Theory of the Energy Gap". In: *Phys. Rev. Lett.* 51 (20 1983), pp. 1888–1891. DOI: 10.1103/PhysRevLett.51.1888. URL: https://link.aps.org/doi/10.1103/PhysRevLett.51.1888.

[102] John P. Perdew and Mel Levy. "Physical Content of the Exact Kohn-Sham Orbital Energies: Band Gaps and Derivative Discontinuities". In: *Phys. Rev. Lett.* 51.20 (1983), pp. 1884–1887. DOI: 10.1103/PhysRevLett.51.1884.

[103] M. Lannoo, M. Schlüter, and L. J. Sham. "Calculation of the Kohn-Sham potential and its discontinuity for a model-semiconductor". In: *Phys. Rev. B* 32 (6 1985), pp. 3890–3899. DOI: 10.1103/PhysRevB.32.3890. URL: https://link.aps.org/doi/10.1103/PhysRevB.32.3890.

[104] R. W. Godby, M. Schlüter, and L. J. Sham. "Accurate Exchange-Correlation Potential for Silicon and Its Discontinuity on Addition of an Electron". In: *Phys. Rev. Lett.* 56.22 (1986), pp. 2415–2418. DOI: 10.1103/PhysRevLett.56.2415.

[105] R. W. Godby, M. Schlüter, and L. J. Sham. "Self-energy operators and exchange-correlation potentials in semiconductors". In: *Phys. Rev. B* 37 (17 1988), pp. 10159–10175. DOI: 10.1103/PhysRevB.37.10159. URL: https://link.aps.org/doi/10.1103/PhysRevB.37.10159.

[106] Y. M. Niquet and X. Gonze. "Band-gap energy in the random-phase approximation to density-functional theory". In: *Phys. Rev. B* 70 (24 2004), p. 245115. DOI: 10.1103/PhysRevB.70.245115. URL: https://link.aps.org/doi/10.1103/PhysRevB.70.245115.

[107] Myrta Grüning, Andrea Marini, and Angel Rubio. "Effect of spatial nonlocality on the density functional band gap". In: *Phys. Rev. B* 74 (16 2006), p. 161103. DOI: 10.1103/PhysRevB.74.161103. URL: https://link.aps.org/doi/10.1103/PhysRevB.74.161103.

[108] Myrta Grüning, Andrea Marini, and Angel Rubio. "Density functionals from many-body perturbation theory: The band gap for semiconductors and insulators". In: *The Journal of Chemical Physics* 124.15 (2006), p. 154108. DOI: 10.1063/1.2189226. URL: https://doi.org/10.1063/1.2189226.

[109] Takao Kotani. "An optimized-effective-potential method for solids with exact exchange and random-phase approximation correlation". In: *J. Phys.: Condens. Matter* 10 (1998), p. 9241.

[110] Robert van Leeuwen and Evert Jan Baerends. "Energy expressions in density-functional theory using line integrals". In: *Phys. Rev. A* 51 (1 1995), pp. 170–178. DOI: 10.1103/PhysRevA.51.170. URL: https://link.aps.org/doi/10.1103/PhysRevA.51.170.

[111] J. J. Mortensen, L. B. Hansen, and K. W. Jacobsen. "Real-space grid implementation of the projector augmented wave method". In: *Phys. Rev. B* 71 (3 2005), p. 035109. DOI: 10.1103/PhysRevB.71.035109. URL: https://link.aps.org/doi/10.1103/PhysRevB.71.035109.

[112] J Lindhard. "No Title". In: *Kgl. Danske Vidensk. Selsk. Mat.-Fys, Medd.* 28.8 (1954), p. 8.

[113] Attila Cangi, E. K. U. Gross, and Kieron Burke. "Potential functionals versus density functionals". In: *Phys. Rev. A* 88 (6 2013), p. 062505. DOI: 10.1103/PhysRevA.88.062505. URL: https://link.aps.org/doi/10.1103/PhysRevA.88.062505.

[114] Ayoub Aouina, Matteo Gatti, and Lucia Reining. "Strategies to build functionals of the density, or functionals of Green's functions: what can we learn?" In: *Faraday Discussions* (2020). DOI: 10.1039/D0FD00068J. URL: https://doi.org/10.1039/D0FD00068J.

[115] N. H. March. "N representability of electron density and first-order density matrix". In: *Phys. Rev. A* 26 (4 1982), pp. 1845–1847. DOI: 10.1103/PhysRevA.26.1845. URL: https://link.aps.org/doi/10.1103/PhysRevA.26.1845.

[116] R.W.G. Wyckoff. *Crystal structures*. Second. Vol. 1. New York: Interscience Publishers, 1963.

[117] A. F. Schuch and R. L. Mills. "New Allotropic Form of He^3". In: *Phys. Rev. Lett.* 6 (11 1961), pp. 596–597. DOI: 10.1103/PhysRevLett.6.596. URL: https://link.aps.org/doi/10.1103/PhysRevLett.6.596.

[118] P. Ziesche. "Cumulant 2-matrix of the high-density electron gas and the density matrix functional theory". In: *International Journal of Quantum Chemistry* 90.1 (2002), pp. 342–354. DOI: https://doi.org/10.1002/qua.969. eprint: https://onlinelibrary.wiley.com/doi/pdf/10.1002/qua.969. URL: https://onlinelibrary.wiley.com/doi/abs/10.1002/qua.969.

[119] K. Rapcewicz and N. W. Ashcroft. "Fluctuation attraction in condensed matter: A nonlocal functional approach". In: *Phys. Rev. B* 44 (8 1991), pp. 4032–4035. DOI: 10.1103/PhysRevB.44.4032. URL: https://link.aps.org/doi/10.1103/PhysRevB.44.4032.

[120] Martin Panholzer, Matteo Gatti, and Lucia Reining. "Nonlocal and Nonadiabatic Effects in the Charge-Density Response of Solids: A Time-Dependent Density-Functional Approach". In: *Phys. Rev. Lett.* 120 (16 2018), p. 166402. DOI: 10.1103/PhysRevLett.120.166402. URL: https://link.aps.org/doi/10.1103/PhysRevLett.120.166402.

[121] Xavier Gonze et al. "A brief introduction to the ABINIT software package". In: *Z. Kristallogr* 220 (2005), pp. 558–562.

ECOLE DOCTORALE

Titre : Un nouveau raccourci pour la conception computationnelle des matériaux

Mots clés : Théorie de la matière condensée, Développement de théorie, Conception computationnelle des matériaux

Résumé : La théorie de la fonctionnelle de la densité (DFT) nous apprend que toute propriété d'un système en interaction est une fonctionnelle de la densité électronique de l'état fondamental. L'approche de Kohn-Sham a fait de la DFT une méthode de calcul utile pour étudier la structure électronique des matériaux. Le potentiel d'échange et corrélation (xc) est la quantité clé, mais il reste inconnu. Dans l'approximation de la densité locale (LDA), le système réel est traité localement comme un gaz d'électrons homogène (HEG) dont la densité est égale à la densité locale du système réel. Le potentiel xc est alors importé du HEG, qui sert de modèle. Il a été obtenu, une fois pour toutes, par des calculs de Monte Carlo Quantique (QMC). Ces calculs ont grandement contribué au succès de la DFT dans la modélisation des solides et des molécules. Inspirés par la LDA et l'utilisation du HEG, nous généralisons dans cette thèse l'idée d'utiliser des modèles pour simuler des systèmes réels. Notre approche, appelée "théorie du connecteur" (COT), est une prescription en principe exacte de comment utiliser les données des modèles pour calculer les propriétés des matériaux. La force de la COT est double : premièrement, partir d'une théorie en principe exacte permet de construire des approximations systématiques. Deuxièmement, comme les modèles sont généralement des systèmes plus simples, on peut se permettre de calculer les quantités dans le modèle avec une grande précision. L'avantage est énorme puisque ces calculs sont effectués une fois pour toutes et servent de briques de base pour l'approximation de quantités réelles. Après avoir présenté le schéma général de la COT, nous l'avons utilisé pour construire des fonctionnelles non locales pour le potentiel xc. Nous avons montré que la LDA peut être dérivée comme un cas particulier d'une approximation de la COT. Afin de tester la stratégie de la COT, nous l'avons appliquée pour reproduire une fonctionnelle non locale basée sur la ≪ Weighted Density Approximation ≫. Les résultats ont été très prometteurs: d'une part, nous avons pu obtenir la LDA dans le cadre de la COT en négligeant la partie à longue portée de l'interaction coulombienne. D'autre part, nous avons construit une description non locale qui va au-delà de la LDA. Pour examiner le potentiel xc COT, nous l'avons implémenté dans la boucle Kohn-Sham et avons calculé les densités du silicium, un semi-conducteur, et du chlorure de sodium, un isolant. Comparées aux résultats QMC de référence, les densités produites à partir de ce potentiel xc COT étaient très précises. Indépendamment du COT, nous avons examiné la question de l'obtention du potentiel xc à partir de la densité QMC. L'objectif principal était de comparer les propriétés du potentiel xc exact à la COT et d'autres approximations DFT. Nous avons abordé diverses questions techniques liées à l'algorithme d'inversion, qui a été appliqué pour la première fois aux solides, notamment l'effet d'une base incomplète et l'erreur statistique de QMC. Le potentiel xc résultant nous a permis de calculer les énergies xc exactes, les bandes interdites de Kohn-Sham et les structures de bande de Si et de NaCl, et de comparer avec les approximations COT. Cela nous a aussi motivé à construire une fonctionnelle COT pour l'énergie xc. Enfin, nous avons montré que la COT n'est pas limitée à la DFT, en l'utilisant pour estimer la densité sans diagonaliser un hamiltonien à particules indépendantes. Nous avons également expliqué comment utiliser la COT pour approximer des objets non locaux tels que la matrice densité; dans cet exemple, nous avons montré qu'un modèle non homogène peut améliorer les approximations de la COT. Ces modèles plus complexes pourraient être résolus grâce aux capacités de calcul actuelles, et les résultats pourraient être paramétrés grâce aux méthodes d'apprentissage automatique.

Title : A novel shortcut for computational materials design

Keywords : Condensed matter theory, Computational materials design, Theory development

Abstract : Density functional theory (DFT) tells us that any property of an interacting system is a functional of the ground-state electronic density. The Kohn-Sham scheme has made DFT a practical computational tool to study the electronic structure of materials. The main quantity that needs to be approximated is the exchange correlation (xc) potential. In the local density approximation (LDA), the real system is treated locally as a homogeneous electron gas (HEG) with a density equal to the local density of the real system. The xc potential is then imported locally from the HEG, which serves as a model. It has been obtained, once for all, by accurate quantum Monte Carlo calculations (QMC) of the HEG at various densities. These calculations contributed immensely to the success of DFT being one of the most widely used method for modelling solids and molecules. Inspired by the LDA and the use of the HEG, in this thesis we generalise the idea of using models to simulate real systems. Our approach, called "Connector Theory" (COT), is an in principle exact prescription of how to use data from models to calculate quantities in materials. The power of this approach is twofold: first, starting from an in principle exact theory provides a guideline to build systematic and improvable approximations. Second, since models are usually simpler systems, one can also afford high level calculations with great precision for new model quantities. The benefit is enormous since these calculations are done once and for all and serve as building blocks to approximate real quantities. After introducing the general scheme of COT, we used it to build non-local functionals of the density for the xc potential, starting from a linear expansion. We showed that the LDA can be derived as a particular case of the COT approximation. In order to test the COT strategy, we applied it to reproduce a non-local functional of the xc potential based on the weighted density approximation. The results were very promising: on the one hand, we could obtain the LDA within the COT scheme by making the Coulomb interaction short range. On the other hand, we constructed a non-local description of the functional that goes beyond the LDA and the linear expansion. To examine the COT approximation of the xc potential, we implemented it in the self-consistent Kohn-Sham loop and computed the electronic densities of silicon, a semiconductor, and sodium chloride, an insulator. When compared to benchmark QMC results, the densities produced from this COT xc potential were very accurate. This was due to the ability of COT functional to capture a significant amount of the non-local information of the system. Independently of the COT, we have examined the inverse question of obtaining the xc potential from the accurate QMC density. The main aim was to analyse the features of the exact xc potential and to compare them with the COT and other DFT approximations. We addressed various technical issues related to the algorithm of the inversion, which was applied for the first time in solids, including the influence of the basis set and the statistical error of QMC. The inverted xc potential enabled us to determine the exact xc energies, Kohn-Sham band gaps and band structures of Si and NaCl, and to benchmark corresponding COT approximations. This also provided the motivation to build and test a new COT functional optimised for the xc energy. Finally, we demonstrated that COT is not limited to DFT by using it to estimate the density without diagonalising an independent-particle Hamiltonian. We have also explained how to use COT to approximate non-local objects such as the density matrix; in this example, we showed that a non-homogenous model can boost COT approximations. These more complex models could be calculated using nowadays computer capacities, and the results could be interpolated and parametrised using available machine learning techniques.

Institut Polytechnique de Paris
91120 Palaiseau, France